BIOMASS-DERIVED HIGH SURFACE POROUS CARBON FOR ENERGY AND SENSING APPLICATIONS

Thesis

Submitted in partial fulfilment of the requirements for the degree of

DOCTOR OF PHILOSOPHY

By

SHREEGANESH SUBRAYA HEGDE

DEPARTMENT OF CHEMISTRY

NATIONAL INSTITUTE OF TECHNOLOGY KARNATAKA

SURATHKAL, MANGALORE – 575025

JUNE 2024

“आ नो भद्राः क्रतवो यन्तु विश्वतः” – ऋग्वेद

DECLARATION

I hereby declare that the Research Thesis entitled "**BIOMASS-DERIVED HIGH SURFACE POROUS CARBON FOR ENERGY AND SENSING APPLICATIONS**" which is being submitted to the **National Institute of Technology Karnataka, Surathkal** in partial fulfilment of the requirements for the award of the degree of **Doctor of Philosophy** in **Chemistry** is a bonafide report of the research work carried out by me. The material contained in this Research Thesis has not been submitted to any University or Institution for the award of any degree.

Mr. Shreeganesh Subraya Hegde

Register Number: 207543CY501

Department of Chemistry

Place: NITK-Surathkal

Date: 28.06.2024

CERTIFICATE

This is to certify that the Research Thesis entitled "**BIOMASS-DERIVED HIGH SURFACE POROUS CARBON FOR ENERGY AND SENSING APPLICATIONS**" submitted by **Mr. Shreeganesh Subraya Hegde** (Register Number: 207543CY501) as the record of the research work carried out by him, is accepted as the Research Thesis submission in partial fulfilment of the requirements for the award of degree of **Doctor of Philosophy**.

Dr. B. RAMACHANDRA BHAT
Research Guide
Professor
Department of Chemistry
National Institute of Technology Karnataka
Surathkal, Srinivasnagar, MANGALORE - 575 025

Sib Sankar Mal (i/c)
Chairman – DRPC/HOD

विभागाध्यक्ष / H.O.D.
रसायन शास्त्र विभाग/ Chemistry Dept.
राष्ट्रीय प्रौद्योगिकी संस्थान कर्नाटक, सुरत्कल
NITK SURATHKAL
मंगलूरु-५७५ ०२५, कर्नाटक
MANGALURU-575 025, KARNATAKA

Place: NITK-Surathkal

Date: 28.06.2024

ACKNOWLEDGEMENT

I am immensely thankful to Prof. Badekai Ramachandra Bhat, my academic mentor, whose unwavering care, love, and support have been instrumental throughout my doctoral journey. With his guidance, I have been granted the liberty to explore my research projects in ways that have enriched my intellectual development. Under Prof. Bhat's mentorship, I have experienced unparalleled autonomy as a Ph.D. candidate, which has facilitated both my personal and academic progress. He wasn't just a doctoral supervisor to me; he treated me like his own son.

Prof. J. Seetharamappa, who initially sparked my research interest; Prof. Nirmalya Ballav, who helped it flourish; and Prof. B. Ramachandra Bhat, who meticulously nurtured it into fruition, are three figures profoundly etched in my research journey. I am deeply grateful to Bhagavān Rudra for bringing these persons into my life.

I would like to thank my RPAC members, Dr. Beneesh P. B. and Dr. Navin Karanth P., for their insightful suggestions throughout my Ph.D. I am profoundly thankful to the Heads of the Department and Directors of the Institute for offering steadfast support and generosity during my doctoral studies.

I sincerely thank the Department of Chemistry, Central Research Facility, and the National Institute of Technology Karnataka, Surathkal, for providing the necessary research and library facilities. Additionally, I would like to acknowledge the ASEAN-SERB, DST, Govt. of India for the research fellowship.

I applaud all the teaching and non-teaching staff of the department, as well as the institute, for their direct or indirect help and good wishes throughout my research journey. A special thanks to Prof. Udayakumr Dalimba.

I appreciate all my fellow researchers from the depth of my heart for their friendliness towards me. A special thanks to Mr. Shivakumar, Mr. Vighneshwar, and Mr. Dinesh for their timely help and constant support.

I thank Dr. Gil Nonato C. Santos for his hospitality during my visit to De La Salle University, Philippines. Additionally, I am thankful to Dr. Minhaz Uddin Ahmed of Universiti Brunei Darussalam, Brunei, for providing me with the facilities to work with group members and gain exposure to bio-sensing techniques.

I am forever indebted to my Yakshagana guru, Mr. Shashiraja Somayaji, for accepting me as a student and imbuing my research journey with boundless happiness and energy through Yakshagana art.

I would like to express an extreme sense of happiness towards Mr. B.K. Rajesh, my best friend, brother, and well-wisher, who supported me unconditionally at all times.

In the tapestry of my journey, woven with threads of perseverance and dedication, I find myself indebted to the unwavering pillars of love and support provided by my beloved parents, Mrs. Mahalakshmi Hegde and Mr. Subraya Hegde. Despite their limited understanding of the intricacies of research, they wholeheartedly embraced and supported my decisions. Their boundless encouragement, benevolent wishes, and backing have illuminated my path. Their belief in my dreams has been a constant source of inspiration, propelling me towards success. I am profoundly grateful for their enduring presence and unwavering faith in my endeavors. I consider myself immensely fortunate to be blessed with such caring and supportive parents.

Finally, I wish to express my deep appreciation to all those who have helped me directly or indirectly, during my doctoral journey.

SHREEGANESH HEGDE

ಅರ್ಪಣೆ

ತಂದೆಯಂತೆ ರಕ್ಷಿಸುವ ತಾಯಿಗೆ

ತಾಯಿಯಂತೆ ಮುದ್ದಿಸುವ ತಂದೆಗೆ

ಭಾರತೀಯ ವೈಜ್ಞಾನಿಕ ಪರಂಪರೆಗೆ

ABSTRACT

The research thesis titled **'BIOMASS-DERIVED HIGH SURFACE POROUS CARBON FOR ENERGY AND SENSING APPLICATIONS'** explores the synthesis, characterization, and application studies of biomass-derived carbon materials. Through innovative methodologies and meticulous characterization, high-surface porous carbon materials derived from various biomass sources have been tailored to demonstrate exceptional performance in electrochemical energy storage and sensing. Beginning with the investigation of *Tectona grandis* sawdust-derived porous carbon (TPC) and progressing to the refined synthesis of *Mangifera indica* leaf waste-derived activated carbon (MLAC) and *Cocos nucifera* trunk sawdust-derived high-surface carbon (CHSC), each stage demonstrates the transformative potential of converting renewable resources into porous carbon materials with customized properties. These materials exhibited outstanding electrochemical performance, with high specific capacitances, impressive cyclic stabilities, and superior energy densities. Moreover, the study meticulously underscores the importance of optimizing electrolyte conditions to maximize their potential in energy storage. Additionally, the development of a novel electrochemical biosensor utilizing high-surface porous carbon (HSPC) synthesized from *Tamarindus indica* seeds showcases the versatility of biomass-derived carbon in biosensing applications, particularly in the sensitive and selective detection of the dengue virus NS1 protein. The biosensor exhibits exceptional sensitivity, a broad linear range, selectivity, reproducibility, and long-term stability, offering a promising solution to the urgent need for rapid and accurate detection of dengue virus infections, with potential implications for enhancing patient outcomes and controlling disease spread globally.

Keywords: Biomass-derived carbon; Porous carbon; Supercapacitor; Biosensor; Dengue NS1 protein; Electrode material.

CONTENTS

ABBREVIATIONS v

CHAPTER 1 1

INTRODUCTION 1

1.1 BIOMASS-DERIVED CARBON 1

1.1.1 Solid waste as a source of CNS 3

1.1.2 Preparation and activation of solid biomass-derived CNS 5

1.1.3 Effect of morphological diversities on electrochemical performance 7

1.2 SUPERCAPACITOR: A ENERGY STORAGE DEVICE 8

1.2.1 Introduction to supercapacitor 8

1.2.2 Types of supercapacitor 9

1.2.3 Components of the supercapacitor 11

1.2.4 Performance evaluation of supercapacitor 12

1.3 DENGUE BIOSENSORS 12

1.3.1 Introduction to dengue: A arboviral disease 13

1.3.2 Physiology of the virus 14

1.3.3 Dengue diagnosis techniques 16

1.4 SCOPE AND OBJECTIVES OF THE WORK 18

CHAPTER 2 20

SYNTHESIS AND CHARACTERIZATION OF *TECTONA GRANDIS* SAWDUST-DERIVED POROUS GRAPHITIC CARBON FOR HIGH-PERFORMANCE SUPERCAPACITOR 20

2.1 INTRODUCTION 20

2.2 MATERIALS AND METHODS 22

2.2.1 Materials 22

2.2.2 Synthesis of TPC 23

2.2.3 Characterizations....23
2.2.4 Electrode preparation and electrochemical studies....24
2.3 RESULTS AND DISCUSSIONS....24
2.3.1 Structural and morphological analysis....24
2.3.2 Electrochemical performance of electrodes....28
2.4 CONCLUSIONS....32
CHAPTER 3 34
SYNTHESIS AND CHARACTERIZATION OF *MANGIFERA INDICA* LEAF-DERIVED ACTIVATED CARBON FOR LONG-LIFE, HIGH-PERFORMANCE SUPERCAPACITORS 34
3.1 INTRODUCTION 34
3.2 MATERIALS AND METHODS....36
3.2.1 Materials 36
3.2.2 Synthesis of MLAC 36
3.2.3 Characterizations....37
3.2.4 Electrode preparation and electrochemical studies....37
3.3 RESULTS AND DISCUSSIONS....37
3.3.1 Structural and morphological analysis....37
3.3.2 Electrochemical performance of electrodes....44
3.4 CONCLUSIONS....47
CHAPTER 4 49
IMPACT OF ELECTROLYTE CONCENTRATION ON THE ELECTROCHEMICAL ENERGY STORAGE PERFORMANCE OF *COCOS NUCIFERA* TRUNK-DERIVED HIGH-SURFACE CARBON....49
4.1 INTRODUCTION 49
4.2 MATERIALS AND METHODS....52

4.2.1 Materials 52
4.2.2 Synthesis of CHSC 52
4.2.3 Characterizations 53
4.2.4 Electrode preparation and electrochemical studies 53
4.3 RESULTS AND DISCUSSIONS 54
4.3.1 Structural and morphological analysis 54
4.3.2 Electrochemical performance of electrodes 59
4.4 CONCLUSIONS 66
CHAPTER 5 68
ULTRASENSITIVE HIGH-SURFACE POROUS CARBON-BASED ELECTROCHEMICAL BIOSENSOR FOR EARLY DETECTION OF DENGUE VIRUS NS1 PROTEIN 68
5.1 INTRODUCTION 68
5.2 MATERIALS AND METHODS 70
5.2.1 Materials 70
5.2.2 Synthesis of HSPC 71
5.2.3 Instrumentation 71
5.2.4 Construction of the dengue biosensor and electrochemical studies 72
5.2.5 Analysis of NS1 in real blood samples 72
5.2.6 Computational parameters 73
5.3 RESULTS AND DISCUSSIONS 74
5.3.1 Structural and morphological characterizations 74
5.3.2 Electrochemical characterizations 78
5.3.3 Computational results 86
5.4 CONCLUSIONS 90
CHAPTER 6 92

SUMMARY AND CONCLUSIONS 92
6.1 SUMMARY OF RESEARCH WORK 92
6.2 CONCLUSIONS 96
6.3 FUTURE WORK 97
REFERENCES 99
PUBLICATIONS 116
AWARDS & ACHIEVEMENTS 118
CONFERENCES/SYMPOSIUMS/WORKSHOPS 118
BIO-DATA 120

ABBREVIATIONS

CNS	- Carbon nano-structures
TPC	- *Tectona grandis* sawdust-derived porous carbon
MLAC	- *Mangifera indica* leaves-derived activated carbon
CHSC	- *Cocos nucifera* trunk sawdust derived high surface carbon
HSPC	- High-surface porous carbon
NS1 protein	- Non-structural 1 protein
DENV	- Dengue virus
XPS	- X-ray photoelectron spectroscopy
EDX	- Energy-dispersive X-ray spectroscopy
FESEM	- Field emission scanning electron microscopy
TEM	- Transmission electron microscopy
XRD	- X-Ray diffraction
CV	- Cyclic voltammetry
GCD	- Galvanostatic charge-discharge
EIS	- Electrochemical impedance spectroscopy
NMP	- N-Methyl-2-pyrrolidone
PVDF	- Poly(vinylidene fluoride
BSA	- Bovine serum albumin
PBS	- Phosphate buffer saline
PEI	- Polyethylenimine
Ig-G	- Immunoglobulin-G

CHAPTER 1

INTRODUCTION

Abstract: This chapter introduces a comprehensive literature review on biomass-derived carbon materials and presents the basic concepts for supercapacitors as well as dengue disease diagnostics. Additionally, it outlines the scope and objectives of the present research work.

1.1 BIOMASS-DERIVED CARBON

Global population expansion has resulted in an enormous and unconventional increase in worldwide advancement. Consequently, associated needs are growing day by day, causing an explosive rise in creating various types of waste materials (Kumar and Agrawal 2020). An exponential increase in the atmospheric temperature, destructive environmental effects, and the unreplenishable nature of energy supplies have sparked universal attention to the need to find alternative energy sources, value-added chemical products, and fuel (Jaiswal et al. 2022). Biomass-derived material has emerged as a fantastic alternative in this regard. These refer to organic materials originating from plants or animals often regarded as garbage. This garbage are posing significant health and environmental risk, thus showing a considerable challenge for the research world. When solid biomass and agricultural wastes are burned, several pollutants are discharged into the environment (Yao et al. 2023). The sort of biomass feedstock and its types have a significant impact on the nature of emissions. Numerous pollutants are routinely emitted into the atmosphere, including nitrogen oxide, carbon monoxide, and sulphur dioxide. Forest fires are caused by waste biomass, which can potentially raise global greenhouse gas emissions (Liu et al. 2019b).

The correct handling of such a large volume of solid garbage is a primary environmental concern in and of itself (Ferrero et al. 2015a). To successfully address the issue, scientific progress necessitates the development of a novel technique capable of addressing and managing the use of such wastes through the application of

sophisticated scientific technology. In this sense, nanotechnology and nanoscience have been significant blessings to the scientific society. They may concurrently serve as a lifeline for efficiently managing various universal duties, such as solid waste management and the global energy problem. As a result, waste handling solutions must be invented to fully address the challenge of solid waste management. Furthermore, the technological world has a tremendous challenge in developing a new approach for manufacturing ecologically responsible and economically friendly energy storage technologies to address the global energy issue. However, several research groups have published some unique research, such as effective solid waste treatment and an economically favourable synthesis route of carbon nano-structures(CNS) for diverse industrial uses, particularly in the energy sector.

Biological trash, abundant natural resources, or items that may be obtained for free or at a minimal cost are typically used to make biochar. More precisely, animal manure and agricultural by-products are frequently used as raw materials for biochar. These substances are produced in every nation but are rarely used and have disposal issues. Thus, they can be used as feedstocks to make biochar. For instance, trash or by-products from farming production, including corn, peanuts (Liang et al. 2023), sugarcane(Mohamed et al. 2022), oil palm(Gayathiri et al. 2023), and other crop waste, are frequently used to make biochar. The use of biochar as a crucial tool for protecting the atmosphere has subsequently attracted a lot of interest. A blackened product called biochar is created when biomaterials are pyrolyzed in a limited or no oxygen condition. In other words, the carbon-containing substance known as biochar is abundant in minerals and carbon. According to earlier studies, the qualities and many uses of biochar have been linked to its carbon percentage. However, the elemental components of biochar also significantly affect its characteristics and, ultimately, its use in a variety of areas, as the latest scientific advancements have confirmed. Additionally, the elemental components of biochar significantly influence its shape, structure, and other characteristics, including pH, electrical properties, porous structure, and surface area per unit weight (Amalina et al. 2022). The production of these carbons in large quantities is thought to be both inexpensive and environmentally friendly. Hence, activated carbon is frequently utilized for purposes such as soil remediation, energy

production, greenhouse gas reduction, waste management, and enhancement of the soil's capacity to contain nutrients and retain water since it has many positive ecological attributes. It is generally known that the conversion of biomaterials into biochar lowers the atmospheric CO_2 concentration and generates alternative sources (Vijayaraghavan 2021).

1.1.1 Solid waste as a source of CNS

Treatment of solid waste and the demand for renewable energy are two crucial research topics for adopting low-cost solid-waste utilization strategies. The development of low-cost, high-efficiency electrode materials is required to meet the rising demand for green and sustainable energy. Numerous naturally abundant environmental and agro-wastes have been researched to manufacture porous carbon for electrode because of their readily available availability, outstanding performance, and easy processing techniques. These waste materials contain carbon as a skeletal backbone, allowing science and technology to function to a higher degree. In contrast, based on the preparation technique, the activation method can modify the morphological and structural features of the material (Xie et al. 2022). The source and type of biomass are crucial for producing carbon in a commercially sustainable way. Directly burning garbage is a frequent practice since developing nations lack an appropriate disposal technique, which raises atmospheric carbon dioxide concentrations and has a negative impact on both public health and the ecosystem (Jakhar et al. 2023). By transforming such leftovers into value-added products, thermochemical conversion via pyrolysis, gasification, and hydrothermal liquefaction provides an appropriate means of reducing the negative ecological effect of such wastes (Gururani et al. 2022). As a result, agro-forest wastes can be viewed as an environmentally friendly resource for the creation and use of carbon.

The trash produced by a variety of industries includes significant amounts of carbon. These comprise agro-enterprises that create residues like potato peel, orange peel, oilseed cakes, etc., and industries or sawmills in the forest that produce sawdust. Each year, approximately 50 million tonnes of lignin are produced as a byproduct of the pulp and paper industry; less than 5% of this amount is economically used, and the remainder

is burned as dry fuel (Nguyen et al. 2021). The manufacturing methods can be used based on the input. Depending on their accessibility and production in a worldwide context, many sources for the manufacture of carbon may be identified. The bulk of the trash, primarily in the form of lignocellulose, may be attributed to agricultural and forest waste. After the wood is harvested, forestry-related sectors produce debris such as stems, treetops, and branches, among other things, which is referred to as "forestry residual." Rice straw, wheat straw, rice husk, and maize stover are examples of the waste materials produced after crop harvesting that are referred to as "agricultural residues." It either serves as livestock feed or is just left to decompose naturally in the vast farming area. As a result, tobacco (Chen et al. 2017), corncob (Karnan et al. 2017), corn silk (Mitravinda et al. 2018), corn husk (Usha Rani et al. 2020), rice husk (Jin et al. 2019), soybean residue (Ferrero et al. 2015b), sugarcane bagasse (Wang et al. 2018), orange peel (Parveen et al. 2019), lime peels (Ahirrao et al. 2019), banana peels (Liu et al. 2016), onion husks (Wang et al. 2016), coconut coir pith (Sesuk et al. 2019), coconut fibres (Yin et al. 2016), coconut shell (Ashraf et al. 2018), jackfruit shell (Lee et al. 2020), longan shell (Yan 2020), almond shells (Yan 2020), soybean roots(Guo et al. 2016), coffee seed powder (Choi et al. 2019), bacterial cellulose(Ding et al. 2020), pine cones(Gadipelli et al. 2020) and many more bio-waste-derived carbon materials are reported to show good performance as supercapacitor electrodes.

Additionally, sewage sludge produced during the municipal water treatment process in urban facilities can be used as a promising option for the creation of biochar. Wastewater sludge is often disposed of in landfills, fertilizers, and incinerators. These approaches, nevertheless, are risky and constrained in areas with little access to soil (Adhikari et al. 2018). Compared to biochar made from biomass, sewage waste biochar generally has greater hydrogen to carbon ratio and higher levels of N, P, and K (Liu et al. 2018). Additionally, neither the P nor the K content of the biochar would not be altered by the rise in pyrolysis temperature (Yang et al. 2018). Using cattle dung as fertilizer is somewhat constrained by the rising levels of heavy metal ions in the ground. Such heavy metal ions are helped to get immobilized in the carbon framework by the thermal transformation of animal dung into carbon materials (Li et al. 2020). These carbon materials may be used in energy storage technologies such as supercapacitors

since the existence of d-block metals can improve the biochar's capacity for charge storage (Vijayaraghavan 2021).

1.1.2 Preparation and activation of solid biomass-derived CNS

Carbon nanomaterials are carbon-based nanoparticles with a wide range of benefits. So, increasing the yield of different CNS from environmental solid trash substances can be done by following various scientific and technological treatments. Physical vapour deposition (PVD), chemical vapour deposition (CVD), hydrothermal carbonization, torrefaction, organic oxidation-reduction techniques, and pyrolytic heating are the methods for converting carbonic trash into CNS. The properties of these materials are primarily dependent on particular surface interactions and the use of reagents (Tatrari et al. 2021). On the other hand, heating temperature, residence time, atmosphere, pressure, and scan rate are the most critical factors that affect the layer development and fluctuations of the CNS in the pyrolysis reaction. The pyrolysis process is the thermal degradation of biomass in an inert environment to produce carbon materials at temperatures between 300 and 900 degrees Celsius. The quantity and quality of biochar produced are affected by the nature of the raw substance and the adapted parameters or methods (Wei et al. 2019). According to heating rate and temperature, pyrolysis is classified into two types: slow and fast pyrolysis. The slow process uses a lower heat input rate, usually 5–7 °C/min, and a prolonged residence period (greater than one hour), and the rapid process follows a higher heat input rate, usually 100–200 °C/min, and a shorter residence period (less than 10 s) (Dhyani and Bhaskar 2018). Slow pyrolysis produces more charcoal, whereas rapid pyrolysis produces more bio-oil (Al Arni 2018). While using highly moist bio-waste material for biochar synthesis, it's common to dry it first.

The biochar created by the aforementioned thermochemical procedures frequently needs physical or chemical activation in order to improve its surface properties, as well as other characteristics like specific surface area and the porous nature of the material that significantly enhance its charge storage properties (Adeniyi et al. 2024). Hence, activating the biomass waste-derived carbon material is a critical process for developing a porous surface structure and increasing the active area. Physical activation and chemical activation are two methods for producing activated carbon materials from

biomass (Chen et al. 2018b). Physical activation is the process of generating porous carbon structures from waste-derived carbon compounds by utilizing gaseous mediators including hot steam, oxygen, or carbon dioxide (Dong et al. 2018). In contrast, chemical activation is connected with traditional chemical activating agents like acids, bases, or salts (Huo et al. 2020). In physical activation, activation of the waste-derived carbon material is carried out after the carbonation step, whereas in chemical activation, both activation and carbonization of the materials can be done in a one move (Merin et al. 2021). The synthesized carbon material is processed with an activating agent prior to carbonization.

Chemical activation is a widely used method to produce highly porous carbon materials from biomass. This process involves impregnating the biomass with certain chemical agents before heating it to high temperatures. Chemical agents act as dehydrating agents, promoting the formation of cross-linked structures by removing water molecules from the biomass. This leads to a more rigid and porous carbon structure. These agents decompose during heating, leaving behind pores and etching the carbon surface. For instance, KOH reacts with carbon to form K_2CO_3, which produces CO_2, creating additional porosity. These chemicals can also catalyze the gasification of carbon at lower temperatures, producing gases like CO_2 and H_2O that create pores in the carbon matrix. Agents like potassium hydroxide (KOH) can oxidize the biomass, creating more oxygen-containing functional groups. Potassium hydroxide, oxyacids, zinc chloride, and other activating chemical agents are commonly utilized. Chemical activation is more favorable because of the higher yield generation, lower cost, and the ability to generate porous structures at lower temperatures and in less time (Su et al. 2018). The choice of chemical activator depends on several factors, including the type of biomass, desired pore structure, and the final application of the activated carbon. Typically, for energy storage (supercapacitors) and sensing applications, KOH, $FeCl_3$, and $ZnCl_2$ are effective in achieving a high surface area and optimal pore size distribution.

1.1.3 Effect of morphological diversities on electrochemical performance

Despite its average surface area and improper pore size dispersion, immediate utilization of carbon for charge storage techniques is not advantageous. The carbon substance is activated in order to create porosity. The energy storage method for carbon is primarily electrostatic, the various oxidation states of ions aid in energy storage through electrochemical processes. The electrochemical characteristics of CNS enormously vary with the structural features, such as specific surface area and morphological behavior, which highly depend upon the structural framework of the solid waste precursor material. In connection with electrode materials, researchers are constantly looking for carbon electrodes that have a large active surface area, an optimal porous structure to improve the conductivity and capacitance without losing their stability (Jiang et al. 2018). Carbon compounds generated from biomass have sparked a lot of attention in energy storage materials because of their abundant supply and eco-friendly nature.

The electrochemical properties of the produced CNS are significantly connected with morphological features such as graphitization or degree of carbonization, pore volume, pore size, and surface patterns. The extent of carbonization affects the capacitance, power density, total resistance, power transmission, long cycle life, and energy density (Zhai et al. 2022). The hydrophilicity of the synthesized material towards aqueous electrolyte depends on the extent of carbonization. This carbonization would result in better ion diffusion and ion transfer efficiency, which improves the function of the electrode material (Sun et al. 2013). The lower resistance indicates a high level of carbonic activation or carbonization in the sample, implying a higher conductance in the specimen. However, when the degree of graphitization and carbonization progresses, the specific area decreases, resulting in distortions of the relative structure and pore volume (Tatrari et al. 2021). Hence, the primary factors driving changes in electrical and chemical characteristics include differences in surface morphology, changes in the purity of CNS, chemical and thermal permanence, and chemical and structural characteristics. The conductance, capacitive, and storing qualities of CNS are influenced by their extensive surface area. These CNS shows excellent electrical conductance and have a large SSA, hence making them ideal materials for electrodes.

1.2 SUPERCAPACITOR: A ENERGY STORAGE DEVICE

1.2.1 Introduction to supercapacitor

Over the last few decades, the depletion of fossil fuels, environmental contamination, and the release of greenhouse gases has led to significant health risks and disruptions in ecosystems. Adapting to the changing energy landscape necessitates advancing and implementing cost-effective, high-performing, and reliable energy storage solutions to harness the potential of abundant, renewable energy sources. Hence, in recent years, efforts to promote sustainable energy utilization and advance green energy storage technology have gained momentum, aiming to combat the issues arising from high energy consumption and environmental pollution (Mascarenhas et al. 2023; Senthil and Lee 2021). Among the array of electrochemical energy storage technologies, supercapacitors exhibit significant potential for delivering rapid, high-rate power supplies and supporting the versatility of portable electric applications. Due to their unique advantages, encompassing exceptional durability in terms of cycling life, rapid charge and discharge capabilities, outstanding power density, and a solid commitment to environmental sustainability, the supercapacitors distinguish themselves from conventional energy storage options like potassium-ion, sodium-ion, and lithium-ion batteries (Kulurumotlakatla et al. 2020; Yoon et al. 2020; Zhao et al. 2020; Zhu et al. 2022).

Carbon materials, metal oxides, and conducting polymers stand as the three foundational electrode components for supercapacitors. Carbon materials primarily store energy by accumulating charge on the electrode's surface, while the latter two, metal oxides and conducting polymers, rely on Faradaic reactions for their energy storage mechanisms (Adoor et al. 2023). While transition-metal oxides and conducting polymers can yield a considerable specific capacitance, their practical application in supercapacitors is hindered by their high cost, limited voltage operating range (<1.0 V), and relatively short cycling lifespan (Anil Kumar et al. 2020; Kim et al. 2021). Carbon materials exhibit several advantageous qualities, including robust structural stability, extensively developed porosity, customizable surface chemistry, and cost-effectiveness. Consequently, they have emerged as the leading and most promising choice in the field of energy technology.

1.2.2 Types of supercapacitors

The fundamental concept behind a supercapacitor's functionality lies in its capacity to store energy by effectively managing the distribution of ions derived from the electrolyte across the surface area of its electrodes. Supercapacitors are categorized into three classes according to their energy storage mechanisms: electrochemical double-layer capacitors, pseudocapacitors, and hybrid supercapacitors. Electrochemical double-layer capacitors (EDLCs) are comprised of a duo of carbon-based materials functioning as electrodes, alongside an electrolyte and a separator. The distinctive feature of EDLCs lies in their ability to store charge via electrostatic means or through a non-Faradic process, wherein no transfer of charge occurs between the electrode and the electrolyte (Forouzandeh et al. 2020). The application of voltage leads to the accumulation of charge on the surfaces of the electrodes. This charge differential creates an attractive force between opposite charges, prompting ions in the electrolyte to diffuse across the separator and into the pores of the electrode bearing the opposite charge. When a charged object is introduced into an electrolyte, it triggers the formation of an electric double-layer structure. This occurs as the counter charge required to balance the charged surface congregates within the electrolyte, particularly in close proximity to the surface itself (Shin et al. 2022). Numerous theories and models have been proposed to elucidate the intricacies of this interface between an electrode and an electrolyte medium. The storage mechanism inherent in EDLCs enables remarkably rapid energy absorption, release, and enhanced power capabilities. This is achieved without any chemical reactions occurring, thanks to the non-Faradic process, which effectively eliminates the swelling often observed in active materials within batteries during both charging and discharging phases (Tundwal et al. 2024). Nonetheless, the electrostatic surface charging mechanism inherent in EDLC devices imposes constraints on their energy density, prompting current research efforts to focus on enhancing energy performance and expanding the temperature range beyond the limitations of conventional batteries. The performance of EDLCs can be tailored by selecting the appropriate electrolyte, thus offering avenues for modulation and optimization (Otgonbayar et al. 2023).

In contrast to EDLCs, which primarily store charge electrostatically, pseudocapacitors utilize a Faradic process for charge storage. This process entails the transfer of charge between the electrode and the electrolyte, distinguishing it from the purely electrostatic charge storage mechanism employed by EDLCs. The application of potential to a pseudocapacitor triggers reduction and oxidation reactions on the electrode material. This process involves the passage of charge across the double layer, facilitating the flow of Faradic current through the supercapacitor cell (Pavithra et al. 2024). The Faradic process inherent in pseudocapacitors enables them to achieve higher specific capacitance and energy densities compared to EDLCs. Materials such as metal oxides and conducting polymers are examples that have garnered interest in pseudocapacitors. However, owing to their Faradic nature, they undergo reduction-oxidation reactions similar to those observed in batteries, resulting in issues such as instability during cycling and lower power density (Liu et al. 2020b).

EDLCs are known for their excellent cyclic stability and robust power performance, whereas pseudocapacitors excel in providing higher specific capacitance. The hybrid system combines the strengths of both EDLCs and pseudocapacitors by integrating a battery-like electrode for energy storage with a capacitor-like electrode for power delivery within the same cell. By selecting the appropriate combination of electrodes, it becomes feasible to elevate the cell voltage, consequently resulting in enhancements to both energy and power densities (Sadavar et al. 2023). Presently, researchers are directing their attention towards three distinct categories of hybrid supercapacitors, characterized by their electrode configurations. Composite electrodes consist of carbon-based materials with either metal oxides or conducting polymers into a singular electrode, thereby endowing it with both physical and chemical charge storage mechanisms. Carbon-based materials provide a capacitive double layer of charge and possess a high specific surface area, facilitating enhanced contact between pseudocapacitive materials and the electrolyte. This interaction enables the pseudocapacitive material to undergo Faradaic reactions, thereby increasing the capacitance within the composite electrode (Tundwal et al. 2024). Asymmetric hybrids integrate both Faradic and non-Faradic processes by pairing an EDLC with a pseudo-type electrode. In this configuration, the carbon material typically serves as the negative

electrode, while either a conducting polymer or metal oxide functions as the positive electrode (Mohd Abdah et al. 2020).

1.2.3 Components of the supercapacitor

The proper selection of electrolyte, electrode material, current collector, and separator plays a crucial role in determining the overall performance of a supercapacitor. Each component contributes significantly to factors such as energy storage capacity, power density, cycling stability, and overall efficiency of the device (Lakshmi and Vedhanarayanan 2023). Commonly utilized electrode materials in supercapacitors encompass a diverse range, including carbon nanotubes, graphene, activated carbon, conducting polymers, transition metal oxides/sulfides, metal-organic frameworks, and covalent organic frameworks etc. Since this thesis concentrates on biomass-derived carbon materials, table 1.1 presents various environmental and agro-wastes derived carbon materials for supercapacitors. The electrolyte, comprising the salt and solvent, stands as a crucial component in electrochemical supercapacitors. It exerts a significant influence on the formation of the double-layer and the accessibility of pores to electrolyte ions within the system. Electrolytes directly influence both the operating potential window and the resistance of the cell. The energy density is intricately linked to the square of the potential window, while the ionic resistivity inversely affects the power capability of the cell. Consequently, selecting the optimal electrolyte is paramount for achieving high performance characteristics (Pal et al. 2019). A variety of electrolyte types can be employed in supercapacitors, including aqueous electrolytes, organic electrolytes, redox additive electrolytes, and ionic liquids. Separators serve the crucial function of preventing contact and electron transfer between two electrodes in a supercapacitor. It is essential for a separator to possess mechanical strength to ensure device reliability and prevent migration of active materials over time. Low-quality separators can significantly diminish the overall performance of the cell by introducing additional resistance. Therefore, careful selection of a separator is a critical step in the cell formation process (Shulga et al. 2014). The current collector serves the dual function of transporting current from the current source to the electrode and from the electrode to the external load. Additionally, it plays a secondary role in dissipating heat generated within the cell. As a consequence, current collectors must possess electronic

conductivity and durability within the cell environment, capable of withstanding potential chemical degradation caused by electrolytes (Sharma and Chand 2023).

1.2.4 Performance evaluation of supercapacitor

The key performance parameters of a supercapacitor are typically assessed using three primary electrochemical techniques: cyclic voltammetry (CV), Galvanostatic Charge/Discharge (GCD), and Electrochemical Impedance Spectroscopy (EIS). An electrochemical workstation is employed for conducting all these techniques to quantify key factors such as current, voltage, equivalent series resistance, time, and capacitance in both two or three-electrode configurations. The gravimetric specific capacitances (C, F/g) of the cell and single electrode in the two-electrode symmetrical system, energy density (E, Wh/kg), and power density (P, W/kg) can be determined using the galvanostatic charge/discharge (GCD) results. They are calculated respectively using the following equation (Yang et al. 2022a);

$$C_{cell} = \frac{2I \times \Delta t}{m \times \Delta V} \text{ and } C_{electrode} = \frac{4 \times I \times \Delta t}{m \times \Delta V}$$

$$E = \frac{C \times (\Delta V)^2}{2 \times 4 \times 3.6} ; P = \frac{3600 \times E}{\Delta t}$$

In the provided equations, I (A) represents the constant discharge current, Δt (s) signifies the discharge time, m (g) stands for the mass of active material, and ΔV (V) corresponds to the potential change excluding the ohmic drop.

Table 1.1 *Biomass precursor materials and electrochemical performance.*

Precursor	**Activation agent**	**Electrolyte**	**Current Density (Ag^{-1})**	**Specific capacitance (Fg^{-1})**	**Ref.**
Sakura flower	KOH	6M KOH	0.2	265.8	(Ma et al. 2019)
Peanut shell	$ZnCl_2$	1M H_2SO_4	1.0	340	(Xiao 2018)
Rice husk	H_3PO_4	6M KOH	0.05	176	(Wu et al. 2015)
Potato waste	$ZnCl_2$	6M KOH	10	192	(Ma et al. 2015)
Tea leaves	KOH	2M KOH	1.0	330	(Peng et al. 2013)

Banana fibres	$ZnCl_2$	1M Na_2SO_4	0.02	74	(Niu et al. 2017)
Orange peel	KOH	1M H_2SO_4	1.0	460	(Subramani et al. 2017)
Jujube fruit	NaOH	6M KOH	1.0	460	(Yang et al. 2020)
Soyabean pods	NaOH	1M Na_2SO_4	0.5	352.6	(Kong et al. 2020)
Cashew nut shell	KOH	1M Na_2SO_4	1.0	214	(Merin et al. 2021)
Watermelon rind	KOH	6M KOH	1.0	333.4	(Mo et al. 2016)
Mangosteen peels	NaOH	6M KOH	1.0	357	(Yang et al. 2019)
Onion husk	K_2CO_3	1M $TEABF_4$/AC	1.0	188	(Wang et al. 2016)
Sugarcane bagasse	KOH	1M H_2SO_4	1.0	298	(Wang et al. 2018)
Tea waste buds	KOH	6M KOH	1.0	332	(Khan et al. 2020)

1.3 DENGUE BIOSENSORS

1.3.1 Introduction to dengue: A arboviral disease

One of the greatest threats to environmental health and society is the emergence of new human and plant pathogens. Human-pathogenic viruses continue to be a significant factor of disease and death worldwide, as shown by the COVID-19 pandemic, which was sparked by a coronavirus. Despite considerable efforts and recent significant advancements in public healthcare, reducing infectious disease mortality remains a difficult and crucial challenge. As a consequence, any recent or re-emerging contagious disease raises a threat to humanity's survival. More than any other epidemic mechanism, vector-borne viral illnesses create the most incredible damage to human civilization, producing minor to serious infections as well as eventual death. As a result, early detection of this virus is more important than ever to track the spread of viral diseases and save humanity from their negative impacts (Anusha et al. 2019).

Dengue is an arbovirus (viruses transmitted by arthropods) that belongs to the Flavivirus family and causes infectious disease, which raises a threat to humanity’s survival. The Flaviviridae family comprises more than 70 viruses in the genus,

including the West Nile virus, yellow fever virus, and encephalitis viruses like Tick-borne encephalitis virus, Japanese encephalitis virus, and St. Louis encephalitis virus. Many of them are known to cause serious and potentially lethal diseases in humans (Bessaud et al. 2006). In terms of global distribution, this Dengue virus has developed at an exponential rate over the last several decades. One of the most common re-emerging viral diseases is dengue fever. Numerous causes contribute to the present dengue outbreak, including a significant transition in the environment resulting from fast urbanization and high traffic conditions (Chakravarti et al. 2012). High population density, poor hygienic conditions in metropolitan areas, degradation of public health services, and a lack of efficient vector control programs in many nations are the most major macro factors responsible for this surge (Cafferata et al. 2013). The spread of dengue is strongly relying on the weather as well. Temperature rises of even one degree can result in significant increases in transmission potential. In areas with favorable temperatures, factors such as urban poverty and limited surveillance and control capabilities continue to be substantial promoters of dengue spread (Van Kleef et al. 2011). The virus's primary amplification host is humans. Female mosquitoes feed on the dengue virus that is present in the blood of viraemic people. The virus then enters the mosquito's midgut and travels throughout the body over 8 to 12 days. The virus can be transferred to other individuals through further probing or feeding after this extrinsic incubation period. Environmental factors, particularly the ambient temperature, impact the period of sporogony. The mosquito is thus infectious for the entirety of its life. The mosquitos Aedes aegypti are one of the most powerful transmitters for arboviruses. It is exceptionally anthropophilic, bites many times before finishing oogenesis, and thrives close to people (Bhattacharya et al. 2013; Halstead 2002; Rodenhuis-Zybert et al. 2010).

1.3.2 Physiology of the virus

RNA viruses have genomes made up entirely of RNA and do not require a DNA intermediary in their life cycle. This category includes both positive-sense and negative-sense viruses, as well as a wide range of human infections. The Flaviviridae viral family is comprised of four genera of enfolded viruses with a positive-sense single-stranded RNA genomic sequence. These are translated into a single lengthy

polyprotein, which host and viral proteases then process into discrete viral proteins (Ramage and Cherry 2015). The dengue virus is encapsulated, has a size of 50 nm in diameter, and comprises a positive-sense single-stranded RNA genome of nearly 11,000 nucleotides with only a single open reading frame, which encodes a single polyprotein precursor organized in the sequence of NH2-C-prM-E-NS1-NS2A-NS2B-NS3-NS4A-NS4B-NS5-COOH (Bessaud et al. 2006; Darwish et al. 2015).

The three structural proteins (C, prM, E) construct the entire infectious virus particle, also called a virion, due to a co-translational and post-translational modification. The C protein (Capsid protein) envelopes the viral genomic RNA to build the nucleocapsid. This nucleocapsid is surrounded by a lipid bilayer in which the viral pre-membrane protein (prM protein) and envelope protein (E proteins) are inserted. Seven non-structural proteins (NS1,NS2A,NS2B,NS3,NS4A,NS4B,NS5) are required for the viral replication, virion assembly, and evasion of the host immune response and are expressed in infected cells. Non-structural proteins are primarily found in the cytoplasm, where they generate replication products that aid in viral RNA production. DENV NS1, on the other hand, is generated in the endoplasmic reticulum as a hydrophilic membrane-associated homodimer. Since a mutation in the NS1 protein affects RNA synthesis, research of the 3-D structures of the NS1 protein and the viral NS1-NS2A protein catalytic domain will help to understand the configuration of the NS1 subunit and its role in viral pathogenesis. NS2B functions as a chaperone, assisting in folding the NS3 subunit into its active conformation. It is also involved in substrate-enzyme interactions and membrane attachment. DENV non-structural proteins NS3 and NS5, which have several functions and are engaged in enzymatic activities. NS4 is composed of two subunits: NS4A and NS4B. NS4A is engaged in intracellular membrane modulation and its C-terminal end aids in NS4B subunit translocation. However, the NS4B subunit's function is unclear, while new research suggests it may work as an interferon antagonist (Bhakat et al. 2014; Darwish et al. 2015).

Dengue infections were previously thought to be triggered by four antigenically discrete serotypes: Dengue Virus DENV-1, DENV-2, DENV-3, and DENV-4; However, in October 2013, a fifth version, DENV-5, was discovered. Each induces a distinct

immune response in the infected host (Mustafa et al. 2015). Since a person infected with one serologic form of dengue does not acquire immunity to another serotype, infection with other serotypes after the primary infection may cause serious illness. Although all serotypes have a short-term defense, immunity is type-specific after infection (Ashley 2011; Darwish et al. 2015). Any of the dengue virus serotypes can cause a wide range of symptoms and severity. The signs and symptoms of the disease might range from a mild, nonspecific febrile illness to more severe manifestations (Walia et al. 2020). Hence Dengue fever symptoms are sometimes confused with those of other common febrile infections, making early diagnosis extremely challenging.

1.3.3 Dengue diagnosis techniques

DENV infection may have no symptoms or symptoms that are similar to those of other viral infections. Hence, dengue infection is frequently diagnosed based on reported symptoms and physical examination, both of which are ineffective (Izuan Abdul Rashid and Azah Yusof 2018). Because of that, the development of accessible, cost-effective, accurate, quick, and early diagnostic procedures for identifying and detecting dengue diseases has progressed dramatically in recent years. DENV has been diagnosed using classic methods such as cell culture isolation, genomic detection, serological testing, and recently, biosensors and rapid approaches. In clinical circumstances, intact viral particles, viral nucleic acids, viral proteins, and antibodies produced by the patient's immunological response to the virus have been used as bioreceptors to detect dengue infections. Traditional methods such as polymerase chain reaction (PCR), viral culture, enzyme-linked immunosorbent assay (ELISA), and serological antibody detection techniques are used to identify these analytes. However, on the other hand, these conventional methods are sometimes unsuitable for on-the-spot examination as they have many disadvantages. Compared to traditional laboratory-based approaches, biosensors provide exciting alternatives to established diagnostic tests and create affordable, sensitive, quick, miniaturized, and portable platforms. A biosensor is an embedded receptor-transducer device that uses a biological recognition element to provide selected quantitative or semi-quantitative analytical data (Thevenot et al. 1999). In other words, biosensors are precise and sharp analytical tools containing a biological sensing component that can identify and quantify a wide range of biomolecules in a

small number of specific substances or biological samples. Which converts chemical or physical signals into electrical or optical signals that can be processed to determine analyte concentration. This efficiency sets them apart from other methods, enabling the generation of precise and sensitive results in a shorter timeframe.

Biosensors consist of 3 integral components: (a) biorecognition element responsible for target interaction, (b) the transducer/detector element that transforms the bio-signal into a understandable results/output, and (c) a signal processor that presents the signal pathway in a approachable manner (Ozsoz 2012). Among the array of biosensors, electrochemical biosensors stand out for their numerous advantages, including robustness, facile miniaturization, a lower limit of detection, adaptability to small analyte sizes, and the capability to be effectively employed in turbid fluids (Grieshaber et al. 2008). According to an IUPAC recommendation on the definition in 1999, “an electrochemical biosensor is a self-contained integrated device which is capable of providing specific quantitative or semi-quantitative analytical information using a biological recognition element (biochemical receptor) which is kept in direct spatial contact with an electrochemical transduction element” (Thevenot et al. 1999). Generally, an electrochemical biosensor measures changes in electrical properties (such as current, voltage, impedance, and capacitance) due to redox reactions or biomolecular interactions on the electrode surface. An electrochemical cell is used in these sensors to enhance chemical reactions by supplying electrical energy. A three-electrode system is the most commonly utilized electrode design, which comprises a working electrode, a reference electrode, and a counter electrode. In these typical biosensors, the design of the transducer's surface is given high priority in addition to immobilizing the biorecognition component and improving analyte identification. Cyclic voltammetry (CV) and differential pulse voltammetry (DPV) are two commonly used electroanalytical voltammetric techniques. The CV is a valuable method for determining information about the rate of the electrochemical reactions and the redox potential of the analyte, and the DPV is a helpful tool for measuring current variations as a function of voltage and determines the current just before every potential shift. Since this thesis concentrates on dengue NS1 biosensors, table 1.2 presents various reported materials and method of detection.

Table 1.2 *Sensing performance of dengue NS1 biosensors*

Materials	Detection method	Ref.
Polyaminophenol-imprinted films	Impedimetric	(Siqueira Silva et al. 2021)
SAMs composed of 16-MHDA	Impedimetric	(Cecchetto et al. 2017)
Phenylenediamine-indium tin oxide	Fluorescence	(Darwish et al. 2018)
SAM containing PEG-thiol	Impedimetric	(Santos et al. 2018)
Screen-printed gold electrodes	Electrochemical Lateral Flow	(Sinawang et al. 2016)
Gold electrodes modified with SAM	Impedimetric	(Bachour Junior et al. 2021)
Thin film of carbon nanotube-ethylenediamine	Differential pulse voltammetric	(Mendonça et al. 2021)
Screen-printed carbon electrode	Impedimetric	(Nawaz et al. 2018)

1.4 SCOPE AND OBJECTIVES OF THE WORK

The unprecedented global expansion of the population has given rise to a substantial and unconventional surge in worldwide progress. Consequently, the escalating demands associated with this growth are contributing to a surge in the generation of diverse types of waste materials on a daily basis. In addition to this, the depletion of fossil fuels, environmental contamination, and the emission of greenhouse gases have precipitated substantial health risks and disruptions within ecosystems. As a response, scientists are increasingly investigating environmentally friendly and sustainable systems. Therefore, recent studies focusing on the production of activated porous carbon from environmental waste and its utilization across various applications have garnered significant scientific interest. Simultaneously, the development of new carbon

materials with broad applications must align with industrial demands, including considerations for environmental sustainability, cost-effective or straightforward production methods, and the introduction of improved or even innovative desired characteristics. Alongside their remarkable chemical and thermal stability, the heightened surface area, adjustable porosity, and diverse pore sizes of these activated or porous carbons have notably piqued interest. These criteria are met by porous activated carbons derived from cost-effective environmental waste precursors, especially biomass.

Based on this perspective and the literature studies, the present research focuses on utilizing biomass-derived high-surface porous carbon for energy and sensing applications. Specifically, it investigates their potential in supercapacitors for energy storage and electrochemical dengue sensors for disease detection. The study aimed to contribute to the development of sustainable energy solutions and improved healthcare diagnostics through interdisciplinary efforts at the intersection of materials science, electrochemistry, and biomedical science.

The following objectives have been proposed for the present research.

1. To synthesize high-surface porous carbon materials from biomass-derived precursors, with a focus on enhancing surface area, porosity, and structural features.
2. To systematically characterize the synthesized high-surface porous carbon materials using advanced techniques such as BET, FESEM, TEM, XRD, FTIR, and Raman spectroscopy to evaluate their structural, morphological, and chemical properties.
3. To explore the electrochemical properties of synthesized high-surface porous carbon materials for potential energy storage application explicitly focusing on supercapacitor.
4. To evaluate the sensing capabilities of the synthesized high-surface porous carbon materials, particularly in detection of the dengue NS1 protein, through comprehensive electrochemical performance evaluations.

****

CHAPTER 2

SYNTHESIS AND CHARACTERIZATION OF *TECTONA GRANDIS* SAWDUST-DERIVED POROUS GRAPHITIC CARBON FOR HIGH-PERFORMANCE SUPERCAPACITOR

Abstract: This chapter highlights the potential of utilizing *Tectona grandis* sawdust-derived high-surface carbon for supercapacitor applications. It demonstrates the feasibility of converting this waste material into efficient porous carbon materials with substantial graphitization and porosity.

2.1 INTRODUCTION

Over the last few decades, the depletion of fossil fuels, environmental contamination, and the release of greenhouse gases has led to significant health risks and disruptions in ecosystems. As a response, researchers are increasingly investigating environmentally friendly and sustainable systems for energy storage and conversion(Mascarenhas et al. 2023; Pramitha et al. 2023). Renewable energy sources are being integrated into the energy sector, aiming to mitigate environmental pollution by reducing reliance on traditional, fossil fuel-based power methods (Dini et al. 2022). Hence, there has been a growing fascination with nanomaterials due to their electrochemical characteristics, cost-effectiveness, simplicity in production, extensive surface area, and improved electrical as well as magnetic behaviour (Wang et al. 2019, 2022b). In particular, porous activated carbons derived from organic waste have emerged as a significant and innovative concept. This is primarily attributed to their widespread applications in eco-friendly electrochemical sensors, fuel cells, solar cells, catalysis, and energy storage devices such as batteries and supercapacitors (Zhang et al. 2023a). Furthermore, these carbon materials are cost-effective, environmentally friendly, easily accessible, possess high carbon content, exhibit excellent electrical conductivity, and showcase remarkable physicochemical properties (Yin et al. 2023). Specifically, the distinctive crystal structure found in carbon materials derived from

biomass plays a crucial role in facilitating the swift movement of electrolyte ions within electrodes. This characteristic renders them highly promising materials for use as electrodes in supercapacitors (Shaker et al. 2021).

Numerous comprehensive studies have showcased the viability of carbonaceous materials derived from biomass as a competitive and advantageous resource for applications in supercapacitor electrodes and as potential sources of efficient electrochemical power (Wang et al. 2022c). This interest arises from its remarkable attributes, such as high power density, enhanced operational safety, and extended cycle lifespan, which have led to extensive research and exploration in this area (Qiu et al. 2019). Out of all the carbonaceous materials derived from biowaste, activated carbon produced from a lignocellulosic source stands out as the preferred choice. This is due to its expansive specific surface area, adjustable pore structure, notable chemical stability, and favourable electrical conductivity (Peng et al. 2013; Zhang et al. 2017). However, there is a need to further investigate readily available biomass sources, and there is still significant potential for enhancing the preparation strategies. Simultaneously, a comprehensive understanding of the origins and mechanisms underlying this activity remains to be seen. Therefore, further efforts are required to develop straightforward techniques that utilize cost-effective biomass precursors. This will result in the creation of durable electrode materials suitable for energy-related applications (Zhang et al. 2022).

The production of biomass-derived carbon through the conventional method of direct pyrolysis involves three main stages. Initially, at temperatures near 100°C, rapid weight reduction occurs, which can be attributed to water evaporation. Subsequently, within the temperature range of 315 °C to 400 °C, a significant amount of gases is generated, concurrent with the development of the fundamental carbon framework. As the temperature continues to rise, the organic components within biomass cells undergo transformation, leading to the creation of conjugated carbon atoms and forming a char structure (Zhang et al. 2019, 2022). Furthermore, the creation of carbon with sp^2 hybridization and the generation of gases during this process can contribute to enhancing conductivity and the development of a porous framework (He et al. 2019). These effects can be advantageous for utilizing these materials in electrochemical

applications. Nevertheless, the direct carbonization/pyrolysis approach faces challenges in producing carbon materials with inherent porosity and a substantial surface area. Typically, activation processes are necessary for the products to acquire these desired characteristics (Hegde and Bhat 2023). In the process of preparing activated carbon, commonly employed activating agents include steam, CO_2, $ZnCl_2$, H_3PO_4, K_2CO_3, and KOH (Prauchner et al. 2016; Shoaib and Al-Swaidan 2015). Among these options, KOH holds a distinct advantage. This is because its utilization induces more localized reactions with the precursor material, resulting in the creation of higher porosity in the resulting activated carbon (Jain and Tripathi 2014; Lillo-Ródenas et al. 2003).

This study presents a straightforward, inexpensive, and uncomplicated approach to creating porous carbon, referred to as TPC, using Teak sawdust as the starting biomass. This process involves treating the biomass with $FeCl_3$ for carbonization, followed by KOH activation at varying temperatures. This treatment results in the formation of high surface area porous carbons. The study demonstrates that the TPC-850 variant displays remarkable porous and surface properties, high specific capacitance, excellent cyclic stability, and impressive performance when used in a 6.0 M KOH system. As a result, this uncomplicated technique holds significant promise for transforming organic waste into porous, graphitic carbon materials, with substantial potential for applications in sustainable and renewable energy technologies.

2.2 MATERIALS AND METHODS

2.2.1 Materials

KOH pellets, $FeCl_3$, and HCl were obtained from Loba Chemie. Absolute ethanol was sourced from Changshu Hongsheng Fine Chemicals. N-Methyl-2-pyrrolidone (NMP) and poly(vinylidene fluoride) (PVDF) were acquired from Sigma-Aldrich, and TIMCAL C-NERGY SUPER C65 was purchased; all chemicals were used as received. Type 1 ultrapure water was used throughout the experiments to prepare all the solutions. *Tectona grandis* (Teak) sawdust was collected from Beerangod, Honnavara, Uttarakannada, Karnataka, and employed as the precursor material for producing *Tectona grandis* sawdust-derived porous carbon (TPC).

2.2.2 Synthesis of TPC

Tectona grandis sawdust was sun-dried for a week and ground into a powder. It was then thoroughly washed multiple times with ultrapure water, followed by ethanol, and subsequently dried in an oven before being pulverized. The carbonization of pulverized sawdust was done in the first step, followed by chemical activation in the second step. In the first step, pulverized sawdust was mixed in a 1:1 ratio with $FeCl_3$ in the minimum amount of ultrapure water and continuously stirred on a hotplate until it became a solid paste, and then it was placed in a hot air oven at 110 °C for about 24-48 h. Then it was carbonized in an argon gas environment at 400 °C for 1.5 h. In the second step, the carbonized sample was mixed with 10 g of KOH (in a ratio of 1:1 based on the initial weight of biomass used) in ultrapure water with continuous stirring on a hotplate to make it a solid paste, and then it was dried in a hot air oven at about 110 °C for 24–48 h. It was pyrolyzed at various temperatures, including 650 ºC, 750 ºC, and 850 ºC for 90 minutes in a continuous argon environment at the rapid heating rate in a tube furnace to determine the optimal activation temperature. To effectively eliminate residual $FeCl_3$, KOH, and inherent ash minerals, the carbonized samples were immersed in a diluted HCl solution and then rinsed with deionized water until achieving a neutral pH. Finally, ethanol treatment was administered, followed by centrifugation. Before analysing their morphological and electrochemical characteristics, the resulting products TPC-X (denoted as TPC-650, TPC-750, and TPC-850, respectively) were dried at about 110 °C for 24–48 h.

2.2.3 Characterizations

X-ray diffraction (XRD) studies of the synthesized samples were carried out using monochromatic Cu-Kα radiation of a wavelength of 0.154 nm on Malvern PANalytical (Empyrean 3rd Gen, Netherlands) instrument. Raman analysis was done using Compact Raman Spectrometer (Renishaw, UK). FTIR spectrum was recorded by Spectrum Two FT-IR Spectrometer (PerkinElmer, Singapore) in the spectral range of 500-4000 cm^{-1}. The energy dispersive X-ray (EDX) analysis and the field emission scanning electron microscopy (FESEM) images were taken by Carl Zeiss (Germany) instrument. The specific surface area, pore characteristics of the synthesized materials and N_2 adsorption-desorption studies were carried out using an Autosorb (Anton Paar IQ-XR-

XR, Austria) instrument. Before the BET measurement, samples were degassed at 300 ºC in a vacuum for three hours.

2.2.4 Electrode preparation and electrochemical studies

The working electrodes were prepared by drop-casting the NMP solvent-based mixture of 80% TPC, 10% C-NERGY SUPER C65 and 10% PVDF binders on a 1×1 cm^2 grafoil sheet. The mass loading of the active material on the electrode was about 3.0 mg/cm^2. These electrodes were dried in a vacuum oven at 60 °C for overnight. All the electrochemical measurements were carried out in two symmetric electrode system on an electrochemical workstation (Autolab) using a 6 M KOH electrolyte at room temperature. The cyclic voltammetry (CV) and galvanostatic charge-discharge (GCD) measurements were carried out in the potential range from -1 V to 0 V at various scan rates ranging from 10 mV/s to 200 mV/s and current densities ranging from 0.5 to 6 A/g, respectively. The electrochemical impedance spectroscopy (EIS) measurements were carried out in the 10 mHz – 100 kHz range with an amplitude of 10 mV.

2.3 RESULTS AND DISCUSSIONS

2.3.1 Structural and morphological analysis

Powder XRD patterns of TPC-X (650-850 °C) are shown in figure 2.1a. All TPC-X exhibited two characteristic diffraction peaks at 2θ angles of ~26.4° and ~43.5°, which can be attributed to the graphitic carbon planes of (002) and (100). Based on Bragg's law equation ($n\lambda = 2d\sin\theta$), the value of d spacing, or interplanar spacing between 002 planes, was found to be 0.34 nm, explaining the presence of turbostratic carbon structure. TPC-650 showed weak, broadened diffraction peaks at low-angle regions suggesting disordered carbon layer structures. But in the same region, both TPC-750 and TPC-850 showed sharp peaks, which indicate a decrease in the amorphous carbon or an increase in the crystalline structure. Furthermore, the intensity of the peak raised from TPC-750 to TPC-850 samples suggests more development of the orderliness of the carbon layers or graphitic structure at higher temperatures. Further, this improvement in graphitization can be supported by Raman analysis. Figure 2.1b depicts the Raman spectra of KOH-activated TPCs.

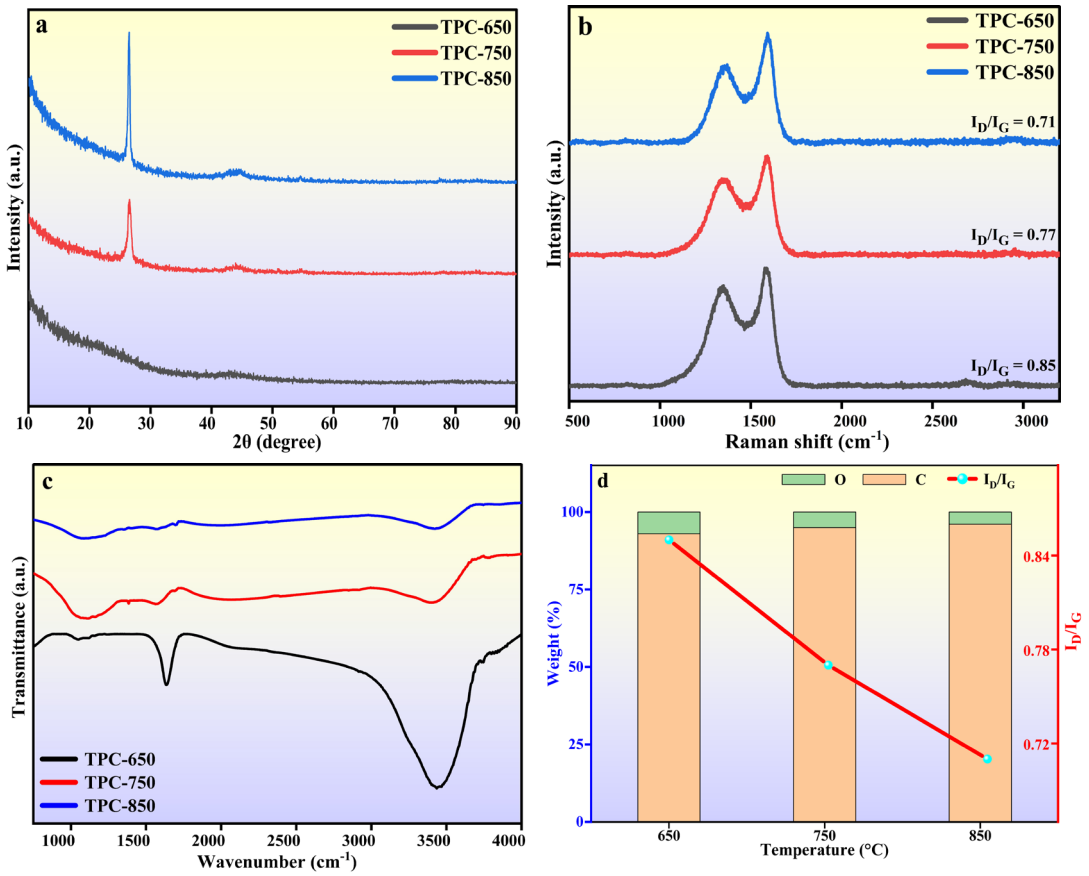

Figure 2.1 *(a) XRD patterns; (b) Raman spectra; and (c) FTIR spectra of TPC-650, TPC-750, and TPC-850 (d) Effect of temperature on elemental weight % and Raman intensity ratio.*

Generally, biomass-derived carbon shows two prominent peaks that are visible in the graph, i.e., the disordered (D) carbon at ~1369 cm^{-1}, which corresponds to the sp^3 defect sites, and the peak positioned at ~1591 cm^{-1} is assigned to the ordered graphitic (G) carbon, correlated to the carbon layer with sp^2 hybridization (Veerakumar et al. 2023). In order to assess the degree of disorder within carbon structures, the intensity ratio of the two bands (I_D/I_G) is frequently used. TPC-850 showed intensity ratios of 0.71, which is considerably lower than those for TPC-750 (0.77) and TPC-650 (0.85). Therefore, the higher I_D/I_G ratio value demonstrates a higher degree of disorder in the carbon structure and the existence of more defects in its framework. The intensity ratio of the D/G band has dropped with the rise in activation temperature from 650 to 850 °C. The TPC-850 displayed the lowest proportion of D/G band intensity because the growth in

crystalline carbon and improved carbon layer stacking occurred at higher temperatures than lower ones (Xu et al. 2021). Figure 2.1d portrays the relation between the graphitization temperature and the I_D/I_G values. In order to further investigate the functional groups present in TPC-X samples, the FT-IR spectroscopic technique was used, as shown in figure 2.1c. For the TPC-650 sample, a broad, strong peak around 3435 cm^{-1} was observed related to the stretching vibrations of the O-H functional moieties. The observed peaks at ~1635 and ~1050 cm^{-1} are due to C=C and C−O stretching vibrations, respectively. As the activation temperature of TPC increases from 650 to 850°C, the peak area diminishes due to the chemical transformation. These could have occurred as a result of the loss and breaking of functional groups in TPC-X.

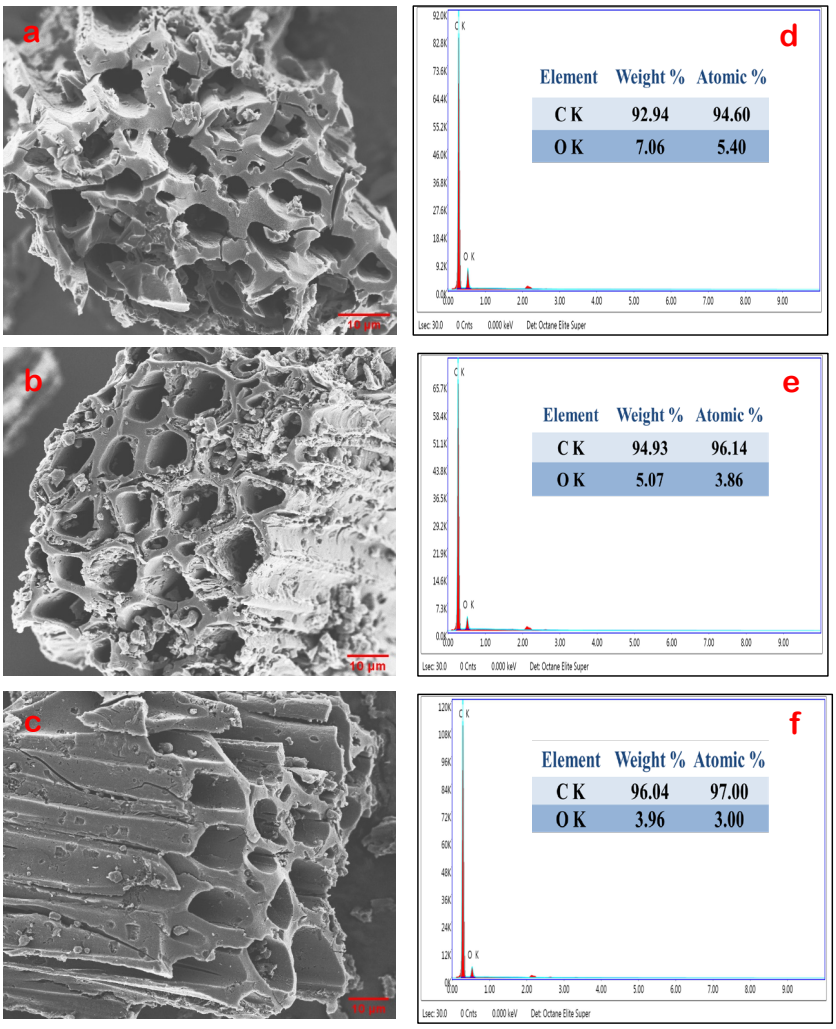

Figure 2.2 *FESEM images (a) TPC-650, (b) TPC-750, (c) TPC-850 and EDX results of (d) TPC-650, (e) TPC-750, (f) TPC-850.*

The surface morphological characteristics of TPC-X were examined using FESEM analysis. In figure 2.2(a-c), the FESEM images reveal the presence of a porous structure throughout the sample, likely responsible for the increase in surface area of the TPC-X samples. Compared to other TPC, the TPC-850 sample stands out due to its copious mesoporous structures and high surface area. Notably, a significant increase in porosity was observed after raising the activation temperature. The presence of numerous interconnected, hollow tube-like porous networks within the carbon texture, varying in dimensions by a few micrometers, indicates their potential suitability for energy storage applications. From the (figure 2.2 d-f) energy dispersive X-ray spectroscopic analysis, the carbon percentage in the TPC samples increased significantly from 92.94% to 96.04% as the pyrolysis temperature rose from 650 °C to 850 °C. Simultaneously, the oxygen percentage decreased from 7.06% to 3.96%, which could likely be due to the breaking down of oxygenated functional groups present in the sample. Hence, it was observed that the pyrolysis temperature notably impacted the oxygen-carbon (O/C) ratios of the TPC samples, leading to a decrease in the ratio from 0.08 to 0.04 as the temperature increased.

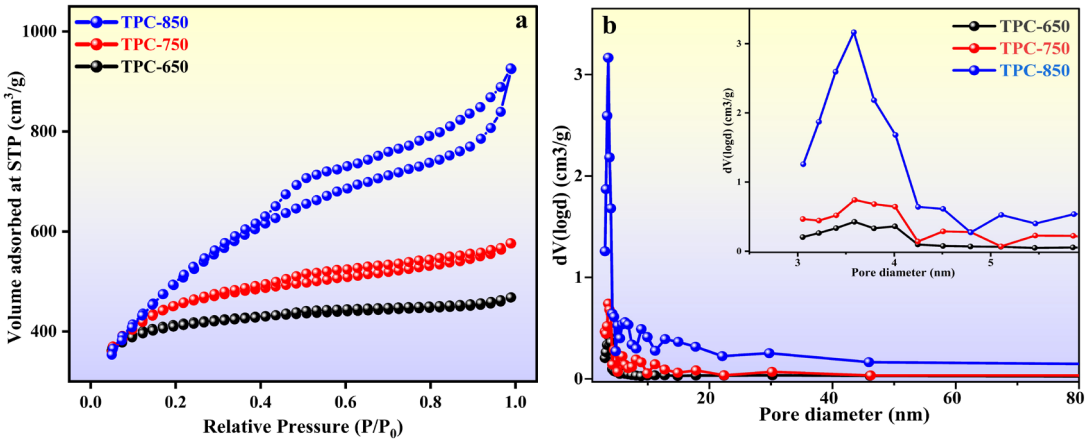

Figure 2.3 *(a) N2 adsorption-desorption isotherms; (b) Pore size distribution curves*

Along with its structural and morphological features, the specific surface area, mean pore diameter, and total pore volume of the activated carbon are also crucial aspects of the energy storage performance of the supercapacitor. In order to investigate the pore structure and specific surface area of TPC-X, N_2 adsorption-desorption measurements

were carried out, as shown in figure 2.3*a*. At a relative pressure of ~ 0.43 to ~ 0.9 (P/P_0), the adsorption curve of TPC-850 has a smooth upward slope, displaying type IV adsorption for hysteresis (Yang et al. 2022a). This adsorption curve demonstrated that the material has a significant quantity of pores and a particular level of mesoporosity. The specific surface areas of TPC-650, TPC-750, and TPC-850 were determined to be 1296, 1466, and 1768 m^2/g, with corresponding pore volumes (at P/P0 = 0.99) of 0.72, 0.89, and 1.43 cm^3/g, respectively. The activation temperature has an impact on the porosity distribution of the TPC materials, as evidenced by the pore-size distribution (figure 2.3b) that was determined from the BJH method. The average pore diameters of TPC-X (X = 650, 750, and 850) were found to be 3.587, 3.589, and 3.582 nm, respectively. Based on the data in table 2.1 and figure 2.3c, it is clear that the TPC-850 sample has high SSAs, pore volumes, and superior textural characteristics when compared to TPC-650 and TPC-750. Additionally, with the substantial porosity of TPC-850 and its significant graphitization level, it has been estimated to offer many active sites for quick ion mobility and considerably improved ionic conductivity. All these results suggest that the TPC-850 sample could be a better candidate for electrochemical energy storage applications.

Table 2.1 *Textural parameters of TPC-X*

Sample	**BET-SSA (m^2/g)**	**Total pore volume (cm^3/g) ***	**Mean pore diameter (nm)**
TPC-650	1296	0.72	3.587
TPC-750	1466	0.89	3.589
TPC-850	1768	1.43	3.582
*Total pore volumes were determined at $P/P_0 = 0.99$			

2.3.2 Electrochemical performance of electrodes

The results and analyses from different structural and morphological investigations showed that TPC-850 was the most suitable electrode material in all TPC-X samples due to its large BET surface area and well-organized mesoporous structure. TPC-650,

TPC-750, and TPC-850 were evaluated as supercapacitor electrodes in a two-electrode cell arrangement with an aqueous 6 M KOH solution functioning as the electrolyte.

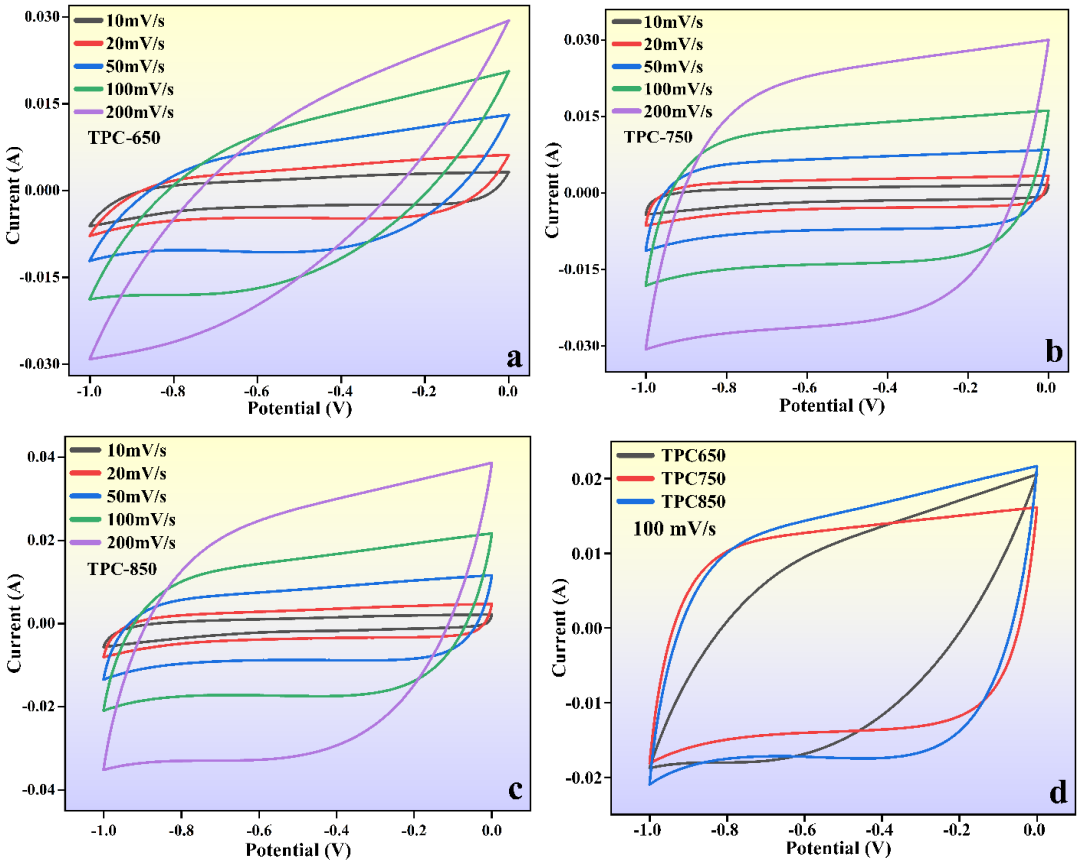

Figure 2.4 *CV curves of (a) TPC-650, (b) TPC-750, (c) TPC-850 at different scan rate (d) comparison CV graph at the scan rate of 100mV/s.*

The cyclic voltammograms of TPC-X electrodes were measured in the potential window of 0 to -1.0 V at a different sweep rate ranging from 10 mV/s to 200 mV/s, as shown in figure 2.4. Nearly square-shaped voltammograms were acquired for all the TPC-X samples during cyclic voltammetry (CV) investigations, demonstrating the typical capacitive electrode behaviour, even under elevated scan rates such as 200 mV/s. The area under the CV curve could be related to the capacitance of the electrode because the capacitance is a measure of the charge stored per unit voltage. The area under the CV curve of the TPC-850 (figure 2.4d) electrode is considerably greater than that of other TPC-X electrodes, which indicates that the TPC-850 electrode has a higher charge storage capacity and, consequently, a higher capacitance. Improved capacitive

performance could result from considerable levels of developed graphitic structure, a well-established pore arrangement, and an augmented surface area in TPC-850. According to the power law, the value of *b* for TPC-850 was calculated to be 1; hence, the charge storage process here is primarily capacitive in nature (specifically EDLC type). Using the Dunn method, capacitive currents were calculated, indicating that the behaviour of TPC-850 is approximately 98.27% EDLC.

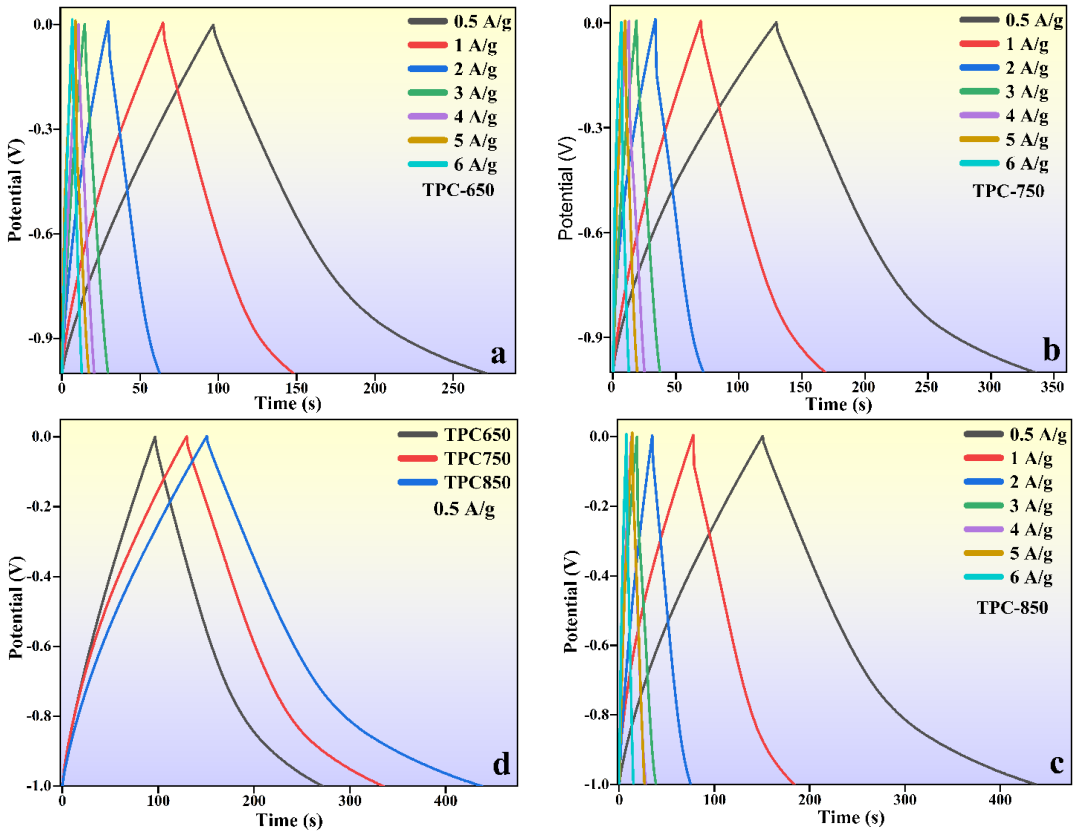

Figure 2.5 *GCD curves of (a) TPC-650, (b) TPC-750, (C) TPC-850 at different current densities (d) comparison GCD graph at the current density of 0.5A/g.*

Figure 2.5 displays the GCD curves of TPC-X-coated electrodes at different current densities varying from 0.5 to 6 A/g in 6 M KOH. The symmetrical shapes observed in all the charge and discharge curves indicate that the electrode material possesses notable electrochemical reversibility. The relatively balanced patterns found in the galvanostatic charge-discharge (GCD) graphs further support their resemblance to the behavior of double-layer capacitors. In all the cases, it was shown that the decrease in

current density has led to an increase in charge-discharge time. Decreased current density reduces the amount of current flowing through the electrode's surface area because, at lower current densities, the movement of ions might be limited by diffusion within the electrode and electrolyte (Dai et al. 2022). Hence, this could lead to slower GCD rates. But at the same time, the discharge time of the capacitor could depend on both its capacitance and the resistance of the circuit through which it is discharging. As depicted in figure 4.5d, the TPC-850 has the most prolonged discharge period compared to TPC-750 and TPC-650. When operating at a current density of 0.5 A/g, the calculated single electrode specific capacitance of TPC-850 was 572 F/g, higher than the 410 F/g of TPC-750 and the 348 F/g of TPC-650. The provided values demonstrate that the electrode, which was predicted to have enhanced electrical conductance due to improved graphitic alignment, could potentially yield advantages for its capacitance performance. Additionally, the existence of hierarchical porous structures in the carbon material may enhance EC behaviour by increasing the accessibility of the electrolyte ions through porous channels (Sesuk et al. 2019).

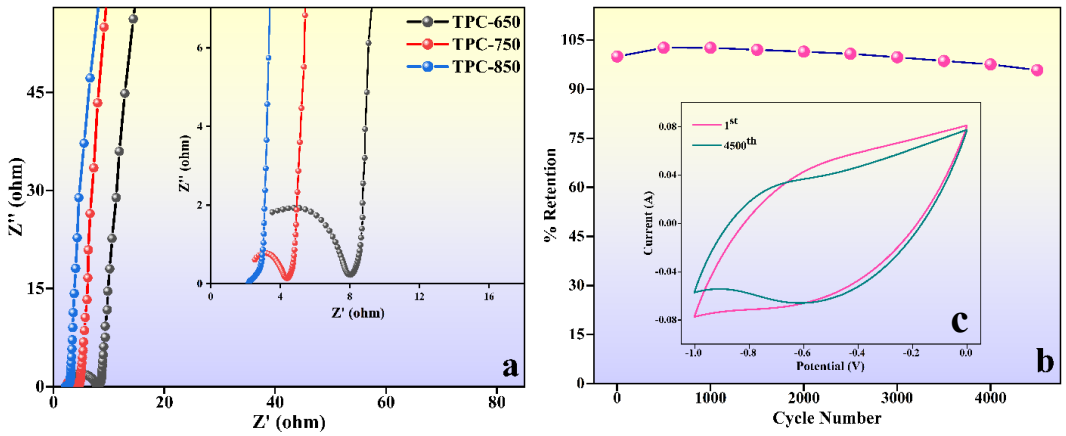

Figure 2.6 *(a) EIS graphs of TPC (b) Cyclic stability (c) 1st and 4500th CV cycle.*

The electrochemical impedance spectroscopy (EIS) measurements carried out in a solution of 6 M KOH, with a frequency range spanning from 10 mHz to 100 kHz, are presented in figure 2.6a. Significantly, the semicircle was situated in the region of higher frequencies, while the straight line appeared in the lower frequency range. These distinct components are essential elements of Nyquist plots, each holding its own significance. The diameter of the semicircle has a significant meaning that describes

the electrical conductivity of the electrodes. A smaller semicircle diameter indicates enhanced electron conductivity and improved capacitive properties (Veerakumar et al. 2023). When compared to TPC-750 and TPC-650, the TPC-850 electrode displays the smallest semicircle diameter in the high-frequency range and exhibits a steeper or more linear behaviour in the low-frequency region. These characteristics suggest reduced resistance, heightened ion diffusion, rapid migration, and favourable electrochemical double-layer capacitor (EDLC) traits. This improved electrochemical performance can be attributed to an increased level of graphitization, a high specific surface area (SSA), and a more structured porous structure (Liu et al. 2021; Tian et al. 2019). Subsequently, the study delved into the cyclic performance as depicted in figure 2.6b to evaluate the stability of the TPC-850 electrode, a crucial characteristic for energy storage devices such as supercapacitors. The TPC-850 supercapacitor electrode displayed impressive electrochemical cyclic stability, maintaining 95.83% of its initial capacity even after completing 4,500 cycles. Figure 2.6c illustrates the cyclic voltammetry (CV) curves for both the 1st and 4,500th cycles of the TPC-850 electrode at a scan rate of 500 mV/s in a 6.0 M KOH solution. Consequently, the TPC-based supercapacitor demonstrates its potential suitability for utilization in extensive industrial applications in the future.

2.4 CONCLUSIONS

This study offers a promising approach to repurposing agricultural waste biomass into valuable porous carbon materials with potential applications in energy storage. In summary, *Tectona grandis* sawdust, as agricultural residue, was effectively converted into new porous carbons using an easy and relatively inexpensive KOH activation method. This method was carried out at carbonization temperatures ranging from 650 to 850 °C. The FESEM analysis reveals the presence of enormous hollow tube-like porous networks in the TPC samples. BET analysis showed a specific surface area of 1768 m^2/g and corresponding pore volumes (at $P/P_0 = 0.99$) of 1.43 cm^3/g for TPC-850. With these unique properties, TPCs demonstrated an excellent electrochemical energy storage capacity with a high specific capacitance (572 F/g at 0.5 A/g) at a potential range of 0 to -1.0 V in a 6.0 M KOH solution. Significantly, TPC-850 demonstrated remarkable electrochemical cyclic stability, retaining 95.83% of its initial capacity even

after undergoing 4,500 cycles at a scan rate of 500 mV/s. It suggests that our study opens up the possibility of synthesizing activated carbon produced from waste biomass with a significant level of graphitization, abundant hierarchical porous structure, and excellent pore volume, thereby opening the door to its use in energy storage. Consequently, this study showcases an effective approach to managing waste biomass resources into an environmentally favourable production of energy storage devices. It also offers significant potential for the widespread utilization of advanced renewable energy solutions on a larger scale. However, further optimization may be required to adapt it for a large-scale industrial approach.

****

CHAPTER 3

SYNTHESIS AND CHARACTERIZATION OF *MANGIFERA INDICA* LEAF-DERIVED ACTIVATED CARBON FOR LONG-LIFE, HIGH-PERFORMANCE SUPERCAPACITORS

Abstract: This chapter describes the investigation of *Mangifera indica* leaf waste-derived activated carbon as an electrode material for long-life, high-performance supercapacitors. The study provides a promising route for utilizing waste biomass as a low-cost, sustainable electrode material.

3.1 INTRODUCTION

The overuse and exploitation of fossil fuels such as coal and oil have presented contemporary civilization with a mounting array of critical energy challenges and environmental degradation (Kreps 2020; Ramos et al. 2022). As a result, the majority of nations worldwide have implemented dual-carbon policies, which involve concerted efforts to foster the creation and utilization of green, renewable resources. This approach aims to tackle the aforementioned challenges while sustaining rapid economic development (Jiang et al. 2022). Recent studies focusing on the production of activated porous carbon from environmental waste and its utilization across various applications have garnered significant scientific interest (Balahmar et al. 2017). Simultaneously, the development of new carbon materials with broad applications must align with industrial demands, including considerations for environmental sustainability, cost-effective or straightforward production methods, and the introduction of improved or even innovative desired characteristics (Hegde and Bhat 2024b; Mascarenhas et al. 2023). Alongside their remarkable chemical and thermal stability, the heightened surface area, adjustable porosity, and diverse pore sizes of these activated or porous carbons have notably piqued interest (Serafin et al. 2019). These criteria are met by porous activated carbons derived from cost-effective environmental waste precursors, especially biomass. Most significantly, biomass is ideally suited for the preparation of carbon

electrode materials for energy storage devices like supercapacitors due to its extremely high percentage of carbon content and unique physiochemical properties (Bi et al. 2019).

Carbon materials possess key characteristics such as electrical conductivity, low electrical resistance, a substantial specific surface area, and the ability to physically adsorb a significant amount of charges onto their surface. As a result, supercapacitors constructed from carbon-based materials often exhibit favourable attributes, including a high specific capacitance, prolonged lifespan, and outstanding performance stability (Wang et al. 2022a). However, carbon nanotubes, graphene materials, and fullerene stand out as highly esteemed carbon-based electrode materials. Still, their intricate synthetic processes and high manufacturing costs often render them unsuitable for widespread commercial adoption (Zhang et al. 2023b). Due to their straightforward synthesis, cost-effectiveness, adaptable pore structures, and exceptional chemical and thermal stability, porous activated carbon materials exhibit immense potential in this regard (Serafin et al. 2019). Food wastes, municipal solid wastes, agricultural and animal wastes, along with other environmental waste sources, have been extensively utilized in the production of porous activated carbon via carbonization and activation processes. The properties of these porous activated carbons can be tailored by manipulating parameters such as the activator/carbon precursor ratio, activation pyrolysis temperature, and the choice of activating agents, such as $ZnCl_2$, $FeCl_3$, H_3PO_4, K_2CO_3, KOH, etc (Hegde and Bhat 2023). Here, dead *Mangifera indica* leaves waste was employed as the feedstock, and porous activated carbon was synthesized using a two-step process with changing temperatures. XRD, Raman spectroscopy, FTIR, FESEM, EDX, TEM, XPS, and BET investigations have been used to study the different physicochemical aspects of the produced material. Finally, the electrochemical performance of synthesized activated carbon materials was assessed as electrodes for the supercapacitors.

3.2 MATERIALS AND METHODS

3.2.1 Materials

KOH pellets, $FeCl_3$, and HCl were purchased from Loba Chemie. Absolute ethanol was purchased from Changshu Hongsheng Fine Chemicals, N-Methyl-2-pyrrolidone (NMP), and Poly(vinylidene fluoride) (PVDF) were purchased from Sigma-Aldrich, grafoil sheets, TIMCAL C-NERGY SUPER C65 were purchased and were used as-received. Type 1 ultrapure water (Elga Veolia) was used throughout the experiments to prepare all the solutions. Dead *Mangifera indica* leaves (DML) was collected near Beerangod, Honnavara, Uttarakannada, Karnataka and used as a precursor material to prepare *Mangifera indica* leaves-derived activated carbon (MLAC).

3.2.2 Synthesis of MLAC

Dead *Mangifera indica* leaves (DML) was sun-dried for a week and ground into a powder. It was then thoroughly washed multiple times with ultrapure water, followed by ethanol, and subsequently dried in an oven before being pulverized. The carbonization of pulverized DML was done in the first step, followed by chemical activation in the second step. In the first step, pulverized DML was mixed in a 1:1 ratio with $FeCl_3$ in the minimum amount of ultrapure water and continuously stirred on a hotplate until it became a solid paste, and then it was placed in a hot air oven at 110 °C for about 24-48 h. Then it was carbonized in an argon gas environment at 400 °C for 1.5 h. In the second step, the carbonized sample was mixed with 10 g of KOH in ultrapure water with continuous stirring on a hotplate to make it a solid paste, and then it was dried in a hot air oven at about 110 °C for 24–48 h. It was pyrolyzed at various temperatures, including 525 ºC, 625 ºC, and 725 ºC for 90 minutes in a continuous argon environment at the rapid heating rate in a tube furnace to determine the optimal activation temperature. To effectively eliminate residual $FeCl_3$, KOH, and inherent ash minerals, the carbonized samples were immersed in a diluted HCl solution and then rinsed with deionized water until achieving a neutral pH. Finally, ethanol treatment was administered, followed by centrifugation. Before analysing their morphological and electrochemical characteristics, the resulting products MLAC-X (denoted as MLAC-525, MLAC-625, and MLAC-725, respectively) were dried at about 110°C for 24–48h.

3.2.3 Characterizations

X-ray diffraction studies of the synthesized samples were carried out using monochromatic Cu-Kα radiation of a wavelength of 0.154 nm on Malvern PANalytical (Empyrean 3rd Gen, Netherlands) instrument. Raman analysis was done using Compact Raman Spectrometer (Renishaw, UK). FTIR spectrum was recorded by Spectrum Two FT-IR Spectrometer (PerkinElmer, Singapore) in the spectral range of 500-4000 cm^{-1}. The energy dispersive X-ray analysis and the FESEM images were taken by Jeol (Japan) instrument. TEM images were taken using the JEOL JEM-2100. XPS was used to confirm the elemental composition in the sample. The specific surface area, pore characteristics of the synthesized materials and N_2 adsorption-desorption studies were carried out using an Autosorb (Anton Paar IQ-XR-XR, Austria) instrument. Before the BET measurement, samples were degassed at 300 ºC in a vacuum for three hours.

3.2.4 Electrode preparation and electrochemical studies

The working electrodes were prepared by drop-casting the NMP solvent-based mixture of 80% MLAC, 10% C-NERGY SUPER C65 and 10% PVDF binders on a 1×1 cm^2 grafoil sheet. The mass loading of the active material on the electrode was 3.00 mg/cm^2. These electrodes were dried in a vacuum oven at 60 °C for overnight. All the electrochemical measurements were carried out in two symmetric electrode system on an electrochemical workstation (Autolab) using a 6 M KOH electrolyte at room temperature. The cyclic voltammetry (CV) and galvanostatic charge-discharge (GCD) measurements were carried out in the potential range from -1 V to 0 V at various scan rates ranging from 10 mV/s to 200 mV/s and current densities ranging from 0.5 to 6 A/g, respectively. The electrochemical impedance spectroscopy (EIS) measurements were carried out in the 10 mHz – 100 kHz range with an amplitude of 10 mV. The cyclic stability of the electrodes was studied using the CV technique at a scan rate of 500 mV/s for up to 10,001 cycles.

3.3 RESULTS AND DISCUSSIONS

3.3.1 Structural and morphological analysis

Powder XRD patterns of MLAC-X (5250-725 °C) are shown in figure 3.1a. All TPC-X exhibited two characteristic diffraction peaks at 2θ angles of ∼26° and ∼43°, which

can be attributed to the graphitic carbon planes of (002) and (100), respectively (Yang et al. 2022a). The broadness of the peaks suggests that the activated carbon compounds possess amorphous structures and exhibit low levels of graphitization. However, with the increase in pyrolysis temperature from 525°C to 725°C, there is a noticeable increase in peak intensity and a reduction in peak broadness, indicating an enhancement in graphitization. Further, this improvement in graphitization can be supported by Raman analysis.

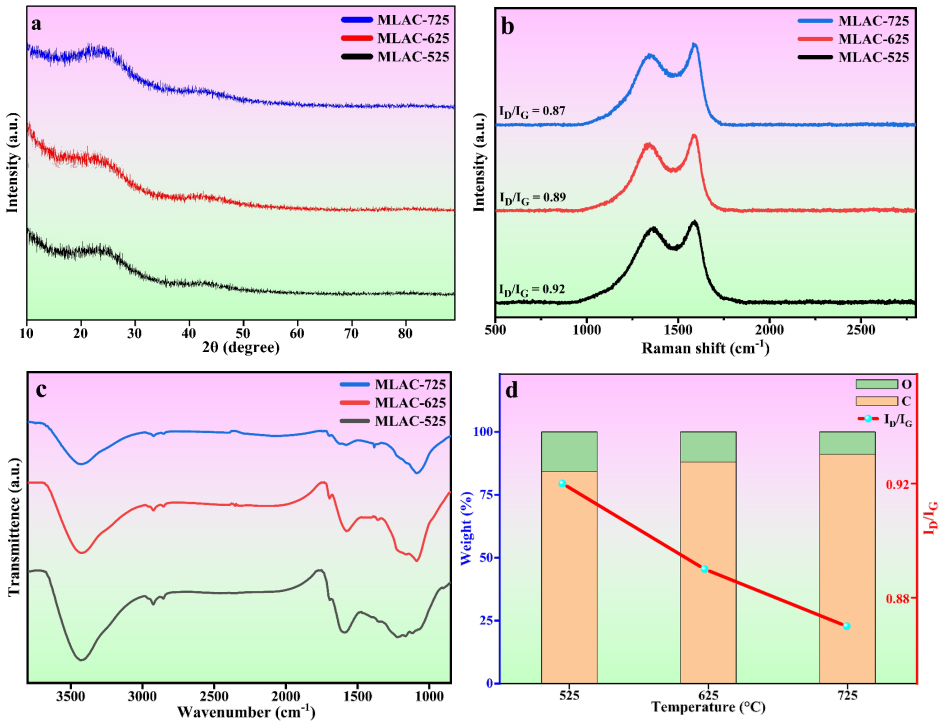

Figure 3.1 *(a) XRD patterns, (b) Raman spectra, (c) FTIR spectra, (d) Effect of temperature on elemental weight % and Raman intensity ratio.*

Raman spectroscopy, a non-destructive characterization method, was used to examine the extent of changes in the order of the arrangement of carbon structures in MLAC-525, MLAC-625, and MLAC-725 during the graphitization phase and also to figure out the microstructural changes that occurred during the activation. The D-band, which originates from disordered carbon, can be seen in all Raman spectra (figure 3.1b) of materials between 1339 cm^{-1} to 1364 cm^{-1}, while the characteristic G-bond, which comes from sp^2-hybridized graphitic carbon, can be seen between 1581 cm^{-1} to 1591 cm^{-1}. A commonly utilized method to assess the degree of disorder in carbon structures

involves calculating the intensity ratio of two distinct bands, referred to as I_D/I_G. The peak intensity of XRD and the I_D/I_G value in the Raman spectra are measures of graphitic order or crystallinity in the activated carbon and are inversely related. The increase in peak intensity in the XRD pattern is a result of an improvement in crystallinity or the development of graphitic orders, which leads to a decrease in the value of the I_D/I_G ratio in the Raman spectra (Jiang et al. 2017). The I_G/I_D values of MLAC-525, MLAC-625, and MLAC-725 are 0.92, 0.89, and 0.87, respectively. Figure 3.1d portrays the relation between the graphitization temperature and the I_D/I_G values. When the graphitization temperature of MLAC is raised from 525 °C to 725 °C, the strength of the G band increases while the intensity of the D band decreases, suggesting a growth in the graphitic content with a decrease in defects (Pathak et al. 2022). The defect density or degree of graphitization of activated carbon plays a critical role in enhancing its electrical characteristics when utilized in the fabrication of supercapacitors. The appropriate balance between amorphous and graphitic carbon structures can enhance the active surface area, conductivity, and wettability, all of which are advantageous for enhancing capacitance (Hu et al. 2021; Maria Sundar Raj et al. 2020; Shi et al. 2017; Zhang et al. 2018).

Further, FTIR was used to examine the functional groups of MLAC, as shown in Figure 3.1c. Based on the pertinent literature (Liu et al. 2019a, 2020a; Yu et al. 2018; Zhao and Zhang 2021), the band at 3430 cm^{-1} is associated with the hydroxyl molecule (O-H). The presence of an aliphatic C-H framework, which includes CH_3 and CH_2 in the alkyl group, corresponds to the bands at 2922 cm^{-1}. The functional groups C=O and C=C are attributed to the 1696 cm^{-1} and 1590 cm^{-1} bands, respectively. C-H bending vibration is responsible for the band at 1368 cm^{-1}. The stretching vibration of the C-O can be used to explain the bands at 1094 cm^{-1}. The FTIR spectra of the MLAC showed changes in transmittance as the pyrolysis temperature increased. With the rising preparation temperature of MLAC from 525 °C to 725 °C, the peak at around 3430 cm^{-1} showed a constant reduction in intensity, suggesting the loss of hydroxyl groups. The band at 2922 cm^{-1} had a similar tendency to that of the hydroxyl band, with its strength quickly declining with increasing temperature due to the virtually disappearing C-H bonds. The aliphatic bands show the progressive eradication of the aliphatic structures,

which gradually decrease as the temperature increases. In light of this, it is anticipated that the resulting preparation temperature will cause the rearrangement of the carbon skeleton due to the decomposition and breaking down of the aliphatic framework during activation. In conclusion, the primary chemical modifications that occurred during pyrolysis included dehydration, formation and elimination of carbonyl group, breaking of aliphatic side chains, and creation of aromatic carbon groups (Yu et al. 2018).

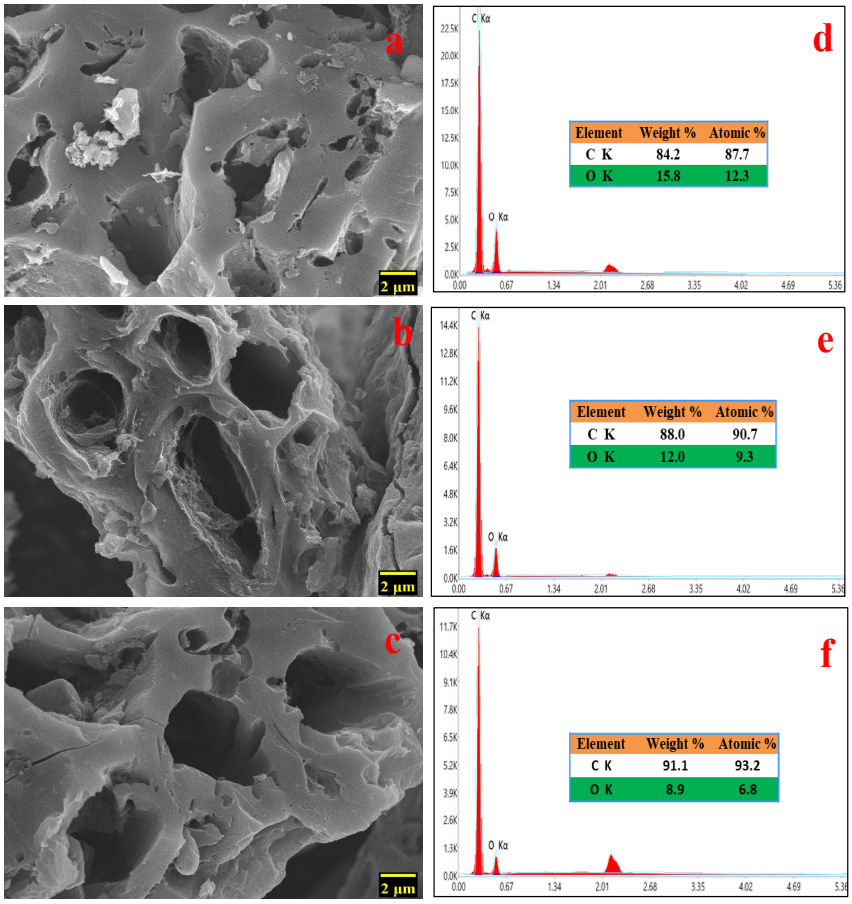

Figure 3.2 *FESEM images of (a) MLAC-525, (b) MLAC-625, (c) MLAC-725 and EDX results of (d) MLAC-525, (e) MLAC-625, (f) MLAC-725.*

The surface morphological characteristics of MLAC samples were examined using FESEM analysis. In figure 3.2(a-c), the FESEM images reveal the presence of a porous structure throughout the sample, likely responsible for the increase in surface area of the MLAC samples. During the high-temperature treatment, activating agents like KOH can play a crucial role in corroding the carbon skeleton, which helps in the development

of pores. Potassium vapours have the ability to penetrate carbon-based materials, resulting in swelling, disturbance of the carbon microstructure, and the creation of new pores (Sevilla and Fuertes 2014). During the pyrolysis process, a significant quantity of small molecules like CO, CO_2, C_xH_y, etc., are liberated from inside the samples, which can also aid in the generation of pore structure. The SEM photographs in figure 3.2(a-c) demonstrate the three-dimensional pore architectures of the MLAC samples. Numerous efficient electrochemical sites become accessible in the presence of pores, as they serve to buffer the electrolyte, facilitate ion diffusion, and enable rapid ion transport to the inner surface (Zhao and Zhang 2021). Due to its highly porous nature, MLAC is expected to offer superior charge accumulation when utilized as electrodes for supercapacitors.

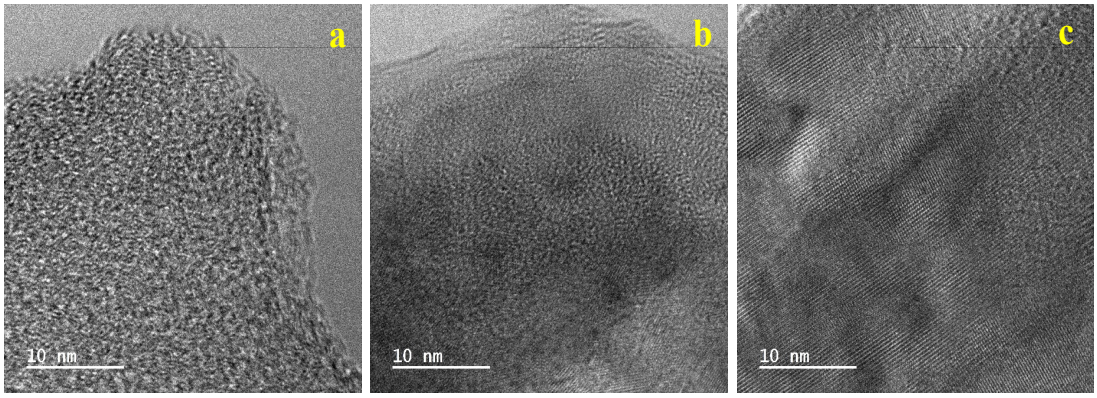

Figure 3.3 *TEM images of (a) MLAC-525, (b) MLAC-625, (c) MLAC-725*

Morphological and physicochemical characteristics of activated carbon, such as area of surface, pore architectures, functional groups on the surface, and also the percentage of elemental compositions, are influenced by the pyrolysis temperature (Tag et al. 2016). With an increase in the pyrolysis temperature from 525 °C to 725 °C, the percentage of carbon in the MLAC samples notably increased from 84.2 to 91.1, with a decline in the percentage of oxygen from 15.8 to 8.9, respectively. Hence, the pyrolysis temperature significantly impacted the oxygen-carbon (O/C) ratios of MLAC, as the ratio decreased from 0.19 to 0.10 with the increase in temperature. The upsurge in percentage carbon content in the X-ray energy dispersive spectroscopy report in figure 3.2(d-f) of MLAC at higher temperatures was a reflection of the degree of carbonization, while the

reduction in percentage oxygen content was probably a result of dehydration processes, the breakdown of oxygenated bonds, and the release of gaseous or low molecular weight by-products containing hydrogen and oxygen (Zhou et al. 2013).

TEM analysis was conducted to acquire additional topographical and morphological insights into the MLAC samples, with the resulting images depicted in figure 3.3. The TEM images clearly demonstrate the coexistence of both amorphous and graphitic features within the MLAC samples. Furthermore, a discernible progression in the formation of ordered structures or graphitic layer-like arrangements is evident from MLAC-525 to MLAC-725, indicating a noticeable transition or evolution in the arrangement of the MLAC samples. This observation is not only visually evident but also finds support in the analyses conducted using both XRD and Raman spectroscopy. Hence, the correlation between TEM imagery and the results from XRD and Raman spectroscopy further strengthens our understanding of the structural changes occurring within the MLAC samples, consistently highlighting the evolving nature of the MLAC samples.

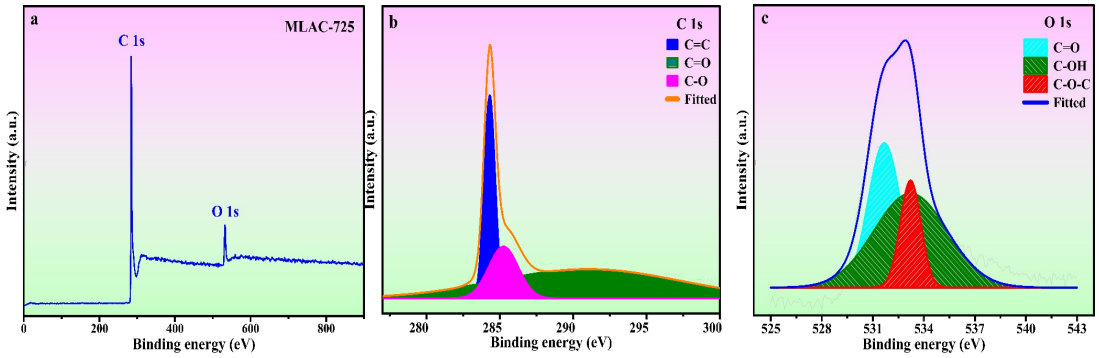

Figure 3.4 *(a) XPS survey; deconvoluted (b) C 1s (c) O 1s spectra of MLAC-725.*

The surface chemical composition analysis of MLAC-725 was conducted through XPS measurements. In figure 3.4a, there are two noticeable peaks observed around ~ 282.42 and ~ 530.42 eV, which can be ascribed to carbon (C 1s, constituting 92.0% of the mass) and oxygen (O 1s, constituting 8.0% of the mass), respectively. The detailed C 1s spectra at higher resolution were analysed, resulting in three distinct peaks (figure 3.4b). These peaks can be attributed to sp^2-bonded carbon (284.4 eV), C-O (286.4 eV), and C=O (288.8 eV). Furthermore, the high-resolution XPS analysis of O 1s spectra

(figure 3.4c) revealed three peaks at 531.6, 532.6, and 533.6 eV, corresponding to C=O, C-OH, and O-C-O, respectively (Zhao and Zhang 2021).

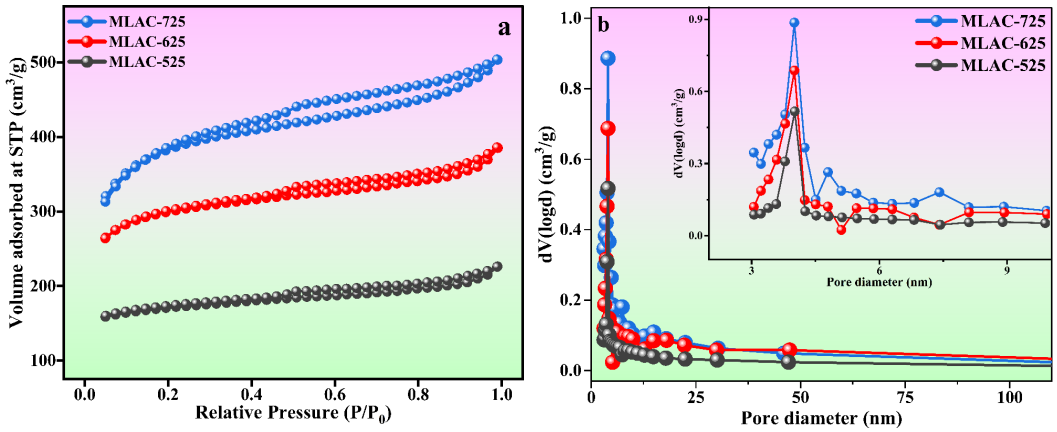

Figure 3.5 *(a) N_2 adsorption-desorption isotherms; (b) Pore size distribution curves.*

Along with its structural and morphological characteristics, the specific area of surface, total pore volume, and pore diameter of activated carbon are also important factors determining its adsorption capability for energy storage technologies (Keppetipola et al. 2021). Figure 3.5 displays the N_2 adsorption-desorption isotherms and pore size distribution for samples of MLAC-525, MLAC-625, and MLAC-725. According to figure 3.5a, all MLAC materials exhibit a classic type IV curve with a distinct H4 type hysteresis loop, indicating the presence of micropores and mesoporous, supported by the pore size distribution curves in figure 3.5b (Sun et al. 2019). Similar pore size distribution patterns were seen in all of the samples, and the peaks appeared nearly at 4 nm. According to their isotherms and pore size distributions, substantial surface areas of all MLAC are primarily due to the presence of a massive number of mesopores. After the carbonization of DML with $FeCl_3$ at 400 °C, the formation of pore structures initiates, leading to an increase in surface area that eventually reaches 405 m^2/g. Furthermore, the specific surface area (SSA) of synthesized MLAC samples rises from 535 to 1233 m^2/g (Table 3.1) with increasing experimental temperature from 525 °C to 725 °C. The carbon structure continues to hydrolysis at a higher rate as the temperature increases, leading to the development of additional micropores and the formation of mesopores, which result in an increased surface area (Chang et al. 2015b). The increased SSA of activated carbon improves its capacity to hold effective charges.

Table 3.1 *Textural parameters of MLAC*

Sample	BET-SSA (m^2/g)	*Total pore volume (cm^3/g)	Mean pore diameter (nm)
MLAC-525	535	0.095	4.01
MLAC-625	946	0.151	4.00
MLAC-725	1233	0.199	4.00
*Total pore volumes were determined at $P/P_0 = 0.99$			

3.3.2 Electrochemical performance of electrodes

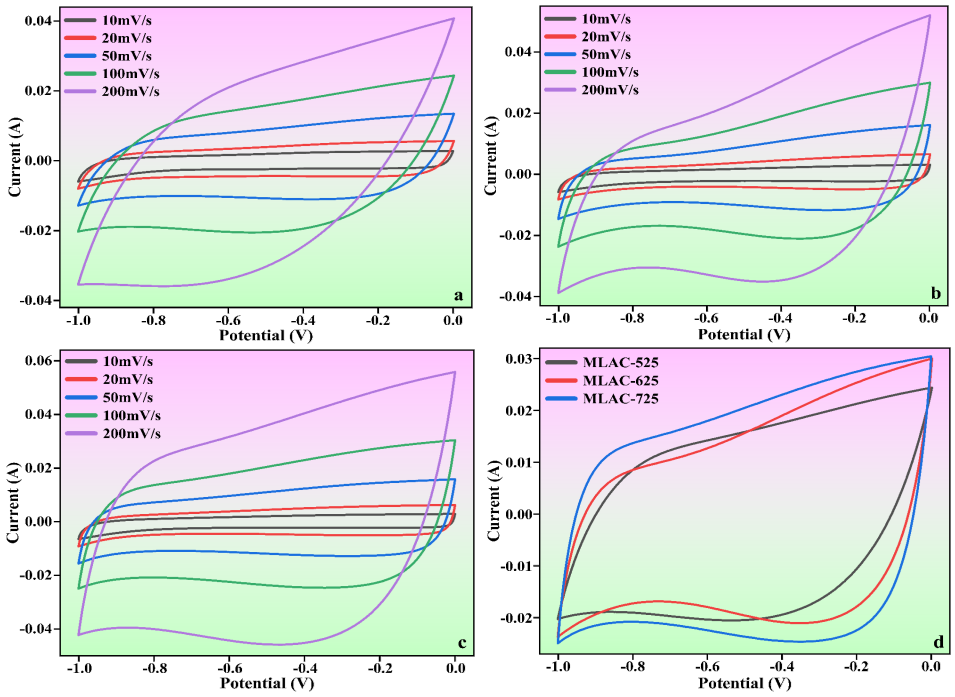

Figure 3.6 *CV curves of (a) MLAC-525, (b) MLAC-625, (C) MLAC-725 (d) all the electrode materials at the scan rate of 100 mV/s.*

The findings and analyses from various structural and morphological studies indicated that MLAC-725, with its high BET surface area and highly ordered mesoporous structure, was the best-suited electrode material in all MLAC samples. To measure the electrochemical performances of MLAC-525, MLAC-625, and MLAC-725 were assessed as electrodes for supercapacitors in a two-electrode cell configuration using an aqueous 6 M KOH solution as an electrolyte. Figure 3.6(a-c) shows the relevant

electrochemical experiment findings of each MLAC electrode at different scan rates ranging from 10 mV/s to 200 mV/s. Further, figure 3.6d compares the capacitive performances of all the samples at the same scan rate of 100 mV/s to identify the electrochemical benefits. Compared to the MLAC-525 and MLAC-625 electrodes, the area of the MLAC-725 electrode on the CV curve was significantly greater, demonstrating the superior capacitive performance of the electrode. Additionally, the impacts of significant levels of developed graphitization, a well-established pore structure, and increased surface area in MLAC-725 materials result in improved capacitive characteristics (Chang et al. 2015a). According to the power law, the value of *b* for MLAC-725 was calculated to be 0.96; hence, the charge storage process here is primarily capacitive in nature (specifically EDLC type). Using the Dunn method, capacitive currents were calculated, indicating that the behaviour of MLAC-725 is approximately 96.59% EDLC.

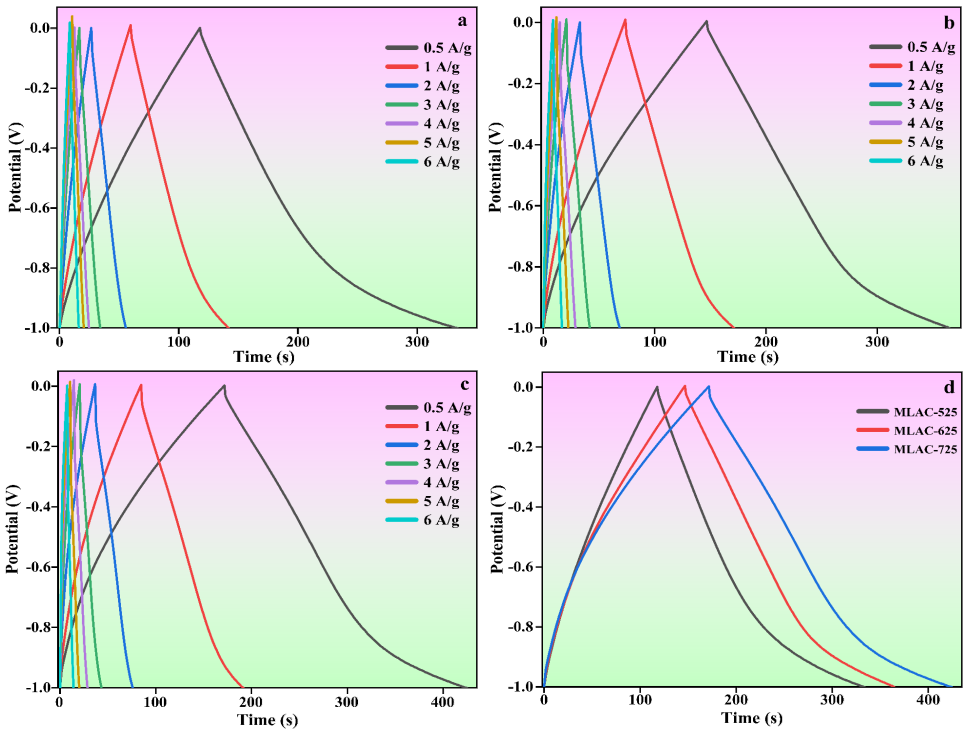

Figure 3.7 *GCD curves of (a) MLAC-525, (b) MLAC-625, (C) MLAC-725 (d) all the electrode materials at the current density of 0.5 A/g.*

Further, galvanostatic charge-discharge (GCD) experiments were performed at different current densities ranging from 0.5 to 6 A/g to compute the specific capacitance

of the MLAC materials. The typical findings are presented in figure 3.7. The fact that all of the GCD plots confirm their capacitor-like behaviour. At a current density of 0.5 A/g, the calculated specific capacitance of MLAC-725 reached 521.65 F/g, higher than the 444.90 F/g of MLAC-625 and the 440.82 F/g of MLAC-525. Because of the results of both physical and chemical activation, MLAC-725 has a significantly higher BET surface area, offering plenty of active sites for energy storage. Thus, it can be assumed that the amount of surface area significantly contributed to improving the material's capacitance by increasing the accumulation of ions at the junction of the electrode and the electrolyte (Madhu et al. 2014). In a hierarchically porous graphitic texture, mesopores operate as easy paths for the ion to enable quick ion transmission, macropores act as ion-buffering reservoirs, and the graphitic structure offers a conductive system for swift charge movement. The combined presence of amorphous and graphitic carbon structures in MLAC-725 might have boosted wettability and increased electrical conductivity, which would be advantageous for capacitance enhancement (Zhao and Zhang 2021).

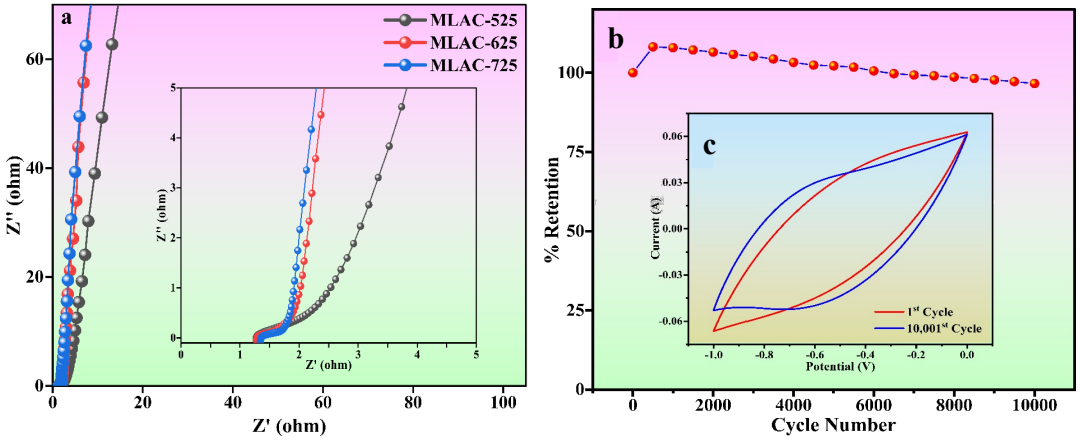

Figure 5.8 *(a) Nyquist plots (b) Cyclic stability (c) 1st and 10,001st CV cycle.*

Figure 5.8a displays the Nyquist plot of the MLAC-525, MLAC-625, and MLAC-725 electrodes over the frequency range of 10 mHz to 100 kHz. In comparison, the MLAC-725 electrode has a very steep slope in the low-frequency zone and a comparatively small semi-circle radius in the high-frequency region. This indicates a faster ion diffusion, migration rate, and low charge transfer resistances suggesting the presence

of a large number of micropores and a more organized microstructure in the MLAC-725 (Liu et al. 2021; Tian et al. 2019). This could be the reason for the significant increase in the ion/charge conductivity inside the active carbon material to improve the rate of capacitive performance (He et al. 2010). The maximum energy density of MLAC-725 was determined to be 17 Wh/kg at a power density of 243 W/kg. Additionally, the cyclic stability of the fabricated electrodes was assessed, considering the importance of prolonged material stability in energy storage devices that undergo repeated cycles. The initial decrease in capacitance followed by an increase in subsequent cycles, observed in a cyclic stability study of a supercapacitor, is a common phenomenon. This behaviour can often be attributed to the activation and conditioning of the electrode materials during the initial cycles. In the early cycles, activation processes such as electrolyte penetration, ion migration, rearrangement of ions, surface restructuring or reorientation, and the formation of a stable interface between the electrode material and the electrolyte may take place, causing an initial decrease in capacitance. As the cycling continues, these processes stabilize, leading to an enhancement in the supercapacitor's performance and an eventual increase in capacitance. This phenomenon is part of the electrochemical processes in the initial stages of supercapacitor operation. The assembled capacitor exhibited exceptional long-term stability, retaining approximately 96.60% of its capacitance after 10,001 cycles at a scan rate of 500 mV/s in a 6M KOH solution (Figure 5.8b). The inset, i.e., figure 5.8c presents a typical cyclic voltammogram for the 1st and 10,001st cycles, demonstrating consistent shapes with minimal deviation, indicative of outstanding capacitance characteristics. All of these superior electrochemical performances underscore the potential of the material as a supercapacitor electrode, derived from biomass waste.

3.4 CONCLUSIONS

In order to create a greener environment, it is suggested in this study that effective regulation may be used to develop efficient porous carbon compounds from waste biomass, which can then be used in energy storage devices like supercapacitors. The dead *Mangifera indica* leaves-derived activated carbons showed high specific surface

areas, large pore volumes, suitable pore size distributions, and a lot of surface functionalities. The impacts of significant levels of developed graphitization, a well-established pore structure, and increased surface area in MLAC-725 materials result in improved capacitive characteristics. The combined presence of amorphous and graphitic carbon structures in MLAC-725 might have boosted wettability and increased electrical conductivity, which would be advantageous for capacitance enhancement. The highest electrochemical performances, i.e., the maximum specific capacitance of 521.65 F/g at a current density of 0.5 A/g, were attained when the specific surface area of the MLAC-725 was raised to 1233 m^2/g. Significantly, it achieved an energy density of 17.4 Wh/kg at a power density of 242.5 W/kg. Furthermore, it demonstrated remarkable electrochemical cyclic stability by retaining 96.60% of its initial capacity even after undergoing 10,001 cycles at a scan rate of 500 mV/s. As a result, this research effectively demonstrates the utilization of waste biomass resources to produce environmentally beneficial energy storage devices, highlighting a promising pathway towards a more sustainable and greener environment. Moreover, it presents substantial possibilities for the extensive adoption of advanced renewable energy solutions at a broader level.

****

CHAPTER 4

IMPACT OF ELECTROLYTE CONCENTRATION ON THE ELECTROCHEMICAL ENERGY STORAGE PERFORMANCE OF *COCOS NUCIFERA* TRUNK-DERIVED HIGH-SURFACE CARBON

Abstract: This chapter unveils a cost-effective approach to supercapacitor development by harnessing the untapped potential of high-porous carbon derived from *Cocos nucifera* trunk sawdust, and offers valuable data regarding its performance under various electrolyte concentrations.

4.1 INTRODUCTION

In recent years, efforts to promote sustainable energy utilization and advance green energy storage technology have gained momentum, aiming to combat the issues arising from high energy consumption and environmental pollution (Mascarenhas et al. 2023; Senthil and Lee 2021). Among the array of electrochemical energy storage technologies, supercapacitors exhibit significant potential for delivering rapid, high-rate power supplies and supporting the versatility of portable electric applications. Due to their unique advantages, encompassing exceptional durability in terms of cycling life, rapid charge and discharge capabilities, outstanding power density, and a solid commitment to environmental sustainability, the supercapacitors distinguish themselves from conventional energy storage options like potassium-ion, sodium-ion, and lithium-ion batteries (Kulurumotlakatla et al. 2020; Yoon et al. 2020; Zhao et al. 2020; Zhu et al. 2022). Carbon materials, metal oxides, and conducting polymers stand as the three foundational electrode components for supercapacitors. Carbon materials primarily store energy by accumulating charge on the electrode's surface, while the latter two, metal oxides and conducting polymers, rely on Faradaic reactions for their energy storage mechanisms (Adoor et al. 2023). While transition-metal oxides and conducting polymers can yield a considerable specific capacitance, their practical

application in supercapacitors is hindered by their high cost, limited voltage operating range (<1.0 V), and relatively short cycling lifespan (Anil Kumar et al. 2020; Kim et al. 2021). Carbon materials exhibit several advantageous qualities, including robust structural stability, extensively developed porosity, customizable surface chemistry, and cost-effectiveness (Hegde and Bhat 2024a). Consequently, they have emerged as the leading and most promising choice in the field of energy technology (Hegde and Bhat 2023).

In the realm of supercapacitors, there is a growing fascination with a wide array of cutting-edge porous carbon materials, including graphene, carbon nanotubes (CNTs), and fullerenes. These innovative carbon materials have gained significant attention in the supercapacitor field due to their precise and well-defined textural structures. Their well-ordered carbon arrangements allow for efficient charge storage and rapid energy release, making them promising candidates for high-performance supercapacitor development. Researchers are continuing their exploration and optimization of these materials to harness their full potential in energy storage and other applications. As a result, a variety of carbon-enriched materials are being actively employed in energy storage applications, particularly in supercapacitors (Mehdi et al. 2023). Biomass, including biomass waste, represents a plentiful and renewable source of carbon. In recent years, there has been a noteworthy surge in the utilization of the inherent structure of biomass. Biomass refers to organic materials derived from living or recently living organisms, such as plants, agricultural residues, wood, and various organic waste products. In other words, biomass is primarily generated through the process of photosynthesis, with the assistance of solar energy, using CO_2 and water. The transformation of biomass into carbon materials is an indirect means of utilizing CO_2 as a carbon source, thus contributing to the sustainable development of energy storage technologies and also in pollution reduction. Traditionally, graphene-like carbon materials derived from biomass possess several vital attributes, including abundant availability, excellent conductivity, a substantial surface area, stable electrochemical performance, and notable mechanical flexibility (Wang and Shi 2015).

When examining the electric double-layer energy storage mechanism, it becomes evident that the high specific capacitance of a carbon electrode is intricately tied to its substantial specific surface area (SSA). This expansive SSA facilitates the availability of a multitude of active sites for the storage of electrolyte ions (Sun et al. 2022; Wang et al. 2022d). In the charge-discharge process of an electric double-layer capacitor (EDLC), ions are repositioned at the electrode surface without engaging in any Faradaic reactions. This unique attribute lends EDLCs exceptional stability and reversibility, leading to a prolonged operational lifespan compared to traditional batteries and capacitors (Mendhe and Panda 2023). As a result, along with the electrode surface area, various factors of the electrolyte, such as ion size, ionic conductivity, mobility, electrolyte viscosity, diffusion coefficient, electrolyte concentration, and other variables, significantly impact the performance of EDLCs (Zhong et al. 2015). The effectiveness of a supercapacitor device relies on the electrical conductivity of its electrolyte. Higher conductivity facilitates a smoother pathway for the transportation of ions toward the electrode surface. The ionic conductivity of an electrolyte, in turn, depends on factors such as the abundance of charge carriers, ion mobility, and the valency of these ions. Consequently, the concentration and the specific solvent used in the electrolyte play a pivotal role in determining the overall conductivity of the fluid. Aqueous electrolytes outperform solid or semi-solid/gel electrolytes in the realm of energy storage due to their liquid-based nature, characterized by low viscosity and rapid ionic conduction (Mendhe and Panda 2023). So, this study aims to explore the impact of different electrolyte concentrations on the electrochemical performance of high-surface carbon derived from biomass waste for green energy storage applications, such as supercapacitors.

This research, introduces a simple, cost-effective, and straightforward method for producing porous carbon material with a high surface area, referred to as CHSC. This innovative process begins with *Cocos nucifera* trunk sawdust as the initial biomass, subjecting it to carbonization through $ZnCl_2$ treatment, followed by KOH activation at different temperatures. The outcome of this treatment is the creation of porous carbons with a remarkable surface area. The investigation reveals that the CHSC-700 variation exhibits outstanding porous and surface characteristics, along with high specific

capacitance, delivering impressive overall performance. Furthermore, an experimental study was carried out to explore the impact of electrolyte concentration on the electrochemical behaviour of an electrode by varying molar concentrations of KOH. The crucial finding was that the best electrochemical performance of the electrode was achieved when a 6 M concentration of KOH was used as the electrolyte. This concentration appeared to be the most effective at facilitating the desired electrochemical responses within the electrode and, as a result, yielded the highest performance.

4.2 MATERIALS AND METHODS

4.2.1 Materials

KOH pellets, $ZnCl_2$, and HCl were purchased from Loba Chemie. N-Methyl-2-pyrrolidone (NMP), and Poly(vinylidene fluoride) (PVDF) were purchased from Sigma-Aldrich and utilized in their original form. Type-1 water (Elga Veolia) was used throughout the experiments to prepare solutions. Raw *Cocos nucifera* (coconut) trunk sawdust waste was collected near Beerangod, Honnavara, Uttarakannada, Karnataka and used as a precursor material to prepare coconut trunk sawdust derived high surface carbon (CHSC).

4.2.2 Synthesis of CHSC

Sun-dried sawdust from raw coconut trunks underwent a one-week drying period. It was subsequently subjected to multiple thorough washes with ultrapure water, followed by an ethanol rinse and subsequent drying in an oven at 110 ºC. The dried material was then pulverized. The preparation of high-surface carbon from coconut trunk sawdust was carried out through a two-step procedure. In the initial step, sawdust was mixed with $ZnCl_2$ in ultrapure water, and the mixture was heated with continuous stirring until it formed a solid paste. This paste was then placed in a hot air oven at 110 °C for 24-48 hours. Subsequently, the $ZnCl_2$-treated sawdust underwent pyrolysis in an argon gas environment at 400 °C for 1.5 hours. The second step involved mixing the pyrolyzed powder sample with KOH in ultrapure water. Again, continuous stirring was applied as the mixture was heated to create a solid paste. This paste was dried at approximately 110 °C for 24-48 hours. The KOH-treated black powder was then heated at various

temperatures (500 ºC, 600 ºC, and 700 ºC) for 90 minutes in a tube furnace with a rapid heating rate in a continuous argon environment to determine the optimal activation temperature. To remove residual $ZnCl_2$, KOH, and inherent ash minerals, the carbonized samples were immersed in a diluted HCl solution and washed with deionized water until they reached a neutral pH. Subsequently, the samples were treated with ethanol and then filtered after centrifugation. Following this, the resulting coconut trunk sawdust-derived high-surface carbon products (CHSC-X, X=500, 600, 700) were dried at 110 °C for 24-48 hours.

4.2.3 Characterizations

X-ray diffraction analysis was conducted using monochromatic Cu-Kα radiation with a wavelength of 0.154 nm. This analysis was performed on a Malvern PANalytical instrument. Raman analysis was carried out using a Compact Raman Spectrometer from Renishaw, equipped with a 532 nm laser source. FTIR spectra were recorded using a Spectrum Two FT-IR Spectrometer from PerkinElmer. Energy dispersive X-ray analysis and FESEM images were obtained using a Carl Zeiss instrument. N_2 adsorption and desorption measurements were done using an Autosorb instrument. The specific surface area was calculated using the BET method. Prior to the surface area measurement, samples were degassed at 300 ºC under vacuum for three hours.

4.2.4 Electrode preparation and electrochemical studies

The working electrodes were prepared through the deposition of a NMP solvent-based mixture consisting of 80% CHSC, 10% C-NERGY SUPER C65, and 10% PVDF binders onto a 1×1 cm^2 grafoil sheet by drop-casting. These electrodes were subsequently dried in a vacuum oven at 60 °C overnight. The active material's mass loading on the electrode was about 3.00 mg/cm^2. All electrochemical measurements were conducted in a two-symmetric electrode system on an electrochemical workstation (Autolab) using KOH electrolyte. Cyclic voltammetry (CV) and galvanostatic charge-discharge (GCD) experiments were carried out over a potential range spanning from -1 V to 0 V, with scan rates ranging from 10 mV/s to 200 mV/s and current densities varying from 0.5 to 5 A/g. Electrochemical impedance spectroscopy (EIS) measurements were performed within the frequency range of 10

mHz to 100 kHz, utilizing a 10-mV amplitude. The cyclic stability of the electrodes was assessed using the CV technique at a scan rate of 500 mV/s, spanning 9,501 cycles.

4.3 RESULTS AND DISCUSSIONS

4.3.1 Structural and morphological analysis

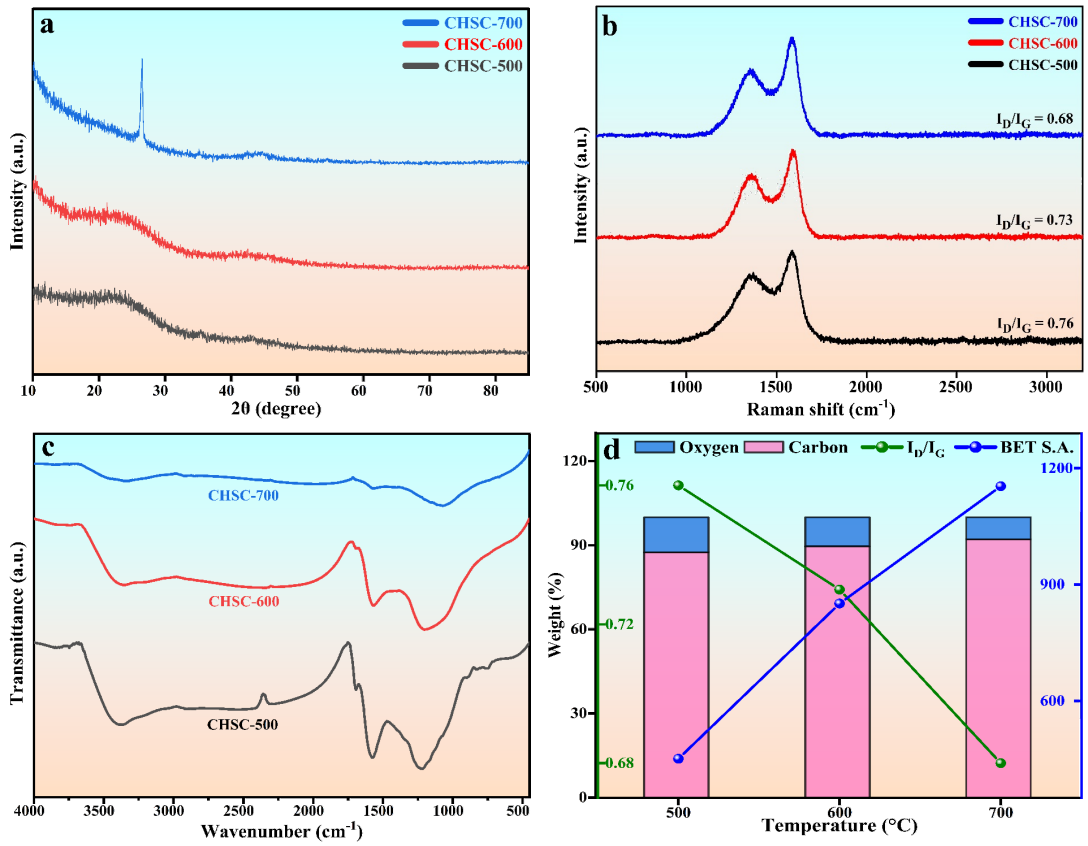

Figure 4.1 *(a) X-Ray diffraction spectrum; (b) Raman spectrum; (c) FTIR spectrum; and (d) Elemental weight % and Raman intensity ratio of CHSC-X (X= 500, 600, 700) samples.*

The structural analysis of the developed carbon material was conducted using XRD analysis. The results revealed that the high surface carbon derived from coconut trunk sawdust (CHSC) exhibits diffraction peaks at ~ 26.5° and ~ 43°, as shown in figure 4.1 a. These peaks correspond to the (002) and (100) planes, respectively. Using Bragg's law equation ($n\lambda = 2d\sin\theta$), the calculated value for the d-spacing, which represents the interplanar spacing between the 002 planes, was determined to be 0.34 nm. The peak at ~ 26.5° signifies a layered graphitic structure, while the broad, weak peak at ~ 43° indicates an essentially amorphous structure with minimal degrees of graphitization

(Sarwar et al. 2021). Therefore, it possesses a turbostratic or random layer lattice structure, representing an intermediate state between the ordered arrangement of graphite and the disordered, amorphous state. However, as the pyrolysis temperature of CHSC increased from 500 °C to 700 °C, there was an increase in peak intensity and a reduction in broadness, indicating enhanced levels of graphitization. Moreover, this observed enhancement in graphitization finds support in the results of the Raman analysis.

To further assess the level of graphitization, the samples underwent Raman spectroscopic analysis, and the outcomes are presented in figure 4.1b. In the spectrum, the distinctive peak at around 1371 cm^{-1} is referred to as the D-band, indicative of disordered carbon, while the peak at approximately 1588 cm^{-1} is recognized as the G-band, typically associated with graphitic carbon. The ratio of the intensities of the D-band to the G-band (I_D/I_G) is commonly used to gauge the extent of carbon graphitization. As the temperature increased from 500 °C to 700 °C, there was a gradual reduction in the I_D/I_G value, signifying a gradual enhancement in the degree of carbon graphitization (Cao et al. 2022). CHSC-700 exhibited an intensity ratio of 0.68, significantly lower than those of CHSC-600 (0.73) and CHSC-500 (0.76) as portrayed in figure 4.1d. Consequently, the higher intensity ratio denotes a greater degree of disorder within the carbon structure and a more prevalent presence of defects in its framework.

FTIR spectroscopy, as shown in figure 4.1c, was employed to provide valuable insights into the functional groups present in the analysed samples. At ~3359 cm^{-1}, a distinct broad peak indicated the O-H stretching vibrations, suggesting the existence of hydroxyl groups in the sample. Another small peak at ~1695 cm^{-1} was indicative of C=O stretching vibrations, implying the presence of carbonyl functional groups. The peak at ~1570 cm^{-1} corresponded to C=C stretching vibrations in aromatic compounds. Additionally, the peak at ~1200 cm^{-1} was associated with C-O stretching vibrations in the compound ("FTIR Functional Group Database Table with Search - InstaNANO" 2023). As the activation temperature rises from 500 °C to 600 °C, the intensity and broadness of the peak decrease and reach negligible when activated at 700 °C. The peak approximately at 3359 cm^{-1} consistently displayed a decrease in intensity, indicating a

continual loss of hydroxyl groups. The C=O band exhibited a comparable trend to that of the O-H band, experiencing a rapid decrease in strength as the temperature increased, attributed to the nearly vanishing carbonyl functional groups. The aliphatic bands in the FTIR spectrum demonstrate the gradual elimination of aliphatic structures, diminishing progressively with the rise in temperature. The carbon skeleton rearrangement occurs through the decomposition and breakdown of the aliphatic framework, along with chemical modifications such as dehydration, decarbonylation, and decarboxylation during the graphitization process (Yu et al. 2018).

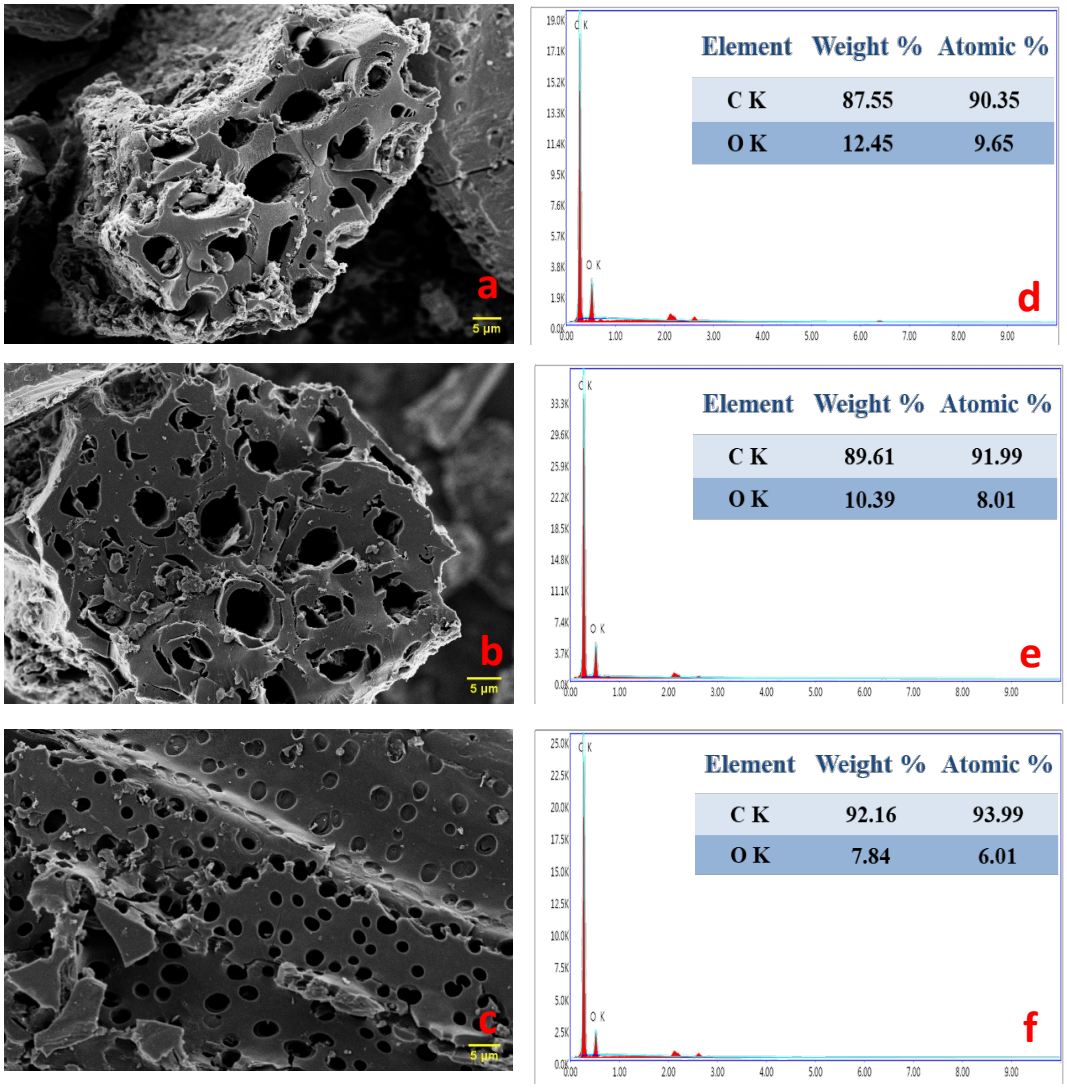

Figure 4.2 *FESEM images (a) CHSC-500, (b) CHSC-600, (c) CHSC-700, and EDX results of (d) CHSC-500, (e) CHSC-600, (f) CHSC-700.*

To gain further insights into the morphology of the CHSCs, FESEM analysis was conducted, as depicted in figure 4.2 (a-c). Sawdust underwent a carbonization process where volatile compounds were eliminated, likely through heating in the absence of oxygen (pyrolysis). This process transformed the sawdust into carbon material, resulting in the creation of a porous structure with varied sizes and shapes. All the samples revealed a diverse array of pores, predominantly induced by KOH activation. KOH, a strong alkali, is known for its potent oxidative properties. Its interaction with the carbon structure leads to decarboxylation reactions, generating small pores within the microstructure (Rajasekaran et al. 2023). This porous structure, resulting from the combination of carbonization and KOH activation, facilitates rapid ion transport. The efficient pathway created by these pores enables the movement of ions during electrochemical measurements. This rapid ion transport is critical for achieving high-performance supercapacitors, as it enhances the device's charge storage and release capabilities. Furthermore, EDAX analysis was performed to ascertain the chemical compositions of the samples, as illustrated in figure 4.2 (d-f). The analysis unveiled a significant presence of carbon and oxygen in the resulting carbon samples. With the elevation of pyrolysis temperature from 500 °C to 700 °C, there was a noticeable surge in the carbon percentage within the CHSC samples, increasing from 87.55% to 92.16%. Correspondingly, the oxygen percentage decreased from 12.45% to 7.84%.

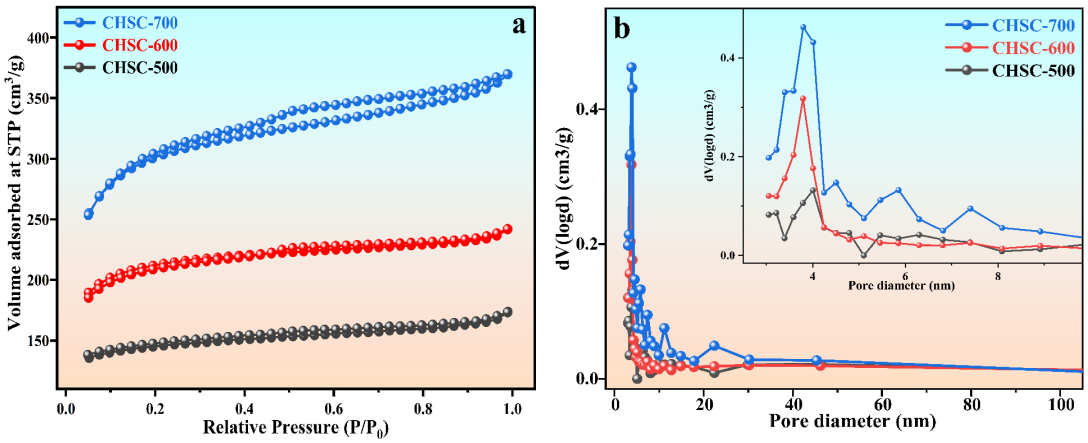

Figure 4.3 *(a) N2 adsorption-desorption isotherms; (b) Pore size distribution curves for CHSC samples.*

Alongside its structural and morphological attributes, the distinct surface area, overall pore volume, and pore diameter of activated carbon play crucial roles in influencing its adsorption capacity for energy storage technologies. N_2 adsorption/desorption measurements were performed to determine pore texture, and figure 4.3 illustrates isotherms and pore size distribution curves for CHSC samples. At a relative pressure ranging approximately from 0.42 to ~ 0.9 (P/P_0), the adsorption profile of CHSC-700 exhibits a smooth ascending trajectory, indicative of type IV adsorption with hysteresis. This distinctive adsorption behaviour signifies the presence of a substantial number of pores and a discernible degree of both microporosity and mesoporosity within the material (Sun et al. 2019). As the temperature rises, the carbon structure undergoes accelerated hydrolysis, fostering the generation of additional pores and consequently contributing to an augmented surface area (Chang et al. 2015b). The specific surface areas, corresponding pore volumes, and the average pore diameters of CHSC samples are listed in table 4.1. The observed results suggest a systematic and consistent evolution in the porous characteristics as a function of the temperature gradient. The enhanced porous structure and increased specific surface area of this activated carbon play a pivotal role in facilitating ion access, particularly during the charge/discharge cycles. This improvement effectively minimizes ion transport time between the electrode and the electrolyte or vice versa, thereby constituting a crucial factor in achieving commendable electrochemical performance.

Table 4.1 *Textural parameters of CHSC-X*

Sample	**BET-SSA (m^2/g)**	**Total pore volume (cm^3/g)**	**Mean pore diameter (nm)**
CHSC-500	451	0.044	4.00
CHSC-600	851	0.056	3.79
CHSC-700	1154	0.11	3.80
*Total pore volumes were determined at $P/P_0 = 0.99$			

4.3.2 Electrochemical performance of electrodes

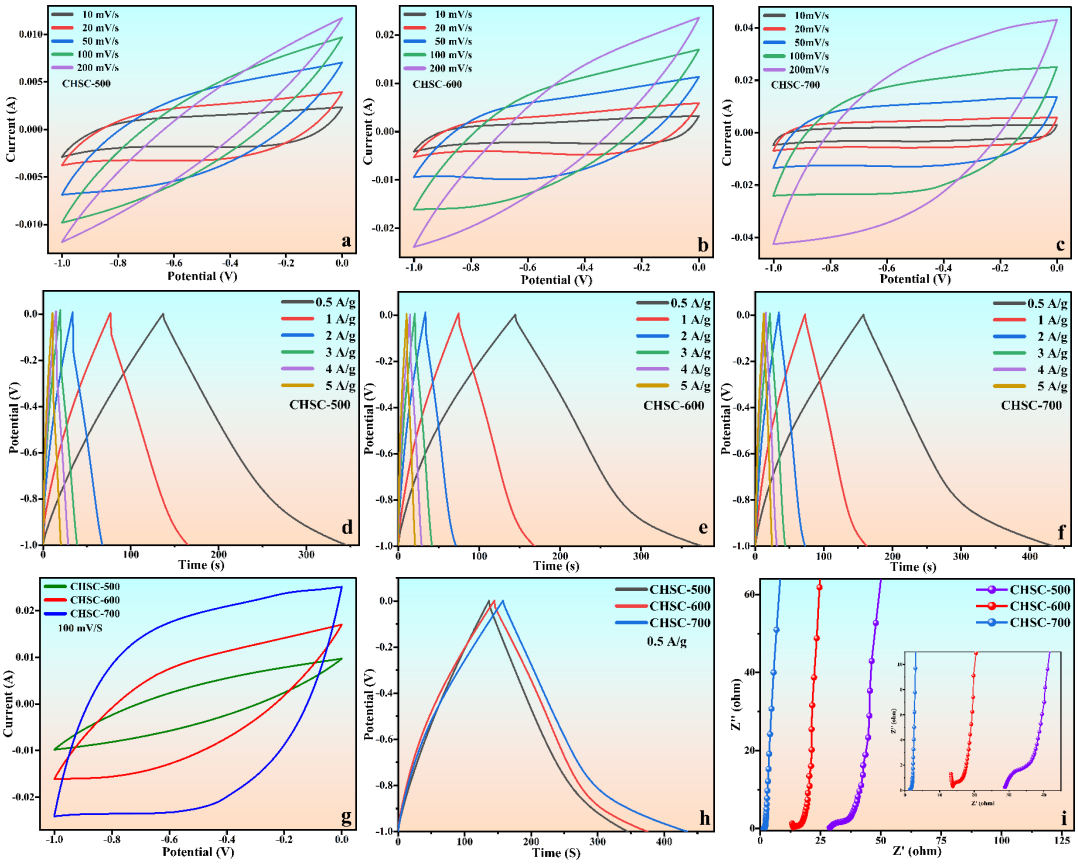

Figure 4.4 *(a-c) CV curves of CHSC-X at various scan rates, (d-f) GCD curves of CHSC-X at different current densities; Comparative (g) CV, (h) GCD, and (i) EIS plots of CHSC-X (X=500,600,700).*

Furthermore, the synthesized materials were fabricated into electrodes and subjected to a comprehensive array of electrochemical evaluations. A two-electrode system was employed to thoroughly scrutinize the electrochemical behaviour of the CHSC samples with a 6 M KOH electrolyte, utilizing cyclic voltammetry, galvanostatic charge-discharge, and impedance analysis. figure 4.4(a-c) illustrates the relevant findings from electrochemical experiments for each CHSC electrode, encompassing a range of scan rates from 10 mV/s to 200 mV/s. Furthermore, figure 4.4g presents a comparative analysis of the capacitive performances of all samples at a consistent scan rate of 100 mV/s, aiming to discern and emphasize the electrochemical advantages among them. During cyclic voltammetric investigations, nearly rectangular-shaped voltammograms were obtained for all CHSC samples, indicative of the characteristic behaviour of

capacitive electrodes. Notably, when compared to the CHSC-500 and CHSC-600 electrodes, the CHSC-700 electrode exhibited a significantly larger rectangular area on the cyclic voltammogram, underscoring its superior capacitive performance. The enhanced capacitive performance witnessed in CHSC-700 can be attributed to the substantial development of a graphitic structure, a well-established arrangement of pores, and an increased specific surface area. According to the power law, the value of b for CHSC-700 was calculated to be 0.99; hence, the charge storage process here is primarily capacitive in nature (specifically EDLC type). Using the Dunn method, capacitive currents were calculated, indicating that the behaviour of CHSC-700 is approximately 97.06% EDLC.

Galvanostatic charge-discharge (GCD) investigations were subsequently carried out at various current densities, ranging from 0.5 to 5 A/g, in 6 M KOH to ascertain the specific capacitance of the CHSC materials. The results of these experiments are visually represented in figure 4.4(d-f, h). Moreover, the pronounced electrochemical reversibility observed in these graphs adds further credence to their resemblance. At a current density of 0.5 A/g, the calculated specific capacitance of a single electrode for CHSC-700 reached 559.27 F/g, surpassing the values of 471.79 F/g for CHSC-600 and 425.36 F/g for CHSC-500. Moreover, the electrochemical impedance spectroscopy measurements supported these findings when performed in a solution of 6 M KOH, with a frequency range of 10 mHz to 100 kHz. Compared to CHSC-600 and CHSC-500, the CHSC-700 electrode exhibited a pronounced incline in the low-frequency range and a relatively diminutive semi-circle radius in the high-frequency domain. These characteristics signify accelerated ion diffusion, a higher migration rate, and reduced charge transfer resistances, pointing towards the existence of numerous and more ordered pore structures in the sample (Liu et al. 2021). The significantly higher surface area, resulting from both physical and chemical activation, provides an abundance of active sites for energy storage. Therefore, the enhancement in material capacitance could be primarily attributed to the increased surface area, facilitating greater ion accumulation at the electrode-electrolyte junction and improved electrical conductance resulting from enhanced graphitic alignment (Sesuk et al. 2019). All these cumulative findings strongly support the proposition that the CHSC-700 sample stands

out as a superior candidate for utilization in electrochemical energy storage applications. Hence, the CHSC-700 sample was employed to delve deeper into the influence of electrolyte concentration on optimizing the capacitive properties of high-surface carbon derived from coconut trunk sawdust waste.

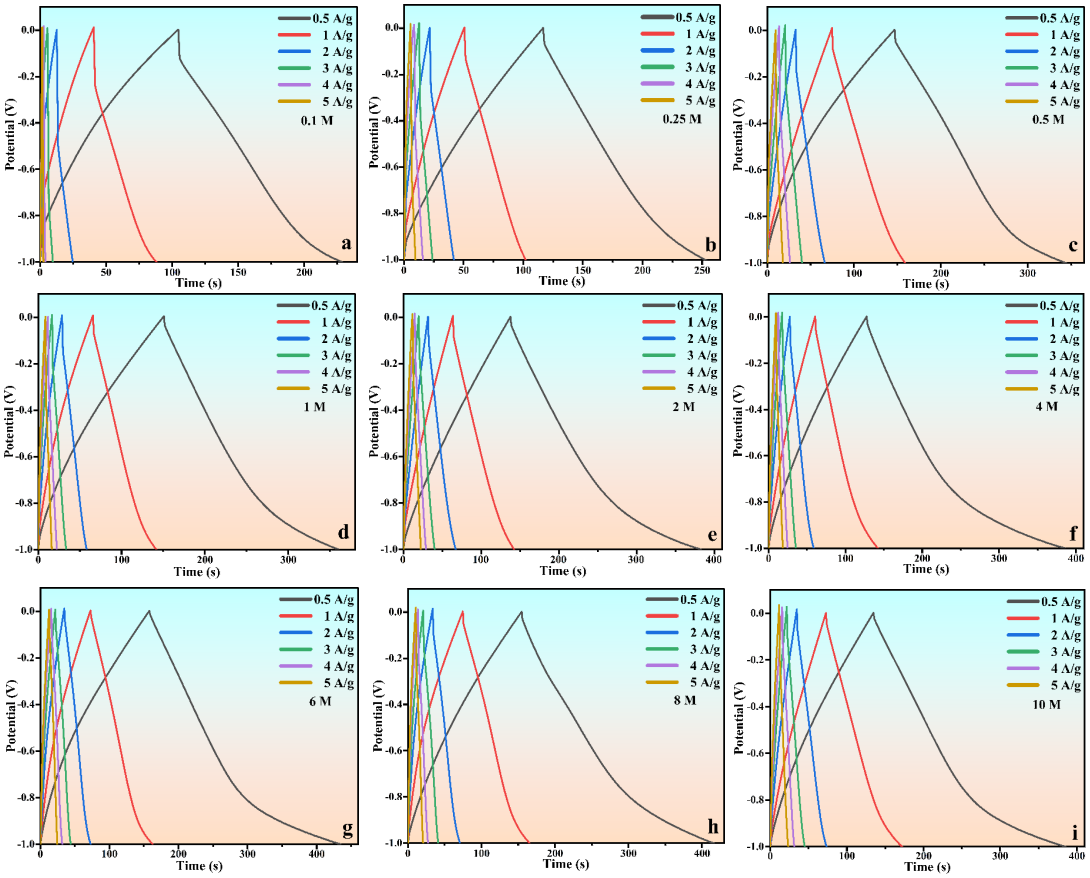

Figure 4.5 *GCD curves of CHSC-700 for (a) 0.1M (b) 0.25M (c) 0.5M (d) 1.0M (e) 2.0M (f) 4.0M (g) 6.0M (h) 8.0M (i) 10.0M concentrations of KOH at various current density.*

Several factors can influence the performance of supercapacitors, and among them, electrolyte concentration stands out as a noteworthy factor. To explore the impact of electrolyte concentrations on the electrochemical performance of CHSC electrodes, a systematic examination was conducted under varying concentrations of aqueous potassium hydroxide (KOH), ranging from 0.1 M to 10.0 M. The results of the galvanostatic charge-discharge (GCD) measurements at different current densities across distinct concentrations of KOH are graphically represented in figure 4.5(a-i).

Additionally, the characteristic specific capacitance values calculated from GCD curves (figure 4.7b) at a current density of 0.5 A/g are systematically presented in table 4.2. It was clearly demonstrated that the specific capacitance of an electrode significantly increased with the rise in KOH concentration from 0.1 M to 6 M. The trend reveals an ascending pattern of specific capacitance with the augmentation of KOH concentration, reaching its peak at 6 M KOH. This observed escalation implies a positive correlation between KOH concentration and specific capacitance, suggesting that higher electrolyte concentrations enhance the electrochemical performance of the system. However, a decrease in specific capacitance is observed beyond this optimal point with further increments in KOH concentration. This decline suggests that beyond a 6 M concentration, increasing the KOH electrolyte concentration may have adverse effects on the electrochemical performance of the system. This observation aligns closely with previous research findings (Krishnan and Biju 2021).

Table 4.2 *Electrochemical performance with various electrolyte concentrations.*

Electrolyte Concentration (M)	Specific Capacitance (F/g)	Energy Density (Wh/kg)	Power Density (W/kg)
0.10	279.56	07.5	220.0
0.25	291.42	08.8	233.3
0.50	414.74	13.0	237.5
1.0	433.16	14.0	241.3
2.0	505.07	16.4	241.6
4.0	529.95	17.3	242.5
6.0	559.27	18.9	246.8
8.0	537.04	17.6	243.0
10.0	514.99	16.7	241.8

When the electrolyte concentration is high, it facilitates more accessible ion transport within the electrode layer. This is because a higher concentration of ions in the electrolyte provides more pathways for ion movement, promoting effective double-layer formation. This effective building-up of a double layer helps in the development

of a stable electrical double layer at the electrode-electrolyte interface, which is crucial for electrochemical energy storage processes. However, when the electrolyte concentration is excessively high, the ion activity may be reduced due to less water hydration. Hydration of ions involves the surrounding water molecules, and ion mobility can decrease if insufficient water molecules are present. Hence, the reduction in ion mobility, caused by less water hydration, can have a negative impact on the overall performance of the electrochemical system. Decreased ion mobility may hinder the efficient transport of ions within the electrode layer, potentially affecting the rate of reactions or processes relying on ion movement (Tsay et al. 2012). Hence, it underscores the importance of finding an optimal balance, as excessively high concentrations of electrolytes can lead to diminishing returns and even a reduction in capacitance.

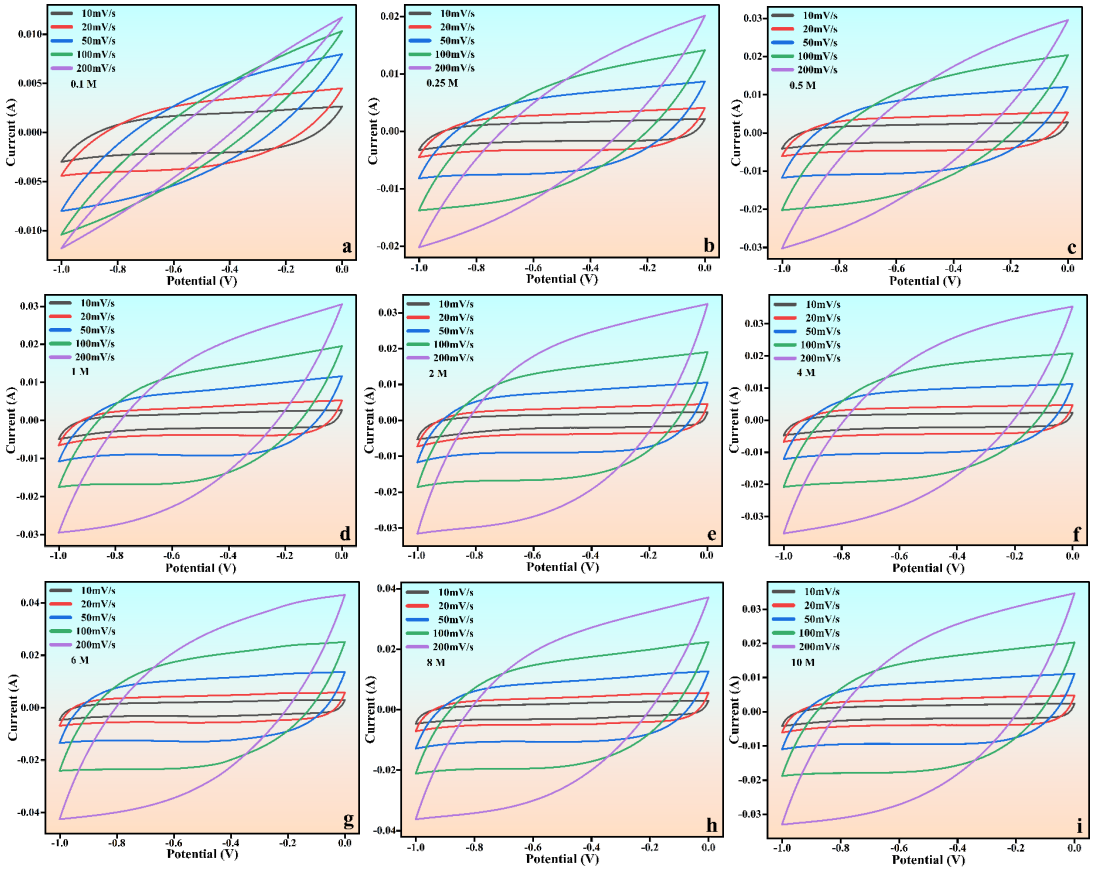

Figure 4.6 *CV curves of CHSC-700 for (a) 0.1M (b) 0.25M (c) 0.5M (d) 1.0M (e) 2.0M (f) 4.0M (g) 6.0M (h) 8.0M (i) 10.0M concentrations of KOH at various scan rate.*

To confirm these findings, CV measurements have been carried out in the potential window of -1 V to 0 V at different scan rates in various concentrations of KOH electrolyte, as visually illustrated in Figure 4.6(a-i). CV curves exhibit neither symmetric nor rectangular shapes for KOH concentrations below 6 M, and they become more distorted at lower electrolyte concentrations. As the KOH concentration increases, CV curves become more rectangular and symmetric, reaching a maximum near rectangular shape (figure 4.7a) when 6 M electrolyte was used. These observations suggest the classic characteristic of a double-layer capacitive type charge storage mechanism involving surface or near-surface charge transfer behaviour, even when operating at a high scan rate of 200 mV/s. The enclosed maximum rectangular area on the CV curve for the 6 M electrolyte was significantly greater than all concentrations, demonstrating superior capacitive performance, and was in good agreement with the GCD findings.

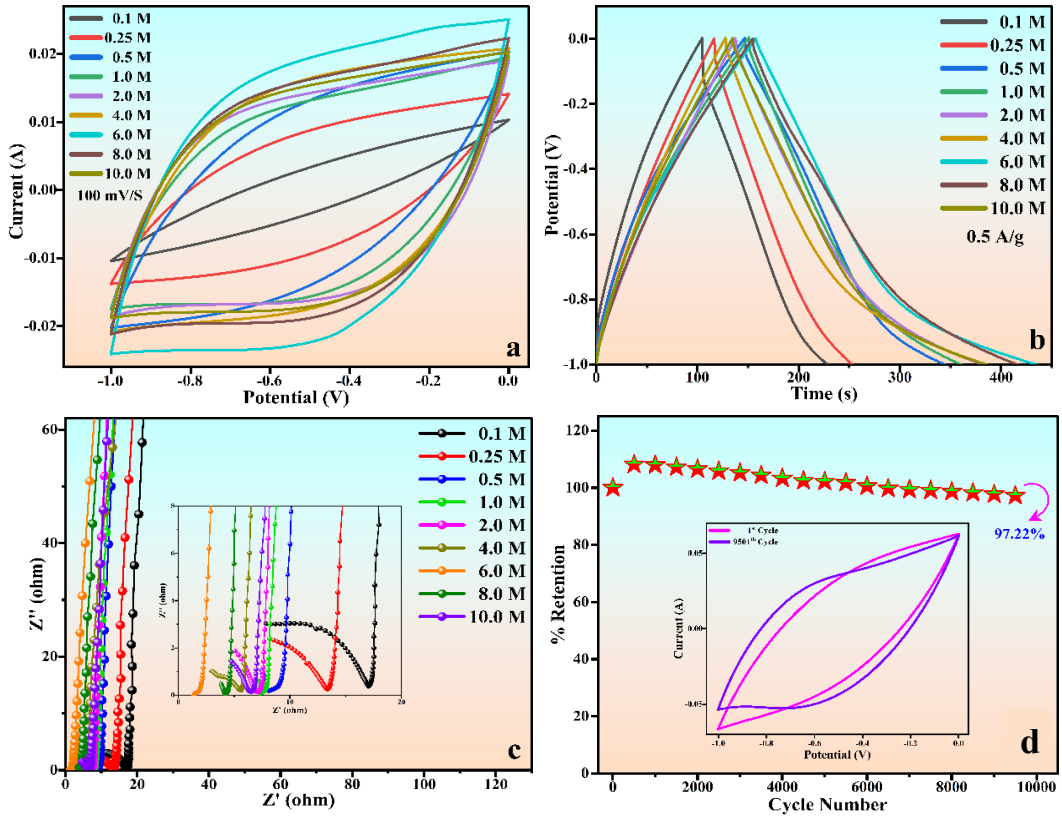

Figure 4.7 *(a) CV, (b) GCD, & (c) EIS plots for at various concentrations of KOH electrolyte; (d) Stability performance.*

The data obtained from the EIS measurements are represented in the form of a Nyquist plot. The typical Nyquist plots for CHSC-700 in various concentrations of KOH are shown in figure 4.7c, covering the frequency range of 10 mHz to 100 kHz. Typically, the Nyquist plot for a supercapacitor comprises three components. Firstly, in the high-frequency region, an intercept on the Z' axis reveals a series resistance. This represents the contact resistance between the electrolyte and electrode surface. Secondly, a semicircle appears in the mid-frequency range, signifying the charge transfer reaction occurring at the interface between the electrode and the electrolyte. Lastly, a straight line at the low-frequency region is attributable to ion diffusion into the electrode material (Teli et al. 2020). The concentrations of electrolytes can influence the ion conductivity within the electrolyte, affecting the charge transfer kinetics and overall electrochemical performance of the electrodes. In comparison, the EIS plot of the electrode measured in 6.0 M electrolyte exhibits a very steep slope in the low-frequency zone and a negligibly small semi-circle radius in the high-frequency region. This indicates faster ion diffusion, a higher migration rate, and low charge transfer resistances. Because a higher concentration of ions in the electrolyte provides more pathways for ion movement, reducing the resistance and promoting effective double-layer formation. Hence, the radius of the semi-circle in the higher frequency region of the Nyquist plot decreases as ionic conductance increases. The specific conductivity of aqueous KOH rises with increasing concentration, reaching a peak at 6 M, but gradually declines with further increments in its molar concentration (Gilliam et al. 2007). So, electrolyte concentration increases beyond 6 M, which diminishes ion activity by impeding water hydration, which is crucial for ion mobility. This decreased ion mobility hinders efficient ion transport within the electrode layer, potentially affecting reaction rates and increasing the resistance. Hence, for 6 M electrolyte, a comparatively lower series resistance is observed in the high-frequency region, which could be attributed to the higher ion/charge conductivity between the electrolyte and electrode surface. All these observations from EIS measurements also confirmed the superior electrochemical performance of the electrode in a 6.0 M electrolyte and were in good agreement with the GCD and CV findings.

The conductance of electrolytes is primarily influenced by the concentration of free charge carriers or ions and their ionic mobilities, playing pivotal roles in assessing electrolyte performance and serving as crucial factors for achieving high power and energy density, prolonged cycling life, and safety in supercapacitor devices (Pal et al. 2019). As discussed, the 6 M KOH electrolyte demonstrates superior conductivity compared to other concentrations, offering advantages in reducing equivalent series resistance and thereby contributing to the development of supercapacitors with significantly enhanced power density (Ramachandran and Wang 2018). Hence, as anticipated, the calculated maximum energy density of 18.9 Wh/kg and power density of 246.8 W/kg were observed at a current density of 0.5 A/g in 6 M KOH. In addition to all these positive electrochemical performances, the effectiveness of a supercapacitor also relies on cyclic stability, which is one of the crucial factors determining its practical viability. To assess the cycling stability of the CHSC-700 sample, exhaustive investigations were conducted at room temperature, spanning an impressive 9501 consecutive CV cycles at a scan rate of 500 mV/s in a 6 M KOH aqueous electrolyte. The electrode exhibited outstanding cycling stability, with a capacitance retention of approximately 97.22%, even after the extensive 9501 cycles. These compelling findings are visually presented in figure 4.7d. The research has practical implications, as it suggests that, in the context of the specific electrode material and electrochemical system studied, a 6.0 M KOH electrolyte concentration is the most suitable choice for achieving optimal performance. This information can be valuable for engineers and researchers working on the design and optimization of electrochemical devices.

4.4 CONCLUSIONS

This research illuminates the promising frontier of utilizing biomass waste, specifically coconut trunk sawdust, as a sustainable precursor for synthesizing high-surface carbon materials with exceptional electrochemical performance. Furthermore, the study delved into the critical role of electrolyte concentration, unraveling its significant impact on the electrochemical behavior of the CHSC electrodes. This systematic exploration revealed that a 6 M KOH electrolyte concentration emerged as the optimal choice, fostering superior ion diffusion, charge transfer, and overall electrochemical

performance. Notably, the CHSC-700 electrode, when tested in a 6 M KOH electrolyte, achieved a specific capacitance of 559.27 F/g at a current density of 0.5 A/g and also displayed excellent cyclic stability, retaining approximately 97.22% capacitance after an extensive 9501 cycles. Furthermore, the Ragone plot showcased the impressive energy and power density of 18.9 Wh/kg and 246.8 W/kg, respectively, at a current density of 0.5 A/g in 6 M KOH. These findings hold promise for the sustainable development of energy storage technologies, highlighting the potential of biomass waste as a renewable carbon source and emphasizing the importance of tailored electrolyte conditions for superior supercapacitor performance. As the world strives for greener and more efficient energy solutions, the outcomes of this research pave the way for innovative advancements in the realm of electrochemical energy storage.

****

CHAPTER 5

ULTRASENSITIVE HIGH-SURFACE POROUS CARBON-BASED ELECTROCHEMICAL BIOSENSOR FOR EARLY DETECTION OF DENGUE VIRUS NS1 PROTEIN

Abstract: This chapter presents the cost-effective and scalable manufacturing process of *Tamarindus indica* seeds-derived carbon, along with its application in the development of an ultrasensitive electrochemical biosensor for dengue detection.

5.1 INTRODUCTION

Infectious diseases transmitted by viruses have the potential to swiftly escalate into widespread pandemics, causing significant upheaval for the global population and disrupting everyday life. Consequently, these factors exert profound impacts on the global economy, leading to unemployment, as well as physical, psychological, and emotional stress, thereby posing a substantial threat to human life (Hegde and Bhat 2022). Dengue stands as the most prevalent arthropod-borne viral infectious disease globally, primarily affecting the people of tropical and subtropical regions. This disease is instigated and disseminated through the bite of *Aedes aegypti* mosquitoes carrying the dengue virus (Bachour Junior et al. 2021). The prevalence of the disease in tropical countries is notably high, primarily attributed to climatic conditions that create favourable environments for the breeding of vector mosquitoes. Upon infection with the disease, dengue manifests with a prominent high fever (approximately 40 °C), accompanied by symptoms such as headache, rashes, and intense joint pain. Complications can escalate to dengue hemorrhagic fever (DHF), characterized by the leakage of plasma fluids. In severe instances, the conditions of DHF can worsen, progressing to dengue shock syndrome (DSS) characterized by circulatory failure. Given the potentially lethal nature of dengue complications, the significance of early and precise diagnosis is paramount for effective disease management and the formulation of appropriate treatment decisions (Siew et al. 2021). The clinical

symptoms associated with this infection frequently overlap with those induced by other arboviruses, creating the potential for confusion. Consequently, the utilization of specific laboratory tests becomes crucial for achieving accurate diagnosis and effective patient management, especially in the areas where these arboviruses are endemic (Andreata-Santos et al. 2020).

The virus comprises three distinct structural proteins: capsid, membrane, and envelope glycoprotein, along with seven non-structural proteins known as NS1, NS2A, NS2B, NS3, NS4A, NS4B, and NS5. Notably, among these proteins, only NS1 is consistently secreted into the bloodstream by the infected host cell, predominantly during the early phase of infection and persisting even after nine days post-onset (Chen et al. 2018a; Figueiredo et al. 2015). Hence, the significance of NS1 as a crucial analyte for dengue detection underscores the development of dengue sensors tailored for NS1 protein identification. Recognizing its pivotal role, various dengue sensors have been suggested for NS1 protein detection, employing diverse transducers such as enzyme-linked immunosorbent assay (ELISA), optical detection relying on localized surface plasmon resonance, fluorescence, amperometric, impedimetric methods, among others (Mendonça et al. 2021). Among these options, label-free electrochemical transducers emerge as a particularly appealing alternative. This preference arises from their potential for effortless portability and rapid detection capabilities, enabling swift point-of-care diagnosis. This stands in contrast to numerous existing detection methods, which often prove time-consuming and labour-intensive (like PCR techniques) (Anusha et al. 2019). In the realm of electrochemical biosensors, the utilization of carbon nanomaterials has emerged as an appealing strategy (Afaque Ansari et al. 2023). This approach enables the attainment of a substantial surface area coupled with notable chemical stability and conductivity, thereby enhancing the sensor's performance (Mendonça et al. 2021; Rao et al. 2018).

This research focused on the design and development of a novel and highly sensitive electrochemical biosensor utilizing high-surface porous carbon for the early detection of dengue virus NS1 protein. In this study, a cost-effective, easy, and simple method was employed for the synthesis of biomass-derived high-surface porous carbon

(HSPC). After numerous detailed physicochemical studies on HSPC, HSPC in aqueous polyethylenimine was incorporated as a sensing platform on a glassy carbon electrode (GCE). Further, this modified GC electrode was functionalized by immobilizing dengue NS1 antibodies, and successively its nonspecific binding sites were obstructed with bovine serum albumin. Various experimental conditions and parameters were optimized to ensure accurate results. Following optimization, the developed sensor exhibited remarkable performance metrics, including superior reproducibility, sensitivity, and a broader linear range compared to existing literature. The sensor demonstrated outstanding selectivity in the presence of other biomolecules and yielded promising results in real sample analysis. This innovative biosensor holds great promise for addressing the pressing need for early detection of dengue virus infections. Its ability to identify the NS1 protein at such high sensitivity levels could revolutionize dengue diagnostics, enabling timely intervention and ultimately improving patient outcomes.

5.2 MATERIALS AND METHODS

5.2.1 Materials

KOH pellets, $ZnCl_2$, HCl, and Cholesterol were purchased from Loba Chemie. KCl, $K_4[Fe(CN)_6]$, $K_3[Fe(CN)_6]$, Bovine serum albumin (BSA), Phosphate buffer saline (PBS), Polyethylenimine (PEI), anhydrous α-D-Glucose, Immunoglobulin-G(IgG) from human serum, and anhydrous Creatinine were purchased from Sigma-Aldrich. Recombinant Dengue Virus 2 NS1 glycoprotein and Dengue virus Type 2 NS1 Monoclonal Antibody were purchased respectively from Abcam and Invitrogen Thermo Fisher Scientific. All chemicals were used as received without any further purification. Type-1 water was used throughout the experiments to prepare solutions. Fresh human serum was directly collected from the Health Care Centre (HCC), NITK. *Tamarindus indica* seeds were collected near Beerangod, Honnavara, Uttarakannada, Karnataka and used as a precursor material to prepare high-surface porous carbon (HSPC).

5.2.2 Synthesis of HSPC

The collected *Tamarindus indica* seeds were cleaned and sun-dried for a week. Subsequently, the dried seeds were ground and washed with water, followed by ethanol. Finally, they were subjected to drying at 110 °C in a vacuum oven. The powder sample underwent treatment with a 1:1 ratio of $ZnCl_2$ and was heated in a minimal amount of water until it formed a solid paste. This mixture was then placed in an oven at 110 °C for a day, and after cooling, it was crushed into a powder. Following this, a rapid heating process was employed for carbonization at 450 °C for 1.5 hours in a horizontal tube furnace under a continuous argon atmosphere. Subsequently, the resulting material was blended with KOH in a 1:1 ratio by weight and heated in a minimal amount of water until it formed a solid paste. Once again, these pastes were transferred into an oven at a temperature of 110 °C for a day, and a mortar-pestle were utilized to create a fine powder from the cooled samples. The obtained powder was placed in a horizontal tubular furnace under a continuous inert argon atmosphere at 650 °C for 1.5 hours. Upon cooling to room temperature, the powder underwent treatment with diluted HCl, with constant stirring overnight at 50 °C. Following this, it was washed with water until achieving a neutral pH, then filtered and ultimately dried completely in a vacuum oven for a day.

5.2.3 Instrumentation

X-ray diffraction (Malvern PANalytical) measurement was conducted using monochromatic Cu-Kα radiation with a wavelength of 0.154 nm. Raman analysis was carried out using a Compact Raman Spectrometer from Renishaw, equipped with a 532 nm laser source. Fourier-transform infrared spectra and thermogravimetric analysis were recorded using a TGA 4000 and Spectrum 2 FT-IR Spectrometer from PerkinElmer. Energy dispersive X-ray analysis and FESEM images were obtained using a Carl Zeiss instrument. TEM images were taken using the JEOL JEM-2100. XPS was used to confirm the elemental composition in the sample using AXIS SUPRA. N_2 adsorption and desorption measurements were done using an Autosorb instrument. The specific surface area was calculated using the BET method. Prior to the surface area measurement, samples were degassed at 300 ºC under vacuum for three hours.

5.2.4 Construction of the dengue biosensor and electrochemical studies

To create the electrochemical dengue sensor, the unmodified glassy carbon electrode (GCE) underwent several rounds of polishing with an alumina slurry, followed by thorough washing with water and sonication in an ultrasonic bath. The fabrication of the dengue biosensor utilized a drop-casting technique, wherein 6 µL of a 1 mg/mL high-surface porous carbon (HSPC) in a 2% polyethylenimine (PEI) aqueous solution was deposited onto the GCE surface, forming HSPC/GCE, and the assembly was then incubated for drying. 4 µL of a 10 µg/mL solution of anti-NS1 was cast on this modified electrode and incubated at room temperature. Thereafter, it was washed with phosphate-buffered saline (PBS) to remove any undesired physical adsorption. Subsequently, a 0.1% bovine serum albumin (BSA) solution was carefully deposited to the surface of the anti-NS1/HSPC/GCE to obstruct nonspecific binding sites, followed by drying. After wash with PBS, the biosensor configuration BSA/anti-NS1/HSPC/GCE was successfully obtained for the detection of the dengue virus NS1 protein. 4 µL of various concentrations of NS1 were incubated on the prepared working electrode at room temperature, and electrochemical responses were recorded. The optimization of experimental conditions and parameters was conducted in successive steps, and the details are provided in the results and discussion section.

All electrochemical studies, including differential pulse voltammetry (DPV) and cyclic voltammetry (CV), were conducted within the potential window of -0.2 V to +0.6 V. An Autolab instrument was employed in a three-electrode assembly comprising a glassy carbon electrode working electrode, a Pt-wire auxiliary electrode, and an Ag/AgCl (3M NaCl) reference electrode. Each experiment was performed with a minimum of three replicates (n = 3) at room temperature, utilizing a 10 mM phosphate-buffered saline (PBS) solution with a pH of 7.4, containing 5 mM $K_4[Fe(CN)_6]/K_3[Fe(CN)_6]$ and 0.1 M KCl.

5.2.5 Analysis of NS1 in real blood samples

The biosensor underwent testing using human serum spiked with dengue NS1 protein to evaluate its performance under realistic conditions. The freshly collected human serum was spiked with three different concentrations of the NS1 protein after being

diluted in PBS buffer. Subsequently, the dengue sensor was incubated with the spiked samples at room temperature, and the electrochemical responses were recorded after rinsing with a PBS solution.

5.2.6 Computational parameters

In silico molecular docking studies were conducted to investigate the interaction between receptor and ligand molecules. Protein-ligand docking was executed employing AutoDock-Vina 1.1.2 software (Trott and Olson 2010). Ligands' chemical structures were drawn using ChemDraw Professional 20.1.1, and their three-dimensional structures were energetically minimized through Chem3D 20.1.1 (Cousins 2005). Crystal structures of dengue type 2 virus non-structural protein (NS1) (PDB ID: 4O6B) (Akey et al. 2014), anti-NS1 (PDB ID: 3UZV, Chain B) (Cockburn et al. 2012), and Bovine serum albumin (BSA) (PDB ID: 4JK4, Chain A) (Sekula et al. 2013) were obtained from the Protein Data Bank (https://www.rcsb.org/). The Modeller tool was utilized to rectify missing residues and atoms in the protein structures (Fiser et al. 2000). Before docking, non-protein components such as cofactors, bound ligands, water molecules, and heteroatoms were removed from the protein's three-dimensional structure. Subsequently, polar hydrogens and Kollman charges were added. The active site of the receptor was identified via the online server COACH (https://zhanggroup.org/COACH/) (Yang et al. 2013). After that, a configuration file was generated, defining the docking boundaries with a cubic grid box of dimensions 100 x 100 x 100 and spacing of -0.362Å, -3.787Å, and 3.824Å along the x, y, and z axes, respectively. Docking was conducted with Vina, setting the exhaustiveness to 16. Protein-protein docking was executed via the ClusPro 2.0 online server (Kozakov et al. 2017). The output files from both protein-ligand and protein-protein docking were analyzed using Biovia Discovery Studio (Baroroh, S.Si., M.Biotek. et al. 2023). Additionally, the isoelectric point and charge of the protein-ligand and protein-protein complexes were calculated using the Prot pi online tool (https://www.protpi.ch/Calculator/ProteinTool) ("Web Based Theoretical Protein pI, MW and 2DE Map" 2009).

5.3 RESULTS AND DISCUSSIONS

5.3.1 Structural and morphological characterizations

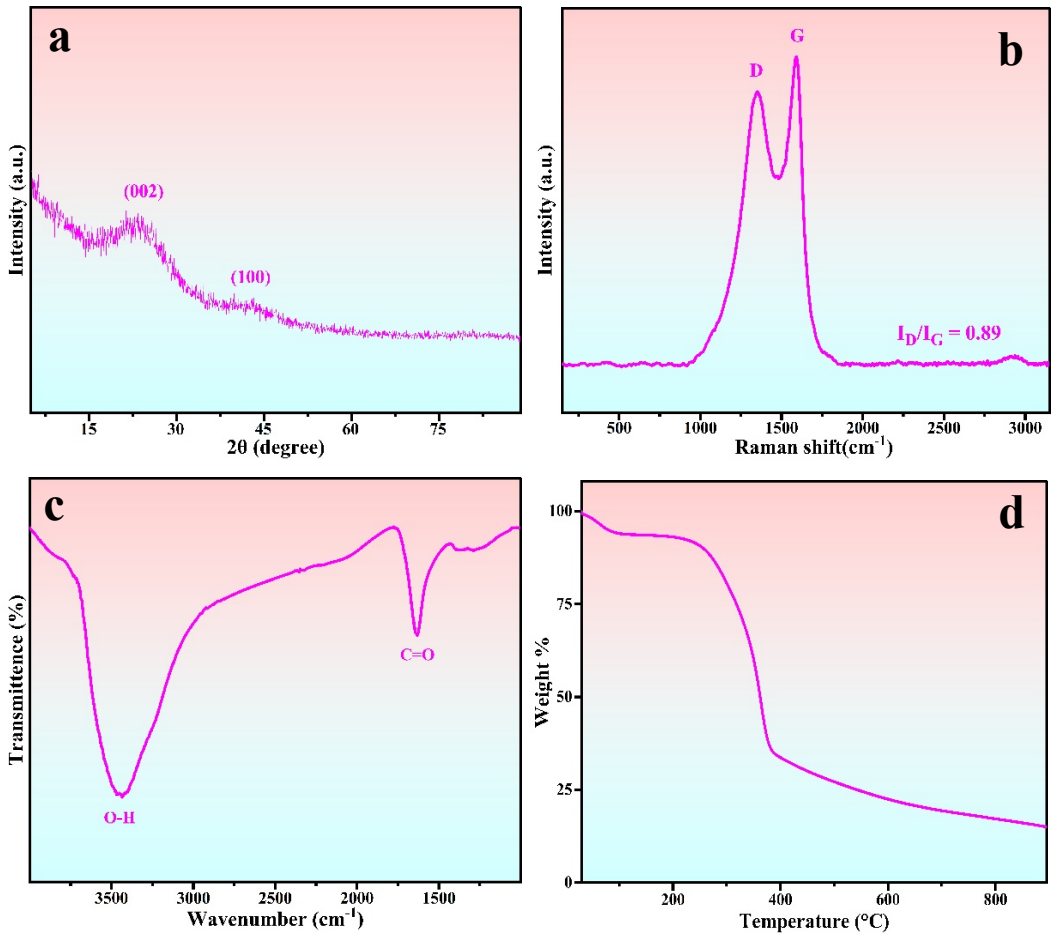

Figure 5.1 *(a) XRD pattern, (b) Raman spectra (c) FTIR spectra of HSPC d) TGA graph of Tamarindus indica L. seed powder.*

The synthesized high-surface porous carbon (HSPC) was comprehensively characterized using various physicochemical techniques, including XRD, Raman spectroscopy, FTIR, FESEM, and BET analysis. Figure 5.1a displays the X-ray diffraction (XRD) pattern of the prepared HSPC, revealing two distinctive peaks typical of activated porous carbon. The broad and well-defined peaks observed at ~24° and ~43° angles correspond to the (002) and (100) planes, respectively, indicating the presence of porous graphitic carbon with an amorphous nature (Pang et al. 2016; Raj et al. 2018). The Raman spectra (figure 5.1b) displays two strong peaks corresponding to the D and G bands. The G-band occurred at 1591 cm^{-1} in HSPC, representing the sp^2-

bonded graphitic region. Additionally, the peak at 1349 cm^{-1}, corresponding to the D-band, occurs due to the presence of amorphous (disordered) carbon in the network. The degree of graphitization in carbonaceous materials is determined by the intensity ratio of the D band to the G band, commonly denoted as I_D/I_G (Hegde and Bhat 2024b). For HSPC, the calculated I_D/I_G value was 0.89, indicating the presence of an amorphous structure. The coexistence of both graphitization and amorphous structures in carbonaceous materials contributes to enhanced conductivity and adsorption performance, respectively (Yang et al. 2022b). FTIR analysis was conducted to investigate the functional groups present in the HSPC material. The FTIR spectrum illustrated in figure 5.1c exhibits a broad absorption peak at approximately 3435 cm^{-1}, indicating the presence of hydroxyl groups. Additionally, the prominent band at 1634 cm^{-1} can be attributed to the C=O stretching. Thermogravimetric analysis (TGA) of the *Tamarindus indica* seed powder was conducted in the temperature range of 30 to 900 °C at a rate of 10 °C/min, and the results are illustrated in figure 5.1d. The initial degradation occurred in the temperature range of 60 - 120 °C, attributed to weight loss resulting from the moisture content present in the sample. Subsequently, significant weight loss was observed between 250−450 °C, which can be linked to the decomposition of hemicellulose and cellulose within the sample (Nandi et al. 2023). The gradual weight loss following this range is indicative of the carbonization of biomass, leading to the formation of carbon consolidation (Ello et al. 2013).

The morphology and microstructure of the HSPC materials were examined using FESEM. Figure 5.2(a-c) display FESEM images of the HSPC samples captured at various magnifications. Notably, the images reveal a well-defined interconnected three-dimensional web-like porous structure on the surface of the HSPC. This characteristic is advantageous, as it provides ample opportunities for the adsorption of the NS1 protein onto the surface of the pores. Furthermore, TEM analysis was conducted to acquire additional topographical and morphological insights into the HSPC samples, with the corresponding images presented in figure 5.2(d-f). The TEM images unequivocally showcase both amorphous and graphitic layer-like arrangement features within the HSPC samples. This observation is visually apparent and substantiated by

analyses conducted using X-ray diffraction and Raman spectroscopy, providing additional support for the identified features.

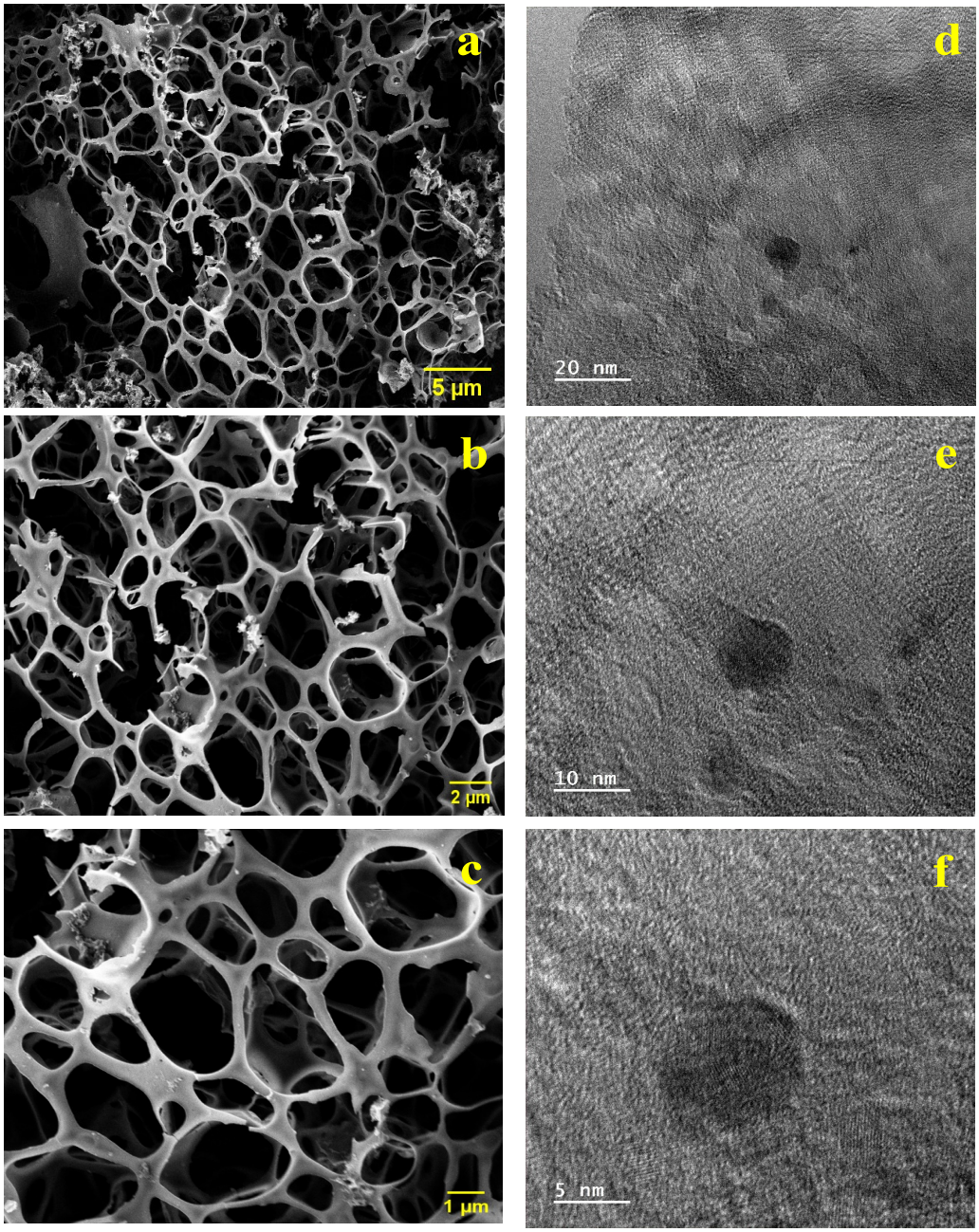

Figure 5.2 *(a-c) FESEM and (d-f) TEM images of HSPC at different magnifications.*

The elemental analysis was conducted through the utilization of EDX and XPS techniques. The EDX (figure 5.3a) analysis unveiled the composition of the HSPC samples, showcasing a predominant 93.65 atomic % of carbon and a minor 6.35 atomic

% of oxygen. The XPS (figure 5.3b) investigation corroborated this compositional determination, providing further validation by confirming a carbon content of 93.1 atomic % and an oxygen content of 6.9 atomic % in the analysed samples. Consequently, these comprehensive studies not only elucidate the elemental composition but also attest to the purity of the HSPC sample.

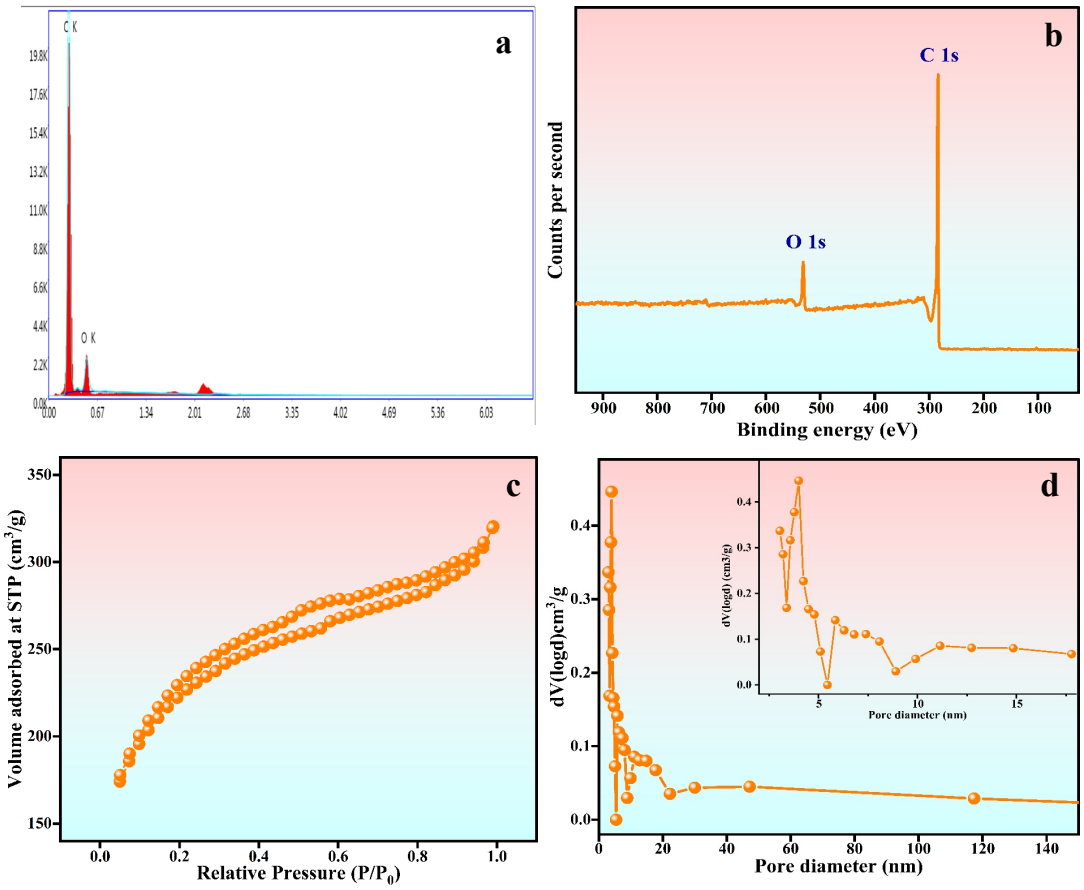

Figure 5.3 *(a) EDX spectra (b) XPS survey spectra (c) BET isotherm (d) Pore size distribution curve of HSPC.*

The surface area and pore structure of the prepared high-surface porous carbon (HSPC) were evaluated through N_2 adsorption−desorption measurements. Figure 5.3c and d illustrate the nitrogen Brunauer-Emmett-Teller (BET) adsorption/desorption isotherms and the corresponding Barrett−Joiner−Halenda (BJH) pore size distribution curves of the HSPC, offering detailed insights into its textural characteristics. The isotherm exhibits a Type IV pattern, and notably, the desorption line deviates from the adsorption

path, forming a loop-like structure within the relative pressure range of ~ 0.25 to ~ 0.95 (P/P_0). These characteristics strongly suggest the presence of both micro and mesopores in the sample. The formation of the loop in the isotherm signifies that adsorbed nitrogen was not released completely, and some remained trapped in the small pores within the HSPC (Nikhil et al. 2022). In figure 5.3d, the corresponding pore size distributions, obtained through the BJH method, further highlight the existence of both micro- and mesopores. The determined average pore diameter, total pore volume, and specific surface area were 4.0 nm, 0.143 cm^3/g, and 747 m^2/g, respectively. The substantial surface area and hierarchical porous structure of HSPCs potentially offer an advantageous pathway for the penetration and transportation of electrolytes (Sha et al. 2018). This characteristic is anticipated to contribute to the enhanced electrochemical performance of HSPCs when utilized as electrode materials in sensors.

5.3.2 Electrochemical characterizations

The electrochemical characterization of bare and high-surface porous carbon-modified glassy carbon electrodes was studied using voltammetric techniques in a 10 mM phosphate-buffered saline (PBS) solution with a pH of 7.4, containing 5 mM $K_4[Fe(CN)_6]/K_3[Fe(CN)_6]$ and 0.1 M KCl. PBS with a pH of 7.4 was chosen for all the electrochemical studies to ensure optimal conditions and reliable results, in alignment with the average pH of physiological fluid in the human body (Hopkins et al. 2024). To assess the impact of surface area, the electrochemically active surface area of both the unmodified glassy carbon electrode (GCE) and the electrode modified with HSPC (HSPC/GCE) was determined through the application of the Randles−Sevick equation using the cyclic voltammetry(CV) technique (Yang et al. 2022b).

$$\boldsymbol{I_{pa} = 2.69 \times 10^5 \times A \times D^{1/2} \times n^{3/2} \times v^{1/2} \times C}$$

Where I_{pa} is the anodic peak current (A), A is the active area of the electrode surface (cm^2), D is the diffusion coefficient of $K_3[Fe(CN)_6]/K_4[Fe(CN)_6]$ i.e., 7.67×10^{-6} cm^2/s, n is the number of electrons transferred in the redox reaction ($1e^-$), v is the scan rate (V/s), C is the concentration of the $K_3[Fe(CN)_6]/K_4[Fe(CN)_6]$ electrolyte (0.005 mol/cm^3). At the scan rate of 100mV/s, the calculated effective electroactive areas for the unmodified GCE and HSPC/GCE were found to be 0.086 cm^2 and 0.130 cm^2,

respectively. The substantial increase of 51.16% in the effective electroactive area for HSPC/GCE is poised to elevate electrocatalytic activity, thereby enhancing overall electrochemical responses.

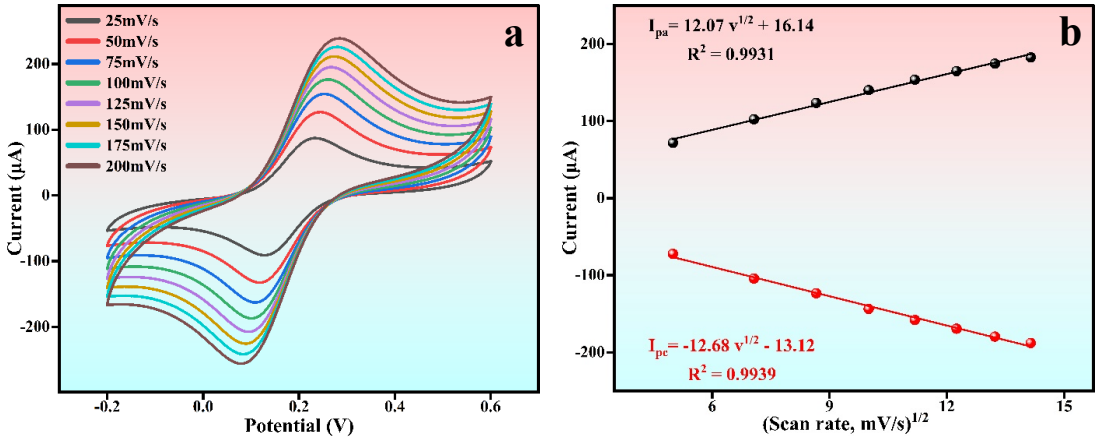

Figure 5.4 *(a) Cyclic voltammograms of HSPC/GCE at different scan rates, (b) anodic and cathodic peak currents v/s square root of scan rates.*

The impact of the scan rate on the electrochemical response of the HSPC-modified GCE was investigated using cyclic voltammetry (CV), as illustrated in figure 5.4a. The anodic peak current (I_{pa}) and the cathodic peak current (I_{pc}) exhibited a consistent increase in their absolute value with the scan rate ranging from 25 mV/s to 200 mV/s. The exceptionally strong linear dependence of the peak current on the square root of the scan rate (figure 5.4b) indicates diffusion-controlled and electrochemically reversible electron transfer processes on the electrode surface (Elgrishi et al. 2018). The linear regression equations can be described as follows: I_{pa} = 12.07 $v^{1/2}$ + 16.14 (R^2 = 0.9931) and I_{pc} = -12.68$v^{1/2}$ - 13.12 (R^2 = 0.9939).

5.3.2.1 Optimization of DENV biosensor

The optimal concentration of HSPC in an aqueous PEI solution plays a crucial role in enhancing the electrochemical response by increasing the active surface area of the bare GCE. Hence, optimization of the HSPC solution was conducted through differential pulse voltammetry (DPV) studies, and the corresponding results are illustrated in figure 5.5a. The study revealed that the DPV current response increases as the concentration of HSPC solutions rises from 0.25 mg/mL to 1 mg/mL. This improvement in electrochemical performance, evidenced by higher current responses in DPV, suggests

an increased surface-active area for electrochemical reactions. Hence, increasing the concentration of high-surface porous carbon enhances electron transfer kinetics on the electrode during electrochemical processes, leading to improved and potentially higher DPV currents. However, no further significant changes occurred beyond this point, and the response reached saturation. Consequently, a concentration of 1 mg/mL for the HSPC solution was employed in all subsequent studies.

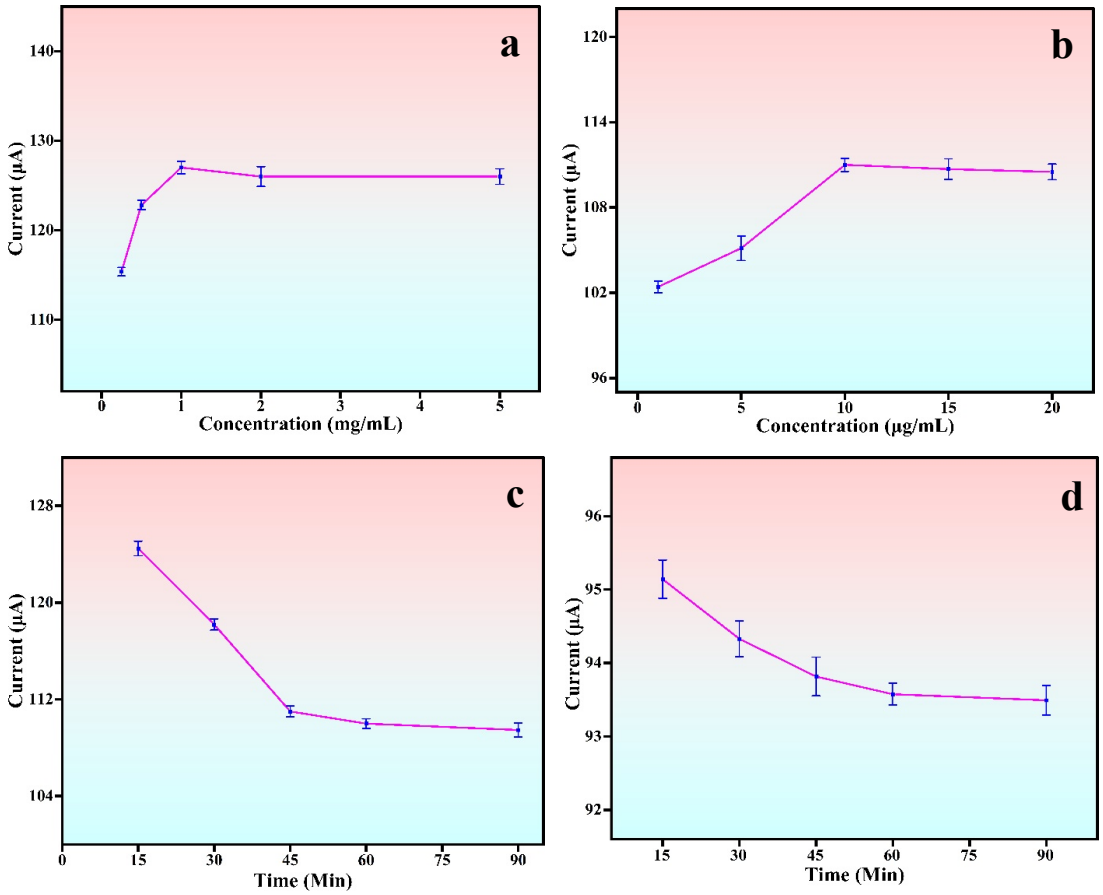

Figure 5.5 *Optimization of (a) HSPC concentration, (b) antibody concentration, (c) incubation time of anti-NS1, (d) incubation time of NS1 protein.*

In pursuit of optimal sensing performance from the sensor, meticulous optimization of essential experimental conditions, including the concentration of anti-NS1, incubation time of anti-NS1, and NS1, was carefully conducted. The crafting of an efficient electrochemical sensor relies significantly on the pivotal step of immobilizing the biomolecules on the detection surface. Hence, a meticulous fine-tuning process was

undertaken for the concentration of anti-NS1 and the duration of binding, ensuring precision in the fabrication of the electrochemical sensor. After incorporating the anti-NS1 solution onto the HSPC/GCE, a noticeable reduction in the DPV current response was observed. This reduction can be attributed to the immobilization of anti-NS1, which reduces the active surface area of the electrode. The concentration of anti-NS1 increased from 1 μg/mL to 10 μg/mL, the corresponding current value also increased as depicted in figure 5.5b. However, the peak current did not exhibit a significant change beyond an antibody concentration of 10 μg/mL. This noted phenomenon can be attributed to the saturation of HSPC surface active sites available for the immobilization of anti-NS1. So, the concentration of 10 μg/mL for the anti-NS1 solution was employed in all succeeding studies.

In order to ascertain the impact of the incubation time, 10 μg/mL of anti-NS1 was drop-cast onto the HSPC/GCE for varying durations, spanning from 15 to 90 minutes. A decline in the DPV current response was observed (figure 5.5c) with an increasing incubation time of up to 60 minutes, indicating saturation of HSPC/GCE binding sites for anti-NS1. Consequently, a 60-minute immobilization period was selected for subsequent investigations. Similarly, the effectiveness of the DENV sensor is significantly impacted by the incubation time of NS1, as a brief duration may hinder the complete binding of NS1 with anti-NS1. As depicted in figure 5.5d, the optimal interaction period for anti-NS1 and NS1 protein was determined to be 60 minutes, and the same duration was used for subsequent experiments.

5.3.2.2 Layer-by-layer studies and analytical performance of the sensor

The layer-by-layer characterization of the developed dengue sensor was conducted after a comprehensive optimization of each layer, utilizing CV and DPV techniques (Figure 5.6 a and b). The current response of HSPC/GCE was significantly higher than that of all other layers, attributable to the increased electrochemical active sites provided by the porous and high surface of the HSPC. The peak current decreased upon immobilizing anti-NS1 on the surface of HSPC/GCE, indicating a reduction in the active surface area of the electrode and suggesting the successful binding of the antibody. Furthermore, the electrochemical response consistently decreases upon

applying a BSA coating on the Anti-NS1/HSPC/GCE surface, suggesting the effective blocking of BSA to the non-specific binding sites of the anti-NS1. Again, the introduction of NS1 protein to the BSA/anti-NS1/HSPC/GCE led to a further reduction in peak current. This observed phenomenon is attributed to the accumulation of NS1 protein layers on the electrode surface after binding with the anti-NS1 protein, which impedes electron transfer across the electrode interface. The results obtained through DPV closely aligned with the outcomes from CV, as depicted in figure 5.6b, and were consistent with the computational studies. This concordance offers additional validation of the successful construction of the dengue biosensor.

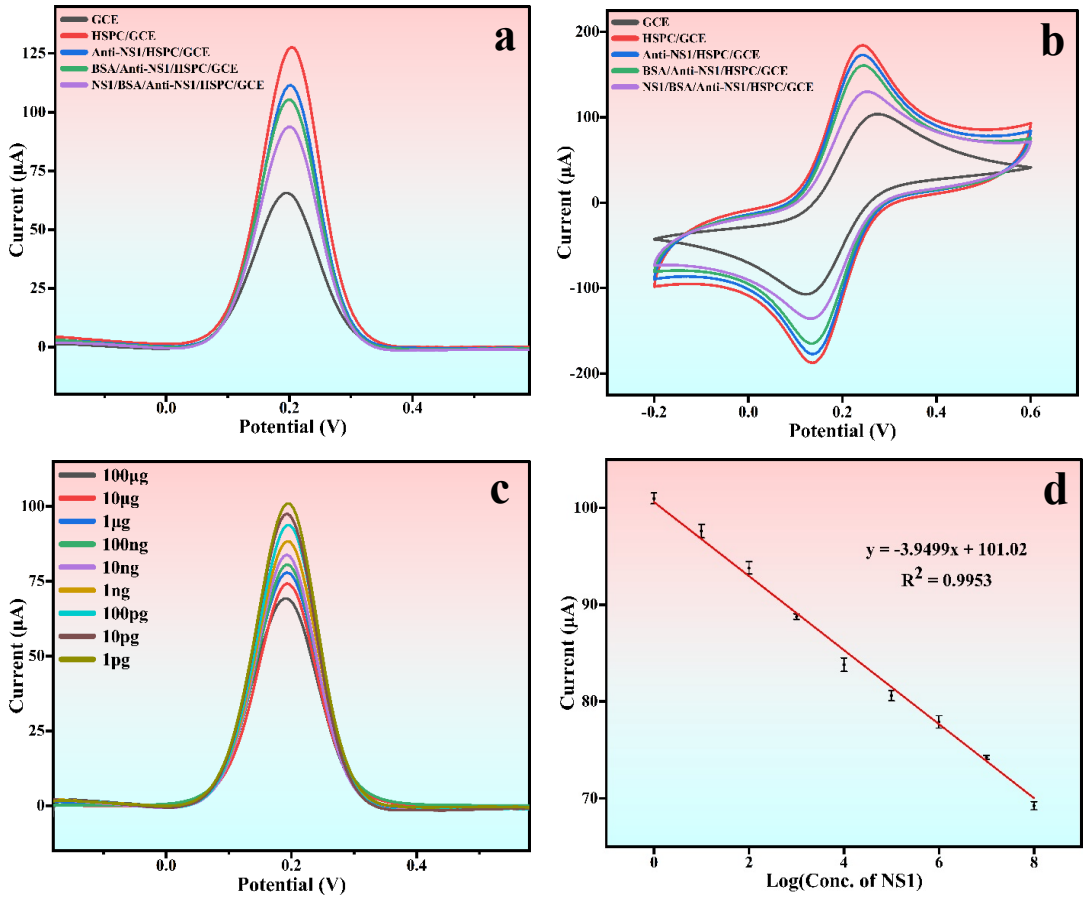

Figure 5.6 *(a) DPV and (b) CV results for each layer (c) DPV curves for different concentration of NS1, (d) Calibration curve of the constructed biosensor.*

Moreover, the analytical response of the developed dengue biosensor was evaluated across a diverse range of NS1 protein concentrations within the optimal working environment. As illustrated in figure 5.6c, the DPV peak current response exhibited a

consistent decline with the escalating concentration of NS1, ranging from 1 pg/mL to 100 µg/mL. According to the computational analysis, the isoelectric point of the NS1 protein and the NS1/BSA/anti-NS1 complex was determined to be 6.069 and 5.988, respectively, carrying a total charge of -13.488 and -31.755, respectively, at pH 7.4. This negatively charged, bulkier protein molecule increases the degree of steric hindrance, which enables effective repulsion of the $[Fe(CN)_6]^{3-/4-}$ anion, thereby hindering its access to the surface of the electrode (Kareem et al. 2024). Additionally, an increase in NS1 protein concentration may result in the formation of a protein layer on the electrode surface, acting as a barrier. The combination of steric hindrance and electrostatic repulsion may further impact the electrochemical behaviour with an increasing concentration of the NS1 protein, potentially reducing current values. Figure 5.6d demonstrates a commendable level of linearity within the range of 100 µg/mL to 1 pg/mL, as evidenced by the graph depicting the logarithm of NS1 concentration against the DPV response. The linear regression equation, y = -3.95x + 101.02, along with a correlation coefficient (R^2) of 0.9953, signifies the high precision in detecting NS1. The limit of detection (LOD) for the DENV biosensor was determined to be 0.665 pg/mL. This sensor demonstrated its efficacy in NS1 detection through its expansive dynamic range and remarkably low detection limit. A comparative analysis with previous studies on DENV detection (Table 5.1) reveals that the developed sensor surpasses them with its broader linear range and outstanding LOD, establishing it as a reliable method for the ultrasensitive detection of DENV NS1 protein.

Table 5.1. *Comparative analysis of sensing performance of dengue NS1 biosensors:*

Materials	**Detection method**	**LOD (g/mL)**	**Linear Range (g/mL)**	**Ref.**
Polyaminophenol-imprinted films	Impedimetric	29.3×10^{-6}	50×10^{-6} to 200×10^{-6}	(Siqueira Silva et al. 2021)
SAMs composed of 16-MHDA	Impedimetric	3×10^{-9}	10×10^{-9} to 2×10^{-6}	(Cecchetto et al. 2017)

Phenylenediamine-indium tin oxide	Fluorescence	15×10^{-9}	15×10^{-9} to 500×10^{-9}	(Darwish et al. 2018)
SAM containing PEG-thiol	Impedimetric	1.2×10^{-9}	5×10^{-9} to 1×10^{-6}	(Santos et al. 2018)
Screen-printed gold electrodes	Electrochemical Lateral Flow	0.5×10^{-9}	1×10^{-9} to 25×10^{-9}	(Sinawang et al. 2016)
Gold electrodes modified with SAM	Impedimetric	0.022×10^{-9}	100×10^{-9} to 10×10^{-12}	(Bachour Junior et al. 2021)
Thin film of carbon nanotube-ethylenediamine	Differential pulse voltammetric	6.8×10^{-9}	20×10^{-9} to 800×10^{-9}	(Mendonça et al. 2021)
Screen-printed carbon electrode	Impedimetric	0.3×10^{-9}	1×10^{-9} to 200×10^{-9}	(Nawaz et al. 2018)
High-surface porous carbon-Polyethylenimine	Differential pulse voltammetric	6.65×10^{-13}	100×10^{-6} to 1×10^{-12}	This work

5.3.2.3 Selectivity, reproducibility, and stability of the DENV sensor

Selectivity or specificity plays a crucial role in the successful implementation of sensors in diagnostic and monitoring applications. Therefore, rigorous testing is essential to evaluate the biosensor's response to potentially interfering substances, helping address any issues related to false positive or negative results (Nawaz et al. 2018). To assess the specificity of the biosensor, an evaluation was conducted by scrutinizing additional biomolecules, including glycine, creatinine, glucose, and cholesterol, at a concentration of 100 pg/mL to identify any potential interferences during the detection step. Figure 5.7a illustrates minimal signal variation between BSA and other interfering biomolecules, while a significant contrast in the DPV peak current was evident when NS1 was employed. The computational study reveals that there was no significant

binding or interaction between Anti-NS1 and glycine, creatinine, glucose, or cholesterol, as the observed binding energies for them are insignificant. Consequently, there were no changes in the effective charge on the protein, leading to negligible alterations in the current value. This underscores the high selectivity of NS1 in the developed biosensor.

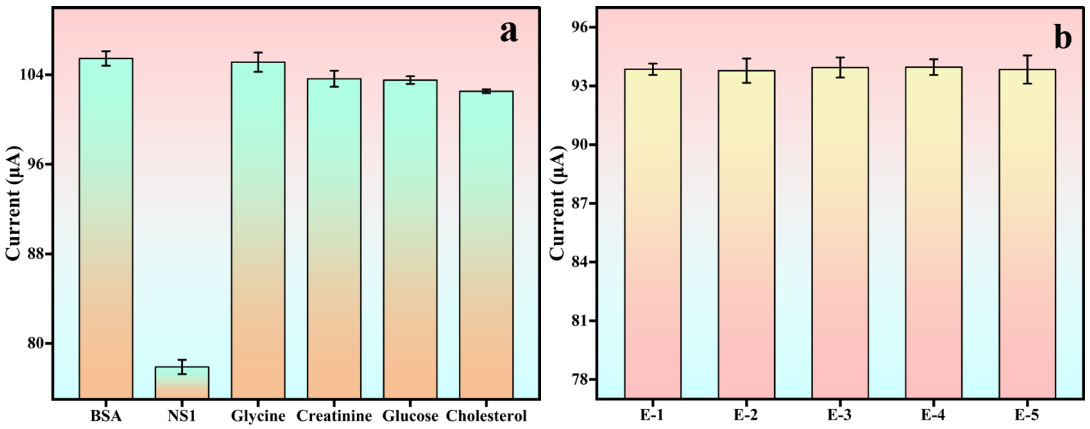

Figure 5.7 *(a) Selectivity, (b) reproducibility studies of the developed DENV sensor*

Furthermore, to assess the efficacy of the constructed DENV sensor, key indicators such as repeatability and long-term stability were examined. Reproducibility was investigated by testing five distinct GC electrodes to detect NS1 at the same concentration (100 pg/mL) under identical experimental conditions, and the results are depicted in figure 5.7b. The calculated standard deviation, amounting to 0.45, indicates the commendable repeatability demonstrated by the fabricated sensor. The assessment of the long-term stability of the immunosensor was carried out by storing the fabricated biosensor in a refrigerator for designated durations. Impressively, even after 5 days of storage, the constructed immunosensor preserved approximately 99.13% of its initial signal. Extending the storage to 11 days showed a DPV current retention of about 96.9%, affirming the exceptional stability of the constructed DENV sensor.

5.3.2.4 Detection of dengue NS1 in human serum: A real sample analysis

Early detection of NS1 in actual blood samples is an essential aspect of an effective management strategy for dengue disease treatment. Hence, a recovery study was conducted by the standard addition method to evaluate the practicability and effectiveness of the constructed dengue biosensor in real blood samples. The human

serum sample was spiked with three different concentrations of a standard NS1 solution. The experimental results are summarized in table 5.2. These findings demonstrate the feasibility and significance of the proposed system for detecting dengue NS1 in actual samples, highlighting the remarkably straightforward and uncomplicated nature of the detection process.

Table 5.2 *Results of the spiked sample analysis*

Spiked concentration (ng/mL)	Detected concentration (ng/mL)	% Recovery	RSD (%)
0.1	0.1036	103.60	1.46
100	98.24	98.24	0.12
100000	992313	99.23	0.72

5.3.3 Computational results

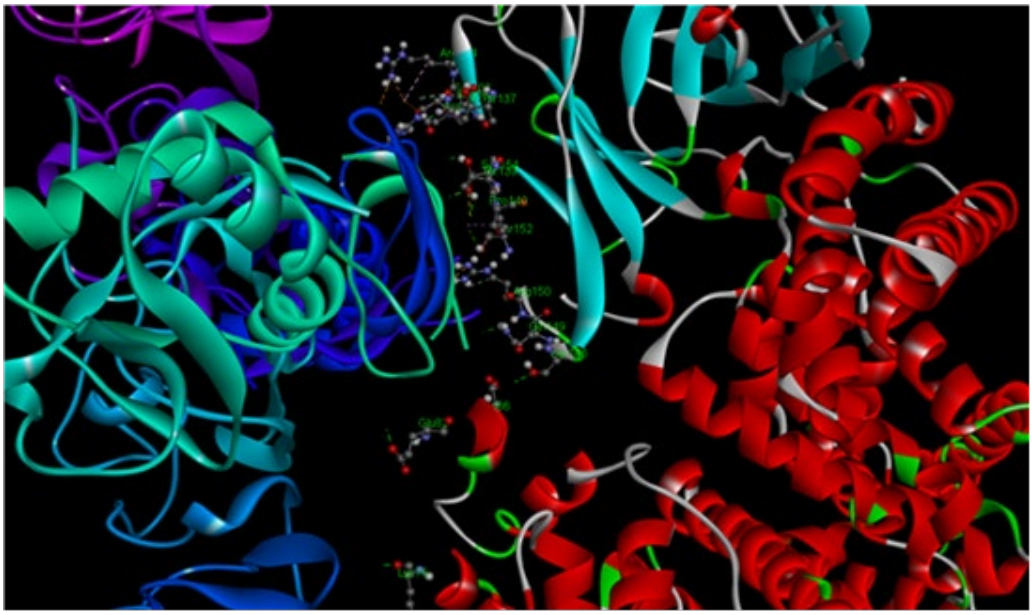

Figure 5.8 *3D docking pose of the anti-NS1-BSA-NS1 complex.*

Protein-protein docking, a computational method, predicts spatial protein interactions, aiding in determining complex structures involving two or more proteins through structural analysis. This study was focused on the interaction between NS1 and anti-NS1 proteins. NS1 protein comprises three significant domains: the hydrophobic β-roll

(dimerization domain, amino acids 1-29), the wing (connector subdomain, amino acids 30-37, and 152-180, α/β subdomain, amino acids 38-151), and the -ladder (amino acids 181-352). These domains play crucial roles in viral RNA replication, DENV production, and the modulation of host immune responses (Chen et al. 2018a). To analyze the interaction between anti-NS1 and NS1, the respective active sites were identified from the crystal structure of anti-NS1 and NS1. Inactive sites of anti-NS1 were blocked using BSA(Chain-A), and the resulting complex was subsequently docked with the active site of the NS1 protein (as illustrated in figure 5.8) to investigate the potential interactions between these proteins and their binding mechanisms. The docking analysis revealed that NS1 docked within the active site of the BSA/anti-NS1 complex with a binding energy of -1034.4 kcal/mol. A total of eleven hydrogen bonds, four salt bridges and 159 non-bonded contacts were identified between BSA(Chain-A) and anti-NS1. The eight amino acids of the NS1(Chain-A) protein: Ser2, Lys11, Glu12, Leu13, Cys15, Cys4, Gly16, and Ser17, form hydrogen bonds with corresponding amino acids from the BSA/anti-NS1: Thr139, Gln149, Arg150, Arg150, Thr152, Ser154, Ser154, and Arg156, respectively, with bond distances of 2.81 Å, 2.78 Å, 2.78 Å, 2.61 Å, 3.23 Å, 3.04 Å, 2.83 Å, and 2.81 Å. The amino acid Glu12 from the NS1(Chain-A) protein form salt bridge with corresponding amino acid Arg150 from the BSA/anti-NS1 with a bond distance of 2.78 Å. Similarly, the three amino acids of the NS1(Chain-B) protein: Gly161, Trp28, and Trp28, form hydrogen bonds with corresponding amino acids from the BSA/anti-NS1: Arg150, Ser203, and Thr205, respectively, with bond distances of 2.69 Å, 2.92 Å, and 2.85 Å. A total of 95 non-bonded contacts were identified between NS1(Chain-A & Chain-B) and the BSA/anti-NS1 complex. Again, two hydrogen bonds, two salt bridges and 21 non-bonded contacts were observed between BSA(Chain-A) and NS1(Chain-A). Both chains of NS1, i.e., Chain-A and Chain-B, interacted with each other and formed 37 hydrogen bonds, two salt bridges, and 373 non-bonded contacts. All the interactions between BSA, anti-NS1, and NS1 are schematically illustrated in figure 5.8. Furthermore, docking studies involving BSA/anti-NS1 with glucose, glycine, creatinine, and cholesterol were conducted to confirm the selective binding mechanism of

BSA/antiNS1 with NS1. The binding energy for these complexes are summarized in table 5.3.

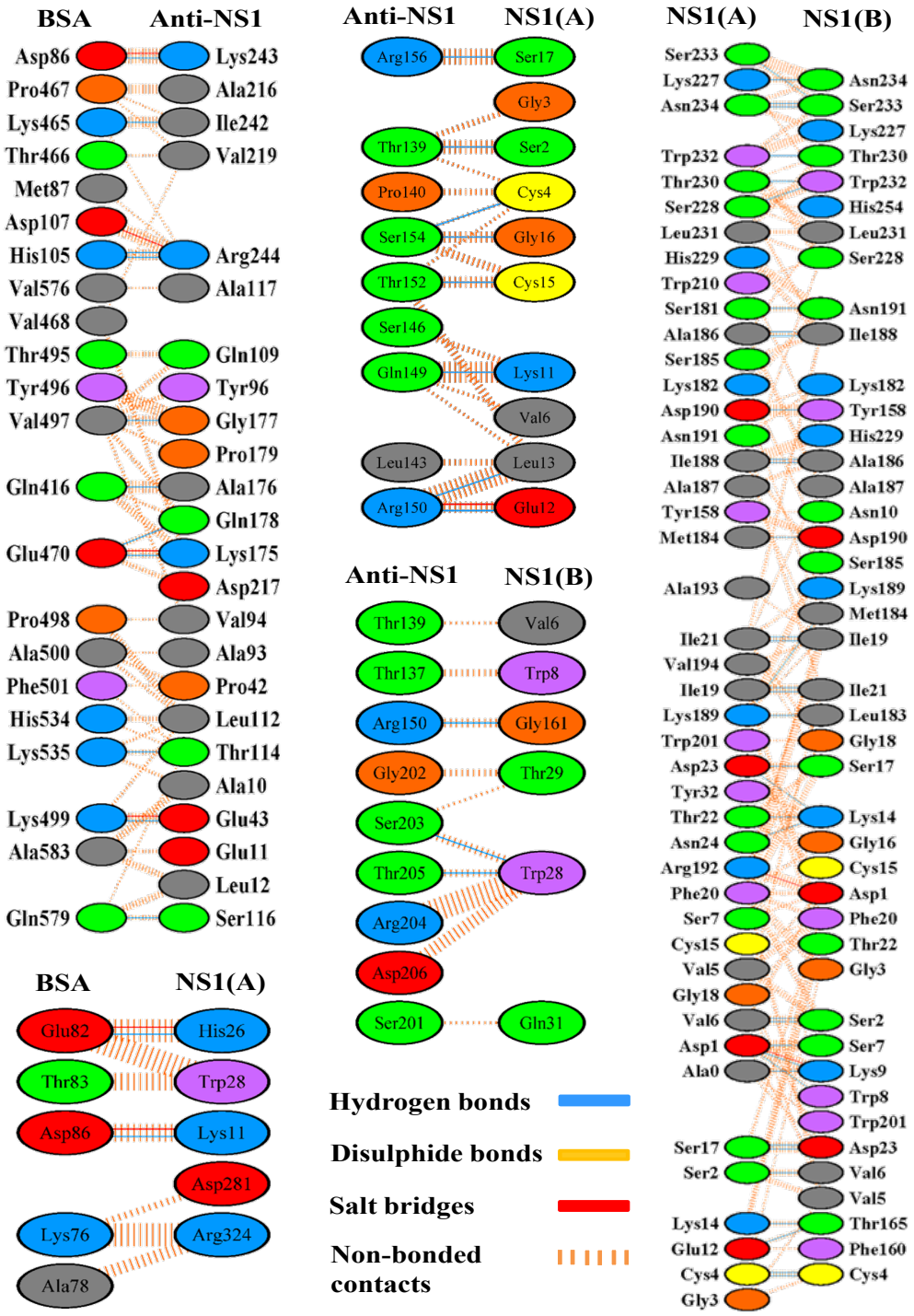

Figure 5.8 *Interactions of active site amino acid residues of BSA/anti-NS1 complex with the active site amino acid residues of NS1 protein.*

The isoelectric point (pI) and charge on the protein or complex play a crucial role, especially in the electrochemical sensing platform, as they are pH-dependent. The pH of a protein's environment affects its net charge relative to its isoelectric point (pI), wherein at pI, the protein carries no net charge due to a balance between positive and negative charges. However, when the pH is below the pI, the protein tends to become positively charged due to excess protons. Conversely, when the pH is above the pI, the protein tends to be negatively charged because there is a relative deficit of protons. Therefore, identifying pI and charge on the protein/complex at a specific pH is crucial to confirm the sensor's electrochemical response. To facilitate comparative analysis, pI and charge of anti-NS1, BSA, NS1, BSA/anti-NS1, NS1/BSA/anti-NS1, and BSA/anti-NS1 with other biomolecules such as glucose, glycine, creatinine, and cholesterol complexes were computationally studied, and the values are summarized in table 5.3. Notably, all the complexes are negatively charged since their pI values are lower than the pH 7.4.

Table 5.3 *Binding energy, charge, and isoelectric point of the protein/complex.*

Protein or Complex	**Binding energy (kcal/mol)**	**Isoelectric point (pI)**	**Charge (Z) at pH 7.4**
anti-NS1	-	7.854	+1.084
BSA	-	5.694	-20.228
NS1	-	6.069	-13.488
BSA/anti-NS1	-708.40	5.920	-18.436
NS1/BSA/anti-NS1	-1034.4	5.988	-31.755
Glucose/BSA/anti-NS1	-6.7	5.920	-18.436
Glycine/ BSA/anti-NS1	-4.0	5.920	-18.436
Creatinine/ BSA/anti-NS1	-5.2	5.920	-18.436
Cholesterol/BSA/anti-NS1	-8.6	5.920	-18.436

When the protein analyte binds to the receptor, it changes the charge density either on the electrode surface or in the solution adjacent to it. This alteration in charge density can influence the movement of electron transfer reactions at the electrode, consequently impacting the measured current. The experimental findings clearly show that the binding of NS1 to BSA/anti-NS1 causes a decrease in the measured current. This decrease is attributed to the increased negative charge of the NS1/BSA/anti-NS1 complex. Consequently, there is heightened repulsion between the electrode and the complex, leading to a reduction in electron transfer at the electrode interface. However, when glucose, glycine, creatinine, or cholesterol were drop-casted to the surface of BSA/anti-NS1, there was only a negligible change in current. This minimal effect occurs because there is no alteration in the net charge or isoelectric point of the BSA/anti-NS1 with glucose, glycine, creatinine, and cholesterol systems. This lack of change is primarily because these analyte molecules are neutral and bind to the surface of BSA/anti-NS1 with negligibly lower binding energy than NS1. Thus, the theoretical analyses closely align with the experimental findings.

5.4 CONCLUSIONS

This study presents a comprehensive investigation into the development of a novel electrochemical biosensor for the early detection of dengue virus NS1 protein. Leveraging the distinctive properties of high-surface porous carbon (HSPC), synthesized through a cost-effective and straightforward method using *Tamarindus indica* seeds, the study achieved remarkable advancements in dengue diagnostics. Structural and morphological characterizations elucidated the unique properties of HSPC, including its porous structure and high surface area (747 m^2/g), providing ample opportunity for biomolecular interactions at the nanoscale, which are pivotal for enhanced electrochemical performance. Layer-by-layer construction and optimization efforts further refined the sensor's performance, unveiling remarkable results: a 51.16% increase in the effective electroactive surface area upon HSPC modification, setting the stage for enhanced electrocatalytic activity. Optimization studies for biomolecule concentration and incubation time meticulously crafted a sensor capable of detecting NS1 protein concentrations as low as 0.665 pg/mL, pushing the boundaries of

sensitivity to unprecedented levels. The analytical performance of the developed biosensor exhibited a broad linear range of 100 µg/mL to 1 pg/mL. Selectivity studies, coupled with computational insights, showcased the biosensor's prowess in distinguishing NS1 protein from potential interfering substances, laying the foundation for reliable diagnostics in complex biological matrices. Moreover, the biosensor exhibited exceptional reproducibility with multiple electrodes and remarkable long-term stability. Real sample analysis using human serum spiked with NS1 protein confirmed the biosensor's efficacy in detecting dengue virus in clinical samples, thereby highlighting its potential as a valuable tool for early diagnosis and effective management of dengue infections. In essence, the presented biosensor offers a promising solution to address the pressing need for rapid and accurate detection of dengue virus infections, with implications for improving patient outcomes and controlling disease spread on a global scale.

****

CHAPTER 6

SUMMARY AND CONCLUSIONS

Abstract: This chapter summarizes the key points of the thesis and offers concluding remarks, as well as providing an overview of future research directions.

6.1 SUMMARY OF RESEARCH WORK

Figure 6.1 *Schematic representation of synthesis of Tectona grandis sawdust-derived porous carbon.*

Initially, a simple, cost-effective, and straightforward method was utilized to produce porous carbon, employing *Tectona grandis* sawdust as the initial biomass source. This process involves treating the biomass with $FeCl_3$ for carbonization, followed by KOH activation. The activation method was carried out at temperatures ranging from 650 to 850 °C and characterized comprehensively. Structural analysis via XRD, Raman, and FTIR revealed a progressive enhancement in graphitic structure and reduction of

functional groups with increasing activation temperature. The FESEM analysis reveals the presence of enormous hollow tube-like porous networks in the *Tectona grandis* sawdust-derived porous carbon (TPC) samples. BET analysis showed a specific surface area of 1768 m^2/g and corresponding pore volumes (at $P/P_0 = 0.99$) of 1.43 cm^3/g for TPC-850. With these unique properties, TPCs demonstrated an excellent electrochemical energy storage capacity with a high specific capacitance (572 F/g at 0.5 A/g) at a potential range of 0 to -1.0 V in a 6.0 M KOH solution. Significantly, TPC-850 demonstrated remarkable electrochemical cyclic stability, retaining 95.83% of its initial capacity even after undergoing 4,500 cycles at a scan rate of 500 mV/s. The findings underscore the viability of TPC-850 as a high-performance supercapacitor electrode material, providing insights into harnessing renewable resources for advanced energy solutions. This work highlighted the potential of utilizing waste biomass for energy storage applications and demonstrated the feasibility of converting it into efficient porous carbon materials with substantial graphitization and porosity.

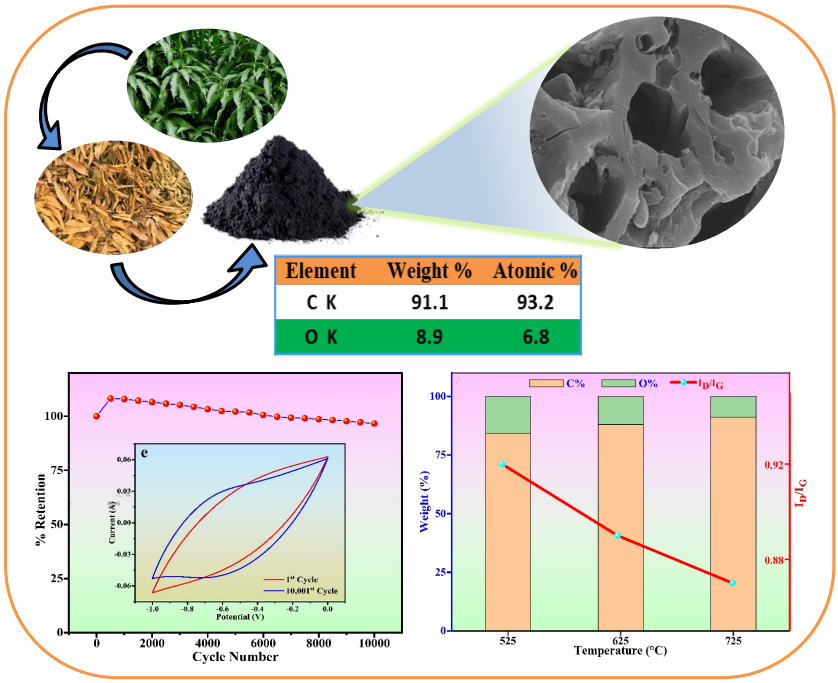

Figure 6.2 *Overview of Mangifera indica leaf-derived carbon for supercapacitor application.*

Following that, the *Mangifera indica* leaf waste-derived activated carbon has been investigated as an electrode material for high-performance supercapacitors. The dried

Mangifera indica leaves were first carbonized and then activated to increase their surface area and pore structure at different temperatures. The activated carbon prepared at 725 °C has shown a high specific capacitance of 521.65 F/g at a current density of 0.5 A/g and also achieved an energy density of 17 Wh/kg at a power density of 243 W/kg in the 6 M KOH electrolyte. Significantly, it has demonstrated remarkable electrochemical cyclic stability, retaining 96.60% of its initial capacity even after undergoing 10,001 cycles at a scan rate of 500 mV/s. The superior electrochemical performance of the activated carbon was attributed to its high surface area of 1233 m^2/g, well-distributed pore size, and excellent degree of graphitization, which all facilitate the rapid diffusion of ions and enhance the accessibility of the electrolyte to the electrode surface.

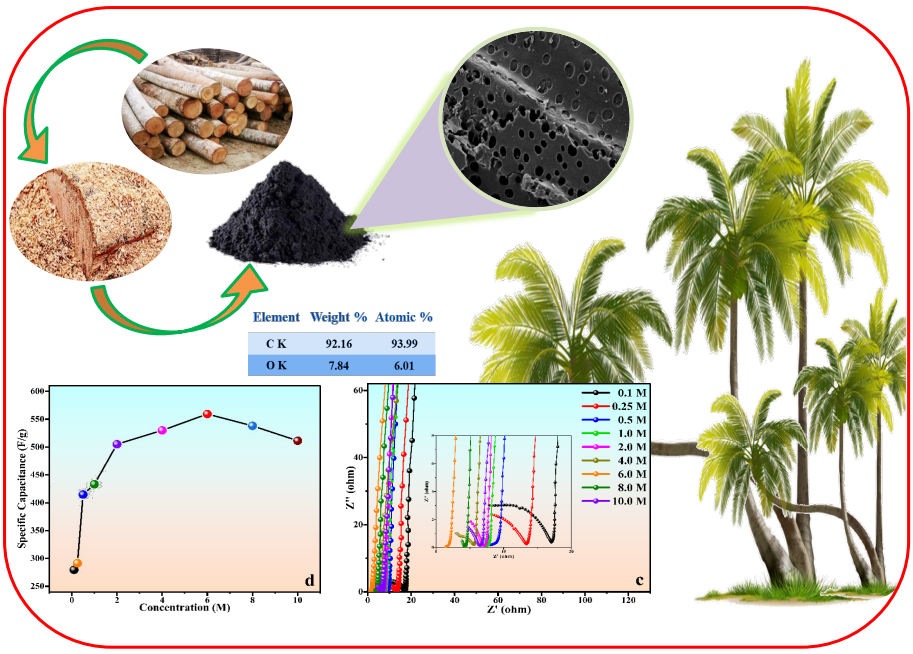

Figure 6.3 *Graphical illustration of Cocos nucifera trunk sawdust-derived carbon for supercapacitor application.*

Subsequently, the development of supercapacitor electrode was carried out by harnessing the untapped potential of *Cocos nucifera* trunk sawdust-derived high-surface carbon (CHSC). Through a meticulous process involving $ZnCl_2$ treatment and KOH activation at varying temperatures, CHSC-700 emerged as a standout electrode material with exceptional structural characteristics, boasting enhanced graphitization

and a specific surface area of 1154 m^2/g. Furthermore, the study delved into the critical role of electrolyte concentration, unraveling its significant impact on the electrochemical behavior of the CHSC electrodes. To explore the importance of electrolyte concentrations, a systematic examination was conducted under varying concentrations of aqueous potassium hydroxide, ranging from 0.1 M to 10.0 M. This systematic exploration revealed that a 6 M KOH electrolyte concentration as the optimal choice, fostering superior ion diffusion, charge transfer, and overall electrochemical performance. Notably, the CHSC-700 electrode, when tested in a 6 M KOH electrolyte, achieved a specific capacitance of 559.27 F/g at a current density of 0.5 A/g and also displayed excellent cyclic stability, retaining approximately 97.22% capacitance after an extensive 9501 cycles. Furthermore, the Ragone plot showcased the impressive energy and power density of 19 Wh/kg and 247 W/kg, respectively, at a current density of 0.5 A/g in 6 M KOH. These findings held promise for the sustainable development of energy storage technologies, highlighting the potential of biomass waste as a renewable carbon source and emphasizing the importance of tailored electrolyte conditions for superior supercapacitor performance.

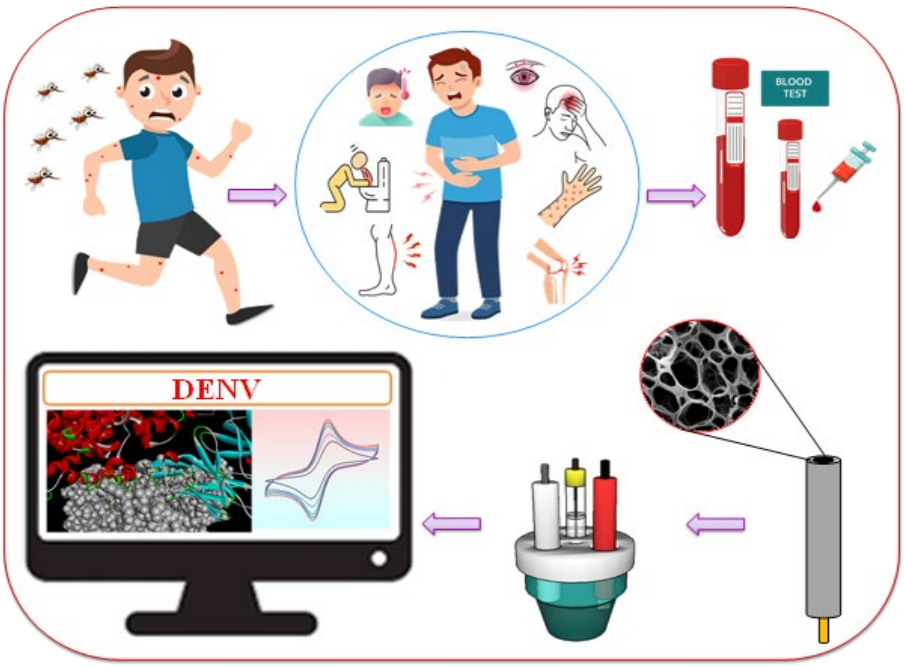

Figure 6.4 *Cartoon representation of dengue disease and electrochemical dengue biosensor.*

Then, a comprehensive investigation was carried out to develop a novel electrochemical biosensor for the early detection of dengue virus NS1 protein. Leveraging the distinctive properties of high-surface porous carbon (HSPC), synthesized through a straightforward method using *Tamarindus indica* seeds, the study achieved remarkable advancements in dengue diagnostics. Structural and morphological characterizations elucidated the unique properties of HSPC, including its porous structure and high surface area (747 m^2/g), providing ample opportunity for biomolecular interactions at the nanoscale, which are pivotal for enhanced electrochemical performance. Layer-by-layer construction and optimization efforts further refined the sensor's performance, unveiling remarkable results: a 51.16% increase in the effective electroactive surface area upon HSPC modification, setting the stage for enhanced electrocatalytic activity. Optimization studies for biomolecule concentration and incubation time meticulously crafted a sensor capable of detecting NS1 protein concentrations as low as 0.665 pg/mL, pushing the boundaries of sensitivity to unprecedented levels. The analytical performance of the developed biosensor exhibited a broad linear range of 100 µg/mL to 1 pg/mL. Selectivity studies, coupled with computational insights, showcased the biosensor's prowess in distinguishing NS1 protein from potential interfering substances, laying the foundation for reliable diagnostics in complex biological matrices. Moreover, the biosensor exhibited exceptional reproducibility with multiple electrodes and remarkable long-term stability. Real sample analysis using human serum spiked with NS1 protein confirmed the biosensor's efficacy in detecting dengue virus in clinical samples, thereby highlighting its potential as a valuable tool for early diagnosis and effective management of dengue infections. In essence, the presented biosensor offered a promising solution to address the pressing need for rapid and accurate detection of dengue virus infections, with implications for improving patient outcomes and controlling disease spread on a global scale.

6.2 CONCLUSIONS

The journey through the innovative utilization of diverse biomass sources to engineer high-performance electrode materials and advanced biosensors has illuminated the path toward sustainable energy solutions and improved healthcare diagnostics. Through

innovative methodologies and meticulous characterization, porous carbon materials derived from various biomass sources have been tailored to exhibit exceptional electrochemical properties, setting new benchmarks in supercapacitor performance. From the initial exploration of *Tectona grandis* sawdust-derived porous carbon (TPC) to the refined synthesis of *Mangifera indica* leaf waste-derived activated carbon (MLAC) and *Cocos nucifera* trunk sawdust-derived high-surface carbon (HSPC), each step has showcased the transformative potential of converting renewable resources into porous carbon materials with tailored properties. These materials have not only exhibited exceptional electrochemical performance, marked by high specific capacitances, impressive cyclic stabilities, and superior energy densities, but have also underscored the importance of meticulous optimization and tailored electrolyte conditions in maximizing their potential. Furthermore, the development of a novel electrochemical biosensor utilizing high-surface porous carbon synthesized from *Tamarindus indica* seeds showcases the versatility of biomass-derived carbon in biosensing applications, particularly in the sensitive and selective detection of the dengue virus NS1 protein. The biosensor's exceptional sensitivity, broad linear range, selectivity, reproducibility, and long-term stability offer a promising solution to the urgent need for rapid and accurate detection of dengue virus infections, with potential implications for enhancing patient outcomes and controlling disease spread globally.

These findings underscore the immense potential of converting waste biomass into value-added carbon materials, thereby contributing to environmental sustainability and technological innovation in energy storage and biosensing realms. Collectively, these endeavors highlight the synergy between materials science, renewable resource utilization, and technology in addressing pressing societal challenges. As we continue to innovate and collaborate toward a greener future, the potential for transformative impact in the energy and healthcare sectors remains boundless.

6.3 FUTURE WORK

The research findings demonstrated the feasibility of utilizing *Tectona grandis* sawdust, *Mangifera indica* leaves, *Cocos nucifera* trunk sawdust, and *Tamarindus indica* seeds; further research could explore various biomass sources. Investigating different

agricultural, forestry, and food waste types could unveil novel carbon precursors with unique structural and chemical properties, potentially leading to materials with enhanced electrochemical performance and biosensing capabilities. Future studies could delve deeper into optimizing the activation methods and conditions to tailor the porous carbon materials' porosity, surface chemistry, and electrochemical properties. Further, composite materials could be synthesized and characterized by combining porous carbon with conductive polymers, metal oxides, or other nanomaterials to enhance the overall electrochemical performance and sensing capabilities. Future research could focus on developing cost-effective and scalable synthesis routes compatible with large-scale manufacturing processes, paving the way for the commercialization and widespread adoption of these materials in various other applications as well.

****

REFERENCES

Adeniyi, A. G., Iwuozor, K. O., Emenike, E. C., Ajala, O. J., Ogunniyi, S., and Muritala, K. B. (2024). "Thermochemical co-conversion of biomass-plastic waste to biochar: a review." *Green Chem. Eng.*, 5(1), 31–49.

Adhikari, S., Nam, H., and Chakraborty, J. P. (2018). "Conversion of Solid Wastes to Fuels and Chemicals Through Pyrolysis." *Waste Biorefinery*, Elsevier, 239–263.

Adoor, P., Hegde, S. S., Bhat, B. R., Yethadka, S. N., and Yeenduguli, R. (2023). "Elucidating the Role of Copper-Induced Mixed Phases on the Electrochemical Performance of Mn-Based Thin-Film Electrodes." *ACS Omega*, 8(49), 46640–46652.

Afaque Ansari, M., Juen Liew, W., Padmakumari Kurup, C., and Ahmed, M. U. (2023). "Label-free electrochemical aptasensor for ultrasensitive thrombin detection using graphene nanoplatelets and carbon nano onion-based nanocomposite." *J. Electroanal. Chem.*, 937, 117422.

Ahirrao, D. J., Tambat, S., Pandit, A. B., and Jha, N. (2019). "Sweet-Lime-Peels-Derived Activated-Carbon-Based Electrode for Highly Efficient Supercapacitor and Flow-Through Water Desalination." *ChemistrySelect*, 4(9), 2610–2625.

Akey, D. L., Brown, W. C., Dutta, S., Konwerski, J., Jose, J., Jurkiw, T. J., DelProposto, J., Ogata, C. M., Skiniotis, G., Kuhn, R. J., and Smith, J. L. (2014). "Flavivirus NS1 Structures Reveal Surfaces for Associations with Membranes and the Immune System." *Science (80-.).*, 343(6173), 881–885.

Amalina, F., Razak, A. S. A., Krishnan, S., Sulaiman, H., Zularisam, A. W., and Nasrullah, M. (2022). "Biochar production techniques utilizing biomass waste-derived materials and environmental applications – A review." *J. Hazard. Mater. Adv.*, 7, 100134.

Andreata-Santos, R., Pereira, S. S., Pereira, L. R., Félix, A. C., Romano, C. M., and Ferreira, L. C. de S. (2020). "Specificity of NS1-based immunochromatographic tests for dengue virus with regard to the Zika virus protein." *Int. J. Infect. Dis.*, 95, 276–278.

Anil Kumar, Y., Sambasivam, S., Ahmed Hira, S., Zeb, K., Uddin, W., Krishna, T. N. V., Dasha Kumar, K., Obaidat, I. M., and Kim, H.-J. (2020). "Boosting the energy density of highly efficient flexible hybrid supercapacitors via selective integration of hierarchical nanostructured energy materials." *Electrochim. Acta*, 364, 137318.

Anusha, J. R., Kim, B. C., Yu, K.-H., and Raj, C. J. (2019). "Electrochemical biosensing of mosquito-borne viral disease, dengue: A review." *Biosens. Bioelectron.*, 142, 111511.

Arni, S. Al. (2018). "Comparison of slow and fast pyrolysis for converting biomass into fuel." *Renew. Energy*, 124, 197–201.

Ashley, E. A. (2011). “Dengue fever.” *Trends Anaesth. Crit. Care*, 1(1), 39–41.

Ashraf, C. M., Anilkumar, K. M., Jinisha, B., Manoj, M., Pradeep, V. S., and Jayalekshmi, S. (2018). “Acid Washed, Steam Activated, Coconut Shell Derived Carbon for High Power Supercapacitor Applications.” *J. Electrochem. Soc.*, 165(5), A900–A909.

Bachour Junior, B., Batistuti, M. R., Pereira, A. S., Sousa Russo, E. M. de, and Mulato, M. (2021). “Electrochemical aptasensor for NS1 detection: Towards a fast dengue biosensor.” *Talanta*, 233, 122527.

Balahmar, N., Al-Jumialy, A. S., and Mokaya, R. (2017). “Biomass to porous carbon in one step: directly activated biomass for high performance CO 2 storage.” *J. Mater. Chem. A*, 5(24), 12330–12339.

Baroroh, S.Si., M.Biotek., U., Muscifa, Z. S., Destiarani, W., Rohmatullah, F. G., and Yusuf, M. (2023). “Molecular interaction analysis and visualization of protein-ligand docking using Biovia Discovery Studio Visualizer.” *Indones. J. Comput. Biol.*, 2(1), 22.

Bessaud, M., Pastorino, B. A. M., Peyrefitte, C. N., Rolland, D., Grandadam, M., and Tolou, H. J. (2006). “Functional characterization of the NS2B/NS3 protease complex from seven viruses belonging to different groups inside the genus Flavivirus.” *Virus Res.*, 120(1–2), 79–90.

Bhakat, S., Karubiu, W., Jayaprakash, V., and Soliman, M. E. S. (2014). “A perspective on targeting non-structural proteins to combat neglected tropical diseases: Dengue, West Nile and Chikungunya viruses.” *Eur. J. Med. Chem.*, 87, 677–702.

Bhattacharya, M. K., Maitra, S., Ganguly, A., Bhattacharya, A., and Sinha, A. (2013). “Dengue: a growing menace -- a snapshot of recent facts, figures & remedies.” *Int. J. Biomed. Sci.*, 9(2), 61–7.

Bi, Z., Kong, Q., Cao, Y., Sun, G., Su, F., Wei, X., Li, X., Ahmad, A., Xie, L., and Chen, C.-M. (2019). “Biomass-derived porous carbon materials with different dimensions for supercapacitor electrodes: a review.” *J. Mater. Chem. A*, 7(27), 16028–16045.

Cafferata, M. L., Bardach, A., Rey-Ares, L., Alcaraz, A., Cormick, G., Gibbons, L., Romano, M., Cesaroni, S., and Ruvinsky, S. (2013). “Dengue Epidemiology and Burden of Disease in Latin America and the Caribbean: A Systematic Review of the Literature and Meta-Analysis.” *Value Heal. Reg. Issues*, 2(3), 347–356.

Cao, M., Liu, Y., Sun, K., Li, H., Lin, X., Zhang, P., Zhou, L., Wang, A., Mehdi, S., Wu, X., Jiang, J., and Li, B. (2022). “Coupling Fe 3 C Nanoparticles and N-Doping on Wood-Derived Carbon to Construct Reversible Cathode for Zn–Air Batteries.” *Small*, 18(26).

Cecchetto, J., Fernandes, F. C. B., Lopes, R., and Bueno, P. R. (2017). “The capacitive sensing of NS1 Flavivirus biomarker.” *Biosens. Bioelectron.*, 87, 949–956.

Chakravarti, A., Matlani, M., Kashyap, B., and Kumar, A. (2012). "Awareness of changing trends in epidemiology of dengue fever is essential for epidemiological surveillance." *Indian J. Med. Microbiol.*, 30(2), 222–226.

Chang, B., Guo, Y., Li, Y., Yin, H., Zhang, S., Yang, B., and Dong, X. (2015a). "Graphitized hierarchical porous carbon nanospheres: simultaneous activation/graphitization and superior supercapacitance performance." *J. Mater. Chem. A*, 3(18), 9565–9577.

Chang, B., Yang, B., Guo, Y., Wang, Y., and Dong, X. (2015b). "Preparation and enhanced supercapacitance performance of porous carbon spheres with a high degree of graphitization." *RSC Adv.*, 5(3), 2088–2095.

Chen, H.-R., Lai, Y.-C., and Yeh, T.-M. (2018a). "Dengue virus non-structural protein 1: a pathogenic factor, therapeutic target, and vaccine candidate." *J. Biomed. Sci.*, 25(1), 58.

Chen, H., Guo, Y., Wang, F., Wang, G., Qi, P., Guo, X., Dai, B., and Yu, F. (2017). "An activated carbon derived from tobacco waste for use as a supercapacitor electrode material." *New Carbon Mater.*, 32(6), 592–599.

Chen, W., Yu, H., Lee, S.-Y., Wei, T., Li, J., and Fan, Z. (2018b). "Nanocellulose: a promising nanomaterial for advanced electrochemical energy storage." *Chem. Soc. Rev.*, 47(8), 2837–2872.

Choi, J., Zequine, C., Bhoyate, S., Lin, W., Li, X., Kahol, P., and Gupta, R. (2019). "Waste Coffee Management: Deriving High-Performance Supercapacitors using Nitrogen-Doped Coffee-Derived Carbon." *C*, 5(3), 44.

Cockburn, J. J. B., Navarro Sanchez, M. E., Fretes, N., Urvoas, A., Staropoli, I., Kikuti, C. M., Coffey, L. L., Arenzana Seisdedos, F., Bedouelle, H., and Rey, F. A. (2012). "Mechanism of Dengue Virus Broad Cross-Neutralization by a Monoclonal Antibody." *Structure*, 20(2), 303–314.

Cousins, K. R. (2005). "ChemDraw Ultra 9.0. CambridgeSoft, 100 CambridgePark Drive, Cambridge, MA 02140. www. cambridgesoft.com. See Web site for pricing options." *J. Am. Chem. Soc.*, 127(11), 4115–4116.

Dai, X., Zhang, M., Li, T., Cui, X., Shi, Y., Zhu, X., Wangyang, P., Yang, D., and Li, J. (2022). "Effect of current on electrodeposited MnO2 as supercapacitor and lithium-ion battery electrode." *Vacuum*, 195, 110692.

Darwish, N. T., Alias, Y. B., and Khor, S. M. (2015). "An introduction to dengue-disease diagnostics." *TrAC Trends Anal. Chem.*, 67, 45–55.

Darwish, N. T., Sekaran, S. D., Alias, Y., and Khor, S. M. (2018). "Immunofluorescence–based biosensor for the determination of dengue virus NS1 in clinical samples." *J. Pharm. Biomed. Anal.*, 149, 591–602.

Dhyani, V., and Bhaskar, T. (2018). "A comprehensive review on the pyrolysis of lignocellulosic biomass." *Renew. Energy*, 129, 695–716.

Ding, C., Liu, T., Yan, X., Huang, L., Ryu, S., Lan, J., Yu, Y., Zhong, W.-H., and Yang, X. (2020). "An Ultra-microporous Carbon Material Boosting Integrated Capacitance for Cellulose-Based Supercapacitors." *Nano-Micro Lett.*, 12(1), 63.

Dini, A., Hassankashi, A., Pirouzi, S., Lehtonen, M., Arandian, B., and Baziar, A. A. (2022). "A flexible-reliable operation optimization model of the networked energy hubs with distributed generations, energy storage systems and demand response." *Energy*, 239, 121923.

Dong, S., He, X., Zhang, H., Xie, X., Yu, M., Yu, C., Xiao, N., and Qiu, J. (2018). "Surface modification of biomass-derived hard carbon by grafting porous carbon nanosheets for high-performance supercapacitors." *J. Mater. Chem. A*, 6(33), 15954–15960.

Elgrishi, N., Rountree, K. J., McCarthy, B. D., Rountree, E. S., Eisenhart, T. T., and Dempsey, J. L. (2018). "A Practical Beginner's Guide to Cyclic Voltammetry." *J. Chem. Educ.*, 95(2), 197–206.

Ello, A. S., Souza, L. K. C. de, Trokourey, A., and Jaroniec, M. (2013). "Development of microporous carbons for CO2 capture by KOH activation of African palm shells." *J. CO2 Util.*, 2, 35–38.

Ferrero, G. A., Fuertes, A. B., and Sevilla, M. (2015a). "N-doped porous carbon capsules with tunable porosity for high-performance supercapacitors." *J. Mater. Chem. A*, 3(6), 2914–2923.

Ferrero, G. A., Fuertes, A. B., and Sevilla, M. (2015b). "From Soybean residue to advanced supercapacitors." *Sci. Rep.*, 5(1), 16618.

Figueiredo, A., Vieira, N. C. S., Santos, J. F. dos, Janegitz, B. C., Aoki, S. M., Junior, P. P., Lovato, R. L., Nogueira, M. L., Zucolotto, V., and Guimarães, F. E. G. (2015). "Electrical Detection of Dengue Biomarker Using Egg Yolk Immunoglobulin as the Biological Recognition Element." *Sci. Rep.*, 5(1), 7865.

Fiser, A., Do, R. K. G., and Šali, A. (2000). "Modeling of loops in protein structures." *Protein Sci.*, 9(9), 1753–1773.

Forouzandeh, P., Kumaravel, V., and Pillai, S. C. (2020). "Electrode Materials for Supercapacitors: A Review of Recent Advances." *Catalysts*, 10(9), 969.

"FTIR Functional Group Database Table with Search - InstaNANO." (2023). <https://instanano.com/all/characterization/ftir/ftir-functional-group-search/> (Nov. 10, 2023).

Gadipelli, S., Howard, C. A., Guo, J., Skipper, N. T., Zhang, H., Shearing, P. R., and Brett, D. J. L. (2020). "Superior Multifunctional Activity of Nanoporous Carbons with Widely Tunable Porosity: Enhanced Storage Capacities for Carbon-Dioxide, Hydrogen, Water, and Electric Charge." *Adv. Energy Mater.*, 10(9), 1903649.

Gayathiri, M., Pulingam, T., Lee, K. T., Mohd Din, A. T., Kosugi, A., and Sudesh, K. (2023). "Sustainable oil palm trunk fibre based activated carbon for the adsorption of

methylene blue." *Sci. Rep.*, 13(1), 22137.

GILLIAM, R., GRAYDON, J., KIRK, D., and THORPE, S. (2007). "A review of specific conductivities of potassium hydroxide solutions for various concentrations and temperatures." *Int. J. Hydrogen Energy*, 32(3), 359–364.

Grieshaber, D., MacKenzie, R., Vörös, J., and Reimhult, E. (2008). "Electrochemical Biosensors - Sensor Principles and Architectures." *Sensors*, 8(3), 1400–1458.

Guo, N., Li, M., Wang, Y., Sun, X., Wang, F., and Yang, R. (2016). "Soybean Root-Derived Hierarchical Porous Carbon as Electrode Material for High-Performance Supercapacitors in Ionic Liquids." *ACS Appl. Mater. Interfaces*, 8(49), 33626–33634.

Gururani, P., Bhatnagar, P., Bisht, B., Jaiswal, K. K., Kumar, V., Kumar, S., Vlaskin, M. S., Grigorenko, A. V., and Rindin, K. G. (2022). "Recent advances and viability in sustainable thermochemical conversion of sludge to bio-fuel production." *Fuel*, 316, 123351.

Halstead, S. B. (2002). "Dengue." *Curr. Opin. Infect. Dis.*, 15(5), 471–476.

He, D., Zhao, W., Li, P., Liu, Z., Wu, H., Liu, L., Han, K., Liu, L., Wan, Q., Butt, F. K., and Qu, X. (2019). "Bifunctional biomass-derived 3D nitrogen-doped porous carbon for oxygen reduction reaction and solid-state supercapacitor." *Appl. Surf. Sci.*, 465, 303–312.

He, X., Geng, Y., Qiu, J., Zheng, M., Long, S., and Zhang, X. (2010). "Effect of activation time on the properties of activated carbons prepared by microwave-assisted activation for electric double layer capacitors." *Carbon N. Y.*, 48(5), 1662–1669.

Hegde, S. S., and Bhat, B. R. (2022). "Dengue detection: Advances and challenges in diagnostic technology." *Biosens. Bioelectron. X*, 10, 100100.

Hegde, S. S., and Bhat, B. R. (2023). "Solid Waste-Derived Carbon Materials for Electrochemical Capacitors." *Sustain. Mater. Electrochem. Capacit.*, Wiley, 19–31.

Hegde, S. S., and Bhat, B. R. (2024a). "Sustainable energy storage: Mangifera indica leaf waste-derived activated carbon for long-life, high-performance supercapacitors." *RSC Adv.*, 14(12), 8028–8038.

Hegde, S. S., and Bhat, B. R. (2024b). "Biomass waste-derived porous graphitic carbon for high-performance supercapacitors." *J. Energy Storage*, 76, 109818.

Hopkins, E., Sanvictores, T., and Sharma, S. (2024). "Physiology, Acid Base Balance." Treasure Island (FL).

Hu, W., Xiang, R., Lin, J., Cheng, Y., and Lu, C. (2021). "Lignocellulosic Biomass-Derived Carbon Electrodes for Flexible Supercapacitors: An Overview." *Materials (Basel).*, 14(16), 4571.

Huo, S., Zhao, Y., Zong, M., Liang, B., Zhang, X., Khan, I. U., and Li, K. (2020). "Enhanced supercapacitor and capacitive deionization boosted by constructing inherent N and P external defects in porous carbon framework with a hierarchical porosity."

Electrochim. Acta, 353, 136523.

Izuan Abdul Rashid, J., and Azah Yusof, N. (2018). "Laboratory Diagnosis and Potential Application of Nucleic Acid Biosensor Approach for Early Detection of Dengue Virus Infections." *Biosci. Biotechnol. Res. Asia*, 15(2), 245–255.

Jain, A., and Tripathi, S. K. (2014). "Fabrication and characterization of energy storing supercapacitor devices using coconut shell based activated charcoal electrode." *Mater. Sci. Eng. B*, 183, 54–60.

Jaiswal, K. K., Chowdhury, C. R., Yadav, D., Verma, R., Dutta, S., Jaiswal, K. S., SangmeshB, and Karuppasamy, K. S. K. (2022). "Renewable and sustainable clean energy development and impact on social, economic, and environmental health." *Energy Nexus*, 7, 100118.

Jakhar, R., Samek, L., and Styszko, K. (2023). "A Comprehensive Study of the Impact of Waste Fires on the Environment and Health." *Sustainability*, 15(19), 14241.

Jiang, E., Amiralian, N., Maghe, M., Laycock, B., McFarland, E., Fox, B., Martin, D. J., and Annamalai, P. K. (2017). "Cellulose Nanofibers as Rheology Modifiers and Enhancers of Carbonization Efficiency in Polyacrylonitrile." *ACS Sustain. Chem. Eng.*, 5(4), 3296–3304.

Jiang, L., Sheng, L., and Fan, Z. (2018). "Biomass-derived carbon materials with structural diversities and their applications in energy storage." *Sci. China Mater.*, 61(2), 133–158.

Jiang, T., Yu, Y., Jahanger, A., and Balsalobre-Lorente, D. (2022). "Structural emissions reduction of China's power and heating industry under the goal of 'double carbon': A perspective from input-output analysis." *Sustain. Prod. Consum.*, 31, 346–356.

Jin, H., Wu, S., Li, T., Bai, Y., Wang, X., Zhang, H., Xu, H., Kong, C., and Wang, H. (2019). "Synthesis of porous carbon nano-onions derived from rice husk for high-performance supercapacitors." *Appl. Surf. Sci.*, 488, 593–599.

Kareem, F., Mohd-Naim, N. F., and Ahmed, M. U. (2024). "A novel and ultrasensitive electrochemical immunosensor based on nanocellulose-Ti3C2Tx@ZrO2 nano framework for the detection of ovalbumin." *Int. J. Biol. Macromol.*, 257, 128657.

Karnan, M., Subramani, K., Srividhya, P. K., and Sathish, M. (2017). "Electrochemical Studies on Corncob Derived Activated Porous Carbon for Supercapacitors Application in Aqueous and Non-aqueous Electrolytes." *Electrochim. Acta*, 228, 586–596.

Keppetipola, N. M., Dissanayake, M., Dissanayake, P., Karunarathne, B., Dourges, M. A., Talaga, D., Servant, L., Olivier, C., Toupance, T., Uchida, S., Tennakone, K., Kumara, G. R. A., and Cojocaru, L. (2021). "Graphite-type activated carbon from coconut shell: a natural source for eco-friendly non-volatile storage devices." *RSC Adv.*, 11(5), 2854–2865.

Khan, A., Senthil, R. A., Pan, J., Osman, S., Sun, Y., and Shu, X. (2020). "A new

biomass derived rod-like porous carbon from tea-waste as inexpensive and sustainable energy material for advanced supercapacitor application." *Electrochim. Acta*, 335, 135588.

Kim, H.-J., Naresh, B., Cho, I.-H., Bak, J.-S., Hira, S. A., Sekhar Reddy, P. R., Krishna, T. N. V., Dasha Kumar, K., Mola, B. A., and Kumar, Y. A. (2021). "An advanced nano-sticks & flake-type architecture of manganese-cobalt oxide as an effective electrode material for supercapacitor applications." *J. Energy Storage*, 40, 102702.

Kleef, E. Van, Bambrick, H., and Hales, S. (2011). "THE GEOGRAPHIC DISTRIBUTION OF DENGUE FEVER AND THE POTENTIAL INFLUENCE OF GLOBAL CLIMATE CHANGE." *ISEE Conf. Abstr.*, 2011(1), isee.2011.00337.

Kong, X., Zhang, Y., Zhang, P., Song, X., and Xu, H. (2020). "Synthesis of natural nitrogen-rich soybean pod carbon with ion channels for low cost and large areal capacitance supercapacitor." *Appl. Surf. Sci.*, 516, 146162.

Kozakov, D., Hall, D. R., Xia, B., Porter, K. A., Padhorny, D., Yueh, C., Beglov, D., and Vajda, S. (2017). "The ClusPro web server for protein–protein docking." *Nat. Protoc.*, 12(2), 255–278.

Kreps, B. H. (2020). "The Rising Costs of Fossil-Fuel Extraction: An Energy Crisis That Will Not Go Away." *Am. J. Econ. Sociol.*, 79(3), 695–717.

Krishnan, P., and Biju, V. (2021). "Effect of electrolyte concentration on the electrochemical performance of RGO–KOH supercapacitor." *Bull. Mater. Sci.*, 44(4), 288.

Kulurumotlakatla, D. K., Yedluri, A. K., and Kim, H.-J. (2020). "Hierarchical NiCo2S4 nanostructure as highly efficient electrode material for high-performance supercapacitor applications." *J. Energy Storage*, 31, 101619.

Kumar, A., and Agrawal, A. (2020). "Recent trends in solid waste management status, challenges, and potential for the future Indian cities – A review." *Curr. Res. Environ. Sustain.*, 2, 100011.

Lakshmi, K. C. S., and Vedhanarayanan, B. (2023). "High-Performance Supercapacitors: A Comprehensive Review on Paradigm Shift of Conventional Energy Storage Devices." *Batteries*, 9(4), 202.

Lee, K., Shabnam, L., Faisal, S. N., Hoang, V. C., and Gomes, V. G. (2020). "Aerogel from fruit biowaste produces ultracapacitors with high energy density and stability." *J. Energy Storage*, 27, 101152.

Li, F., Wu, X., Ji, W., Gui, X., Chen, Y., Zhao, J., Zhou, C., and Ren, T. (2020). "Effects of pyrolysis temperature on properties of swine manure biochar and its environmental risks of heavy metals." *J. Anal. Appl. Pyrolysis*, 152, 104945.

Liang, K., Chen, Y., Wang, S., Wang, D., Wang, W., Jia, S., Mitsuzakic, N., and Chen, Z. (2023). "Peanut shell waste derived porous carbon for high-performance supercapacitors." *J. Energy Storage*, 70, 107947.

Lillo-Ródenas, M. ., Cazorla-Amorós, D., and Linares-Solano, A. (2003). "Understanding chemical reactions between carbons and NaOH and KOH." *Carbon N. Y.*, 41(2), 267–275.

Liu, B., Zhang, L., Qi, P., Zhu, M., Wang, G., Ma, Y., Guo, X., Chen, H., Zhang, B., Zhao, Z., Dai, B., and Yu, F. (2016). "Nitrogen-Doped Banana Peel–Derived Porous Carbon Foam as Binder-Free Electrode for Supercapacitors." *Nanomaterials*, 6(1), 18.

Liu, D., Xu, B., Zhu, J., Tang, S., Xu, F., Li, S., Jia, B., and Chen, G. (2020a). "Preparation of Highly Porous Graphitic Activated Carbon as Electrode Materials for Supercapacitors by Hydrothermal Pretreatment-Assisted Chemical Activation." *ACS Omega*, 5(19), 11058–11067.

Liu, D., Zhao, X., Su, R., Hao, Z., Jia, B., Li, S., and Dong, L. (2019a). "Highly Porous Graphitic Activated Carbons from Lignite via Microwave Pretreatment and Iron-Catalyzed Graphitization at Low-Temperature for Supercapacitor Electrode Materials." *Processes*, 7(5), 300.

Liu, Y., Jiang, S. P., and Shao, Z. (2020b). "Intercalation pseudocapacitance in electrochemical energy storage: recent advances in fundamental understanding and materials development." *Mater. Today Adv.*, 7, 100072.

Liu, Z., Ballantyne, A. P., and Cooper, L. A. (2019b). "Biophysical feedback of global forest fires on surface temperature." *Nat. Commun.*, 10(1), 214.

Liu, Z., Hu, J., Shen, F., Tian, D., Huang, M., He, J., Zou, J., Zhao, L., and Zeng, Y. (2021). "Trichoderma bridges waste biomass and ultra-high specific surface area carbon to achieve a high-performance supercapacitor." *J. Power Sources*, 497, 229880.

Liu, Z., Singer, S., Tong, Y., Kimbell, L., Anderson, E., Hughes, M., Zitomer, D., and McNamara, P. (2018). "Characteristics and applications of biochars derived from wastewater solids." *Renew. Sustain. Energy Rev.*, 90, 650–664.

Ma, F., Ding, S., Ren, H., and Liu, Y. (2019). "Sakura-based activated carbon preparation and its performance in supercapacitor applications." *RSC Adv.*, 9(5), 2474–2483.

Ma, G., Yang, Q., Sun, K., Peng, H., Ran, F., Zhao, X., and Lei, Z. (2015). "Nitrogen-doped porous carbon derived from biomass waste for high-performance supercapacitor." *Bioresour. Technol.*, 197, 137–142.

Madhu, R., Sankar, K. V., Chen, S.-M., and Selvan, R. K. (2014). "Eco-friendly synthesis of activated carbon from dead mango leaves for the ultrahigh sensitive detection of toxic heavy metal ions and energy storage applications." *RSC Adv.*, 4(3), 1225–1233.

Maria Sundar Raj, F. R., Jaya, N. V., Boopathi, G., Kalpana, D., and Pandurangan, A. (2020). "S-doped activated mesoporous carbon derived from the Borassus flabellifer flower as active electrodes for supercapacitors." *Mater. Chem. Phys.*, 240, 122151.

Mascarenhas, F. J., Hegde, S. S., and Bhat, B. R. (2023). "Supercapattery." *Sustain.*

Mater. Electrochem. Capacit., Wiley, 279–290.

Mehdi, R., Naqvi, S. R., Khoja, A. H., and Hussain, R. (2023). "Biomass derived activated carbon by chemical surface modification as a source of clean energy for supercapacitor application." *Fuel*, 348, 128529.

Mendhe, A., and Panda, H. S. (2023). "A review on electrolytes for supercapacitor device." *Discov. Mater.*, 3(1), 29.

Mendonça, P. D., Santos, L. K. B., Foguel, M. V., Rodrigues, M. A. B., Cordeiro, M. T., Gonçalves, L. M., Marques, E. T. A., and Dutra, R. F. (2021). "NS1 glycoprotein detection in serum and urine as an electrochemical screening immunosensor for dengue and Zika virus." *Anal. Bioanal. Chem.*, 413(19), 4873–4885.

Merin, P., Jimmy Joy, P., Muralidharan, M. N., Veena Gopalan, E., and Seema, A. (2021). "Biomass-Derived Activated Carbon for High-Performance Supercapacitor Electrode Applications." *Chem. Eng. Technol.*, 44(5), 844–851.

Mitravinda, T., Nanaji, K., Anandan, S., Jyothirmayi, A., Chakravadhanula, V. S. K., Sharma, C. S., and Rao, T. N. (2018). "Facile Synthesis of Corn Silk Derived Nanoporous Carbon for an Improved Supercapacitor Performance." *J. Electrochem. Soc.*, 165(14), A3369–A3379.

Mo, R.-J., Zhao, Y., Wu, M., Xiao, H.-M., Kuga, S., Huang, Y., Li, J.-P., and Fu, S.-Y. (2016). "Activated carbon from nitrogen rich watermelon rind for high-performance supercapacitors." *RSC Adv.*, 6(64), 59333–59342.

Mohamed, F., Shaban, M., Zaki, S. K., Abd-Elsamie, M. S., Sayed, R., Zayed, M., Khalid, N., Saad, S., Omar, S., Ahmed, A. M., Gerges, A., El-Mageed, H. R. A., and Soliman, N. K. (2022). "Activated carbon derived from sugarcane and modified with natural zeolite for efficient adsorption of methylene blue dye: experimentally and theoretically approaches." *Sci. Rep.*, 12(1), 18031.

Mohd Abdah, M. A. A., Azman, N. H. N., Kulandaivalu, S., and Sulaiman, Y. (2020). "Review of the use of transition-metal-oxide and conducting polymer-based fibres for high-performance supercapacitors." *Mater. Des.*, 186, 108199.

Mustafa, M. S., Rasotgi, V., Jain, S., and Gupta, V. (2015). "Discovery of fifth serotype of dengue virus (DENV-5): A new public health dilemma in dengue control." *Med. J. Armed Forces India*, 71(1), 67–70.

N. K., P. S., Jeong, S. M., and Rout, C. S. (2024). "MXene–carbon based hybrid materials for supercapacitor applications." *Energy Adv.*, 3(2), 341–365.

Nandi, R., Jha, M. K., Guchhait, S. K., Sutradhar, D., and Yadav, S. (2023). "Impact of KOH Activation on Rice Husk Derived Porous Activated Carbon for Carbon Capture at Flue Gas alike Temperatures with High CO 2 /N 2 Selectivity." *ACS Omega*, 8(5), 4802–4812.

Nawaz, M. H., Hayat, A., Catanante, G., Latif, U., and Marty, J. L. (2018). "Development of a portable and disposable NS1 based electrochemical immunosensor

for early diagnosis of dengue virus." *Anal. Chim. Acta*, 1026, 1–7.

Nguyen, L. T., Phan, D.-P., Sarwar, A., Tran, M. H., Lee, O. K., and Lee, E. Y. (2021). "Valorization of industrial lignin to value-added chemicals by chemical depolymerization and biological conversion." *Ind. Crops Prod.*, 161, 113219.

Nikhil, Srivastava, S. K., Srivastava, A., Srivastava, M., and Prakash, R. (2022). "Electrochemical Sensing of Roxarsone on Natural Biomass-Derived Two-Dimensional Carbon Material as Promising Electrode Material." *ACS Omega*, 7(3), 2908–2917.

Niu, J., Liang, J., Shao, R., Liu, M., Dou, M., Li, Z., Huang, Y., and Wang, F. (2017). "Tremella-like N,O-codoped hierarchically porous carbon nanosheets as high-performance anode materials for high energy and ultrafast Na-ion capacitors." *Nano Energy*, 41, 285–292.

Otgonbayar, Z., Yang, S., Kim, I.-J., and Oh, W.-C. (2023). "Recent advances in 2D MXene and solid state electrolyte for energy storage applications: Comprehensive review." *Chem. Eng. J.*, 472, 144801.

Ozsoz, M. S. (2012). *Electrochemical DNA Biosensors*. Jenny Stanford Publishing.

Pal, B., Yang, S., Ramesh, S., Thangadurai, V., and Jose, R. (2019). "Electrolyte selection for supercapacitive devices: a critical review." *Nanoscale Adv.*, 1(10), 3807–3835.

Pang, P., Yan, F., Chen, M., Li, H., Zhang, Y., Wang, H., Wu, Z., and Yang, W. (2016). "Promising biomass-derived activated carbon and gold nanoparticle nanocomposites as a novel electrode material for electrochemical detection of rutin." *RSC Adv.*, 6(93), 90446–90454.

Parveen, N., Al-Jaafari, A. I., and Han, J. I. (2019). "Robust cyclic stability and high-rate asymmetric supercapacitor based on orange peel-derived nitrogen-doped porous carbon and intercrossed interlinked urchin-like NiCo2O4@3DNF framework." *Electrochim. Acta*, 293, 84–96.

Pathak, A. D., Potphode, D., and Sharma, C. S. (2022). "Graphitization induced structural transformation of candle soot carbon into carbon nano-onion as a functional anode for metal-ion batteries." *Mater. Adv.*, 3(8), 3610–3619.

Peng, C., Yan, X., Wang, R., Lang, J., Ou, Y., and Xue, Q. (2013). "Promising activated carbons derived from waste tea-leaves and their application in high performance supercapacitors electrodes." *Electrochim. Acta*, 87, 401–408.

Pramitha, A., Hegde, S. S., Bhat, B. R., George, S. D., Sudhakar, Y. N., and Raviprakash, Y. (2023). "Properties of Mn3O4 thin film electrodes prepared using spray pyrolysis for supercapacitor application." *Mater. Chem. Phys.*, 307, 128213.

Prauchner, M. J., Sapag, K., and Rodríguez-Reinoso, F. (2016). "Tailoring biomass-based activated carbon for CH4 storage by combining chemical activation with H3PO4 or ZnCl2 and physical activation with CO2." *Carbon N. Y.*, 110, 138–147.

Qiu, D., Kang, C., Gao, A., Xie, Z., Li, Y., Li, M., Wang, F., and Yang, R. (2019). "Sustainable Low-Temperature Activation to Customize Pore Structure and Heteroatoms of Biomass-Derived Carbon Enabling Unprecedented Durable Supercapacitors." *ACS Sustain. Chem. Eng.*, 7(17), 14629–14638.

Raj, C. J., Rajesh, M., Manikandan, R., Yu, K. H., Anusha, J. R., Ahn, J. H., Kim, D.-W., Park, S. Y., and Kim, B. C. (2018). "High electrochemical capacitor performance of oxygen and nitrogen enriched activated carbon derived from the pyrolysis and activation of squid gladius chitin." *J. Power Sources*, 386, 66–76.

Rajasekaran, S. J., Grace, A. N., Jacob, G., Alodhayb, A., Pandiaraj, S., and Raghavan, V. (2023). "Investigation of Different Aqueous Electrolytes for Biomass-Derived Activated Carbon-Based Supercapacitors." *Catalysts*, 13(2), 286.

Ramachandran, R., and Wang, F. (2018). "Electrochemical Capacitor Performance: Influence of Aqueous Electrolytes." *Supercapacitors - Theor. Pract. Solut.*, InTech.

Ramage, H., and Cherry, S. (2015). "Virus-Host Interactions: From Unbiased Genetic Screens to Function." *Annu. Rev. Virol.*, 2(1), 497–524.

Ramos, J. L., Pakuts, B., Godoy, P., García-Franco, A., and Duque, E. (2022). "Addressing the energy crisis: using microbes to make biofuels." *Microb. Biotechnol.*, 15(4), 1026–1030.

Rao, R., Pint, C. L., Islam, A. E., Weatherup, R. S., Hofmann, S., Meshot, E. R., Wu, F., Zhou, C., Dee, N., Amama, P. B., Carpena-Nuñez, J., Shi, W., Plata, D. L., Penev, E. S., Yakobson, B. I., Balbuena, P. B., Bichara, C., Futaba, D. N., Noda, S., Shin, H., Kim, K. S., Simard, B., Mirri, F., Pasquali, M., Fornasiero, F., Kauppinen, E. I., Arnold, M., Cola, B. A., Nikolaev, P., Arepalli, S., Cheng, H.-M., Zakharov, D. N., Stach, E. A., Zhang, J., Wei, F., Terrones, M., Geohegan, D. B., Maruyama, B., Maruyama, S., Li, Y., Adams, W. W., and Hart, A. J. (2018). "Carbon Nanotubes and Related Nanomaterials: Critical Advances and Challenges for Synthesis toward Mainstream Commercial Applications." *ACS Nano*, 12(12), 11756–11784.

Rodenhuis-Zybert, I. A., Wilschut, J., and Smit, J. M. (2010). "Dengue virus life cycle: viral and host factors modulating infectivity." *Cell. Mol. Life Sci.*, 67(16), 2773–2786.

Sadavar, S., Wang, K. J., Kang, T., Hwang, M., Saeed, G., Yu, X., and Park, H. S. (2023). "Anion storage for hybrid supercapacitor." *Mater. Today Energy*, 37, 101388.

Santos, A., Bueno, P. R., and Davis, J. J. (2018). "A dual marker label free electrochemical assay for Flavivirus dengue diagnosis." *Biosens. Bioelectron.*, 100, 519–525.

Sarwar, A., Ali, M., Khoja, A. H., Nawar, A., Waqas, A., Liaquat, R., Naqvi, S. R., and Asjid, M. (2021). "Synthesis and characterization of biomass-derived surface-modified activated carbon for enhanced CO2 adsorption." *J. CO2 Util.*, 46, 101476.

Sekula, B., Zielinski, K., and Bujacz, A. (2013). "Crystallographic studies of the complexes of bovine and equine serum albumin with 3,5-diiodosalicylic acid." *Int. J. Biol. Macromol.*, 60, 316–324.

Senthil, C., and Lee, C. W. (2021). “Biomass-derived biochar materials as sustainable energy sources for electrochemical energy storage devices.” *Renew. Sustain. Energy Rev.*, 137, 110464.

Serafin, J., Baca, M., Biegun, M., Mijowska, E., Kaleńczuk, R. J., Sreńscek-Nazzal, J., and Michalkiewicz, B. (2019). “Direct conversion of biomass to nanoporous activated biocarbons for high CO2 adsorption and supercapacitor applications.” *Appl. Surf. Sci.*, 497, 143722.

Sesuk, T., Tammawat, P., Jivaganont, P., Somton, K., Limthongkul, P., and Kobsiriphat, W. (2019). “Activated carbon derived from coconut coir pith as high performance supercapacitor electrode material.” *J. Energy Storage*, 25, 100910.

Sevilla, M., and Fuertes, A. B. (2014). “Direct Synthesis of Highly Porous Interconnected Carbon Nanosheets and Their Application as High-Performance Supercapacitors.” *ACS Nano*, 8(5), 5069–5078.

Sha, T., Li, X., Liu, J., Sun, M., Wang, N., Bo, X., Guo, Y., Hu, Z., and Zhou, M. (2018). “Biomass waste derived carbon nanoballs aggregation networks-based aerogels as electrode material for electrochemical sensing.” *Sensors Actuators B Chem.*, 277, 195–204.

Shaker, M., Ghazvini, A. A. S., Cao, W., Riahifar, R., and Ge, Q. (2021). “Biomass-derived porous carbons as supercapacitor electrodes – A review.” *New Carbon Mater.*, 36(3), 546–572.

Sharma, S., and Chand, P. (2023). “Supercapacitor and electrochemical techniques: A brief review.” *Results Chem.*, 5, 100885.

Shi, S., Zhou, X., Chen, W., Chen, M., Nguyen, T., Wang, X., and Zhang, W. (2017). “Improvement of structure and electrical conductivity of activated carbon by catalytic graphitization using N 2 plasma pretreatment and iron(iii) loading.” *RSC Adv.*, 7(71), 44632–44638.

Shin, S.-J., Kim, D. H., Bae, G., Ringe, S., Choi, H., Lim, H.-K., Choi, C. H., and Kim, H. (2022). “On the importance of the electric double layer structure in aqueous electrocatalysis.” *Nat. Commun.*, 13(1), 174.

Shoaib, M., and Al-Swaidan, H. M. (2015). “Optimization and characterization of sliced activated carbon prepared from date palm tree fronds by physical activation.” *Biomass and Bioenergy*, 73, 124–134.

Shulga, Y. M., Baskakov, S. A., Smirnov, V. A., Shulga, N. Y., Belay, K. G., and Gutsev, G. L. (2014). “Graphene oxide films as separators of polyaniline-based supercapacitors.” *J. Power Sources*, 245, 33–36.

Siew, Q. Y., Pang, E. L., Loh, H.-S., and Tan, M. T. T. (2021). “Highly sensitive and specific graphene/TiO2 impedimetric immunosensor based on plant-derived tetravalent envelope glycoprotein domain III (EDIII) probe antigen for dengue diagnosis.” *Biosens. Bioelectron.*, 176, 112895.

Sinawang, P. D., Rai, V., Ionescu, R. E., and Marks, R. S. (2016). “Electrochemical lateral flow immunosensor for detection and quantification of dengue NS1 protein.” *Biosens. Bioelectron.*, 77, 400–408.

Siqueira Silva, M., Moreira Tavares, A. P., Leomil Coelho, L. F., Morganti Ferreira Dias, L. E., Chura-Chambi, R. M., Guimarães da Fonseca, F., Ferreira Sales, M. G., and Costa Figueiredo, E. (2021). “Rational selection of hidden epitopes for a molecularly imprinted electrochemical sensor in the recognition of heat-denatured dengue NS1 protein.” *Biosens. Bioelectron.*, 191, 113419.

Su, X.-L., Chen, J.-R., Zheng, G.-P., Yang, J.-H., Guan, X.-X., Liu, P., and Zheng, X.-C. (2018). “Three-dimensional porous activated carbon derived from loofah sponge biomass for supercapacitor applications.” *Appl. Surf. Sci.*, 436, 327–336.

Subramani, K., Sudhan, N., Karnan, M., and Sathish, M. (2017). “Orange Peel Derived Activated Carbon for Fabrication of High-Energy and High-Rate Supercapacitors.” *ChemistrySelect*, 2(35), 11384–11392.

Sun, L., Gong, Y., Li, D., and Pan, C. (2022). “Biomass-derived porous carbon materials: synthesis, designing, and applications for supercapacitors.” *Green Chem.*, 24(10), 3864–3894.

Sun, L., Tian, C., Li, M., Meng, X., Wang, L., Wang, R., Yin, J., and Fu, H. (2013). “From coconut shell to porous graphene-like nanosheets for high-power supercapacitors.” *J. Mater. Chem. A*, 1(21), 6462.

Sun, N., Li, Z., Zhang, X., Qin, W., Zhao, C., Zhang, H., Ng, D. H. L., Kang, S., Zhao, H., and Wang, G. (2019). “Hierarchical Porous Carbon Materials Derived from Kelp for Superior Capacitive Applications.” *ACS Sustain. Chem. Eng.*, 7(9), 8735–8743.

Tag, A. T., Duman, G., Ucar, S., and Yanik, J. (2016). “Effects of feedstock type and pyrolysis temperature on potential applications of biochar.” *J. Anal. Appl. Pyrolysis*, 120, 200–206.

Tatrari, G., Karakoti, M., Tewari, C., Pandey, S., Bohra, B. S., Dandapat, A., and Sahoo, N. G. (2021). “Solid waste-derived carbon nanomaterials for supercapacitor applications: a recent overview.” *Mater. Adv.*, 2(5), 1454–1484.

Teli, A. M., Beknalkar, S. A., Pawar, S. A., Dubal, D. P., Dongale, T. D., Patil, D. S., Patil, P. S., and Shin, J. C. (2020). “Effect of Concentration on the Charge Storage Kinetics of Nanostructured MnO2 Thin-Film Supercapacitors Synthesized by the Hydrothermal Method.” *Energies*, 13(22), 6124.

Thevenot, D. R., Tóth, K., Durst, R. A., and Wilson, G. S. (1999). “Electrochemical Biosensors: Recommended Definitions and Classification.” *Pure Appl. Chem.*, 71(12), 2333–2348.

Tian, P., Wang, Y., Jia, S., Gao, H., Zhou, S., Xu, H., Song, S., and Zang, J. (2019). “‘Frying’ milk powder by molten salt to prepare nitrogen-doped hierarchical porous carbon for high performance supercapacitor.” *J. Alloys Compd.*, 806, 650–659.

Trott, O., and Olson, A. J. (2010). “AutoDock Vina: Improving the speed and accuracy of docking with a new scoring function, efficient optimization, and multithreading.” *J. Comput. Chem.*, 31(2), 455–461.

Tsay, K.-C., Zhang, L., and Zhang, J. (2012). “Effects of electrode layer composition/thickness and electrolyte concentration on both specific capacitance and energy density of supercapacitor.” *Electrochim. Acta*, 60, 428–436.

Tundwal, A., Kumar, H., Binoj, B. J., Sharma, R., Kumar, G., Kumari, R., Dhayal, A., Yadav, A., Singh, D., and Kumar, P. (2024). “Developments in conducting polymer-, metal oxide-, and carbon nanotube-based composite electrode materials for supercapacitors: a review.” *RSC Adv.*, 14(14), 9406–9439.

Usha Rani, M., Nanaji, K., Rao, T. N., and Deshpande, A. S. (2020). “Corn husk derived activated carbon with enhanced electrochemical performance for high-voltage supercapacitors.” *J. Power Sources*, 471, 228387.

Veerakumar, P., Ramkumar, R., Rajkumar, C., Kim, W. K., and Kim, H. (2023). “Fabrication of Low-Cost and High-Energy Storage Capacitor Electrode from Teak (Tectona grandis) Leaves.” *Energy & Fuels*.

Vijayaraghavan, K. (2021). “The importance of mineral ingredients in biochar production, properties and applications.” *Crit. Rev. Environ. Sci. Technol.*, 51(2), 113–139.

Walia, S. S., Arif, M. A., and Liaqat, J. (2020). “Clinical manifestations and laboratory diagnosis.” *Dengue Virus Dis.*, Elsevier, 115–137.

Wang, B., Wang, Y., Peng, Y., Wang, X., Wang, J., and Zhao, J. (2018). “3-dimensional interconnected framework of N-doped porous carbon based on sugarcane bagasse for application in supercapacitors and lithium ion batteries.” *J. Power Sources*, 390, 186–196.

Wang, C., Yan, B., Zheng, J., Feng, L., Chen, Z., Zhang, Q., Liao, T., Chen, J., Jiang, S., Du, C., and He, S. (2022a). “Recent progress in template-assisted synthesis of porous carbons for supercapacitors.” *Adv. Powder Mater.*, 1(2), 100018.

Wang, D., Liu, S., Fang, G., Geng, G., and Ma, J. (2016). “From Trash to Treasure: Direct Transformation of Onion Husks into Three-Dimensional Interconnected Porous Carbon Frameworks for High-Performance Supercapacitors in Organic Electrolyte.” *Electrochim. Acta*, 216, 405–411.

Wang, D., Mukhtar, A., Humayun, M., Wu, K., Du, Z., Wang, S., and Zhang, Y. (2022b). “A Critical Review on Nanowire-Motors: Design, Mechanism and Applications.” *Chem. Rec.*, 22(8).

Wang, J., Zhang, Q., and Deng, M. (2022c). “Eco-Friendly Preparation of Biomass-Derived Porous Carbon and Its Electrochemical Properties.” *ACS Omega*, 7(26), 22689–22697.

Wang, Mukhtar, Wu, Gu, and Cao. (2019). “Multi-Segmented Nanowires: A High Tech

Bright Future." *Materials (Basel).*, 12(23), 3908.

Wang, N., Zhang, G., Guan, T., Wu, J., Wang, J., and Li, K. (2022d). "Microphase Separation Engineering toward 3D Porous Carbon Assembled from Nanosheets for Flexible All-Solid-State Supercapacitors." *ACS Appl. Mater. Interfaces*, 14(11), 13250–13260.

Wang, X., and Shi, G. (2015). "Flexible graphene devices related to energy conversion and storage." *Energy Environ. Sci.*, 8(3), 790–823.

"Web Based Theoretical Protein pI, MW and 2DE Map." (2009). *J. Comput. Sci. Syst. Biol.*, 02(01).

Wei, J., Tu, C., Yuan, G., Liu, Y., Bi, D., Xiao, L., Lu, J., Theng, B. K. G., Wang, H., Zhang, L., and Zhang, X. (2019). "Assessing the effect of pyrolysis temperature on the molecular properties and copper sorption capacity of a halophyte biochar." *Environ. Pollut.*, 251, 56–65.

Wu, M., Li, L., Liu, J., Li, Y., Ai, P., Wu, W., and Zheng, J. (2015). "Template-free preparation of mesoporous carbon from rice husks for use in supercapacitors." *New Carbon Mater.*, 30(5), 471–475.

Xiao, Z. (2018). "Porous Biomass Carbon Derived from Peanut Shells as Electrode Materials with Enhanced Electrochemical Performance for Supercapacitors." *Int. J. Electrochem. Sci.*, 5370–5381.

Xie, M., Cheng, J., Xu, L., Wang, L., Chen, A., Zhang, S., and Ren, X. (2022). "Preparation of Activated Carbon from Co-Pyrolysis Activation of Fly Ash and Biomass." *Energies*, 15(18), 6636.

Xu, J., He, Q., Xiong, Z., Yu, Y., Zhang, S., Hu, X., Jiang, L., Su, S., Hu, S., Wang, Y., and Xiang, J. (2021). "Raman Spectroscopy as a Versatile Tool for Investigating Thermochemical Processing of Coal, Biomass, and Wastes: Recent Advances and Future Perspectives." *Energy & Fuels*, 35(4), 2870–2913.

Yan, J. (2020). "Nitrogen-doped Oxygen-rich Activated Carbon Derived from Longan Shell for Supercapacitors." *Int. J. Electrochem. Sci.*, 1982–1995.

Yang, J., Chen, Z., Lin, H., Feng, P., Xie, Y., Liang, Y., Zheng, M., Liu, X., Liu, Y., and Xiao, Y. (2022a). "Exfoliating Waste Biomass into Porous Carbon with Multi-Structural Levels for Dual Energy Storage." *ACS Appl. Energy Mater.*, 5(10), 12090–12098.

Yang, J., Roy, A., and Zhang, Y. (2013). "Protein–ligand binding site recognition using complementary binding-specific substructure comparison and sequence profile alignment." *Bioinformatics*, 29(20), 2588–2595.

Yang, V., Arumugam Senthil, R., Pan, J., Rajesh Kumar, T., Sun, Y., and Liu, X. (2020). "Hierarchical porous carbon derived from jujube fruits as sustainable and ultrahigh capacitance material for advanced supercapacitors." *J. Colloid Interface Sci.*, 579, 347–356.

Yang, V., Senthil, R. A., Pan, J., Khan, A., Osman, S., Wang, L., Jiang, W., and Sun, Y. (2019). "Highly ordered hierarchical porous carbon derived from biomass waste mangosteen peel as superior cathode material for high performance supercapacitor." *J. Electroanal. Chem.*, 855, 113616.

Yang, X., He, C., Qiu, Y., Bao, J., Li, P., Chen, Y., Zhou, X., Huang, B., and Zheng, X. (2022b). "Electrochemical sensing based on biomass-derived, hierarchical, porous carbon for simultaneous detection of dopamine and uric acid." *Mater. Chem. Phys.*, 292, 126825.

Yang, Y., Meehan, B., Shah, K., Surapaneni, A., Hughes, J., Fouché, L., and Paz-Ferreiro, J. (2018). "Physicochemical Properties of Biochars Produced from Biosolids in Victoria, Australia." *Int. J. Environ. Res. Public Health*, 15(7), 1459.

Yao, W., Zhao, Y., Chen, R., Wang, M., Song, W., and Yu, D. (2023). "Emissions of Toxic Substances from Biomass Burning: A Review of Methods and Technical Influencing Factors." *Processes*, 11(3), 853.

Yin, L., Chen, Y., Li, D., Zhao, X., Hou, B., and Cao, B. (2016). "3-Dimensional hierarchical porous activated carbon derived from coconut fibers with high-rate performance for symmetric supercapacitors." *Mater. Des.*, 111, 44–50.

Yin, Y., Liu, Q., Zhao, Y., Chen, T., Wang, J., Gui, L., and Lu, C. (2023). "Recent Progress and Future Directions of Biomass-Derived Hierarchical Porous Carbon: Designing, Preparation, and Supercapacitor Applications." *Energy & Fuels*, 37(5), 3523–3554.

Yoon, J.-H., Kumar, Y. A., Sambasivam, S., Hira, S. A., Krishna, T. N. V., Zeb, K., Uddin, W., Kumar, K. D., Obaidat, I. M., Kim, S., and Kim, H.-J. (2020). "Highly efficient copper-cobalt sulfide nano-reeds array with simplistic fabrication strategy for battery-type supercapacitors." *J. Energy Storage*, 32, 101988.

Yu, J., Sun, L., Berrueco, C., Fidalgo, B., Paterson, N., and Millan, M. (2018). "Influence of temperature and particle size on structural characteristics of chars from Beechwood pyrolysis." *J. Anal. Appl. Pyrolysis*, 130, 127–134.

Zhai, Z., Zhang, L., Du, T., Ren, B., Xu, Y., Wang, S., Miao, J., and Liu, Z. (2022). "A review of carbon materials for supercapacitors." *Mater. Des.*, 221, 111017.

Zhang, B., Biswal, B. K., Zhang, J., and Balasubramanian, R. (2023a). "Hydrothermal Treatment of Biomass Feedstocks for Sustainable Production of Chemicals, Fuels, and Materials: Progress and Perspectives." *Chem. Rev.*, 123(11), 7193–7294.

Zhang, C., Lin, S., Peng, J., Hong, Y., Wang, Z., and Jin, X. (2017). "Preparation of highly porous carbon through activation of NH 4 Cl induced hydrothermal microsphere derivation of glucose." *RSC Adv.*, 7(11), 6486–6491.

Zhang, J., Zhang, M., Zeng, Y., Chen, J., Qiu, L., Zhou, H., Sun, C., Yu, Y., Zhu, C., and Zhu, Z. (2019). "Single Fe Atom on Hierarchically Porous S, N-Codoped Nanocarbon Derived from Porphyra Enable Boosted Oxygen Catalysis for Rechargeable Zn-Air Batteries." *Small*, 15(24), 1900307.

Zhang, M., Zhang, J., Ran, S., Sun, W., and Zhu, Z. (2022). “Biomass-Derived sustainable carbon materials in energy conversion and storage applications: Status and opportunities. A mini review.” *Electrochem. commun.*, 138, 107283.

Zhang, X., Li, H., Zhang, K., Wang, Q., Qin, B., Cao, Q., and Jin, L. (2018). “Strategy for Preparing Porous Graphitic Carbon for Supercapacitor: Balance on Porous Structure and Graphitization Degree.” *J. Electrochem. Soc.*, 165(10), A2084–A2092.

Zhang, Y., Pan, H., Zhou, Q., Liu, K., Ma, W., and Fan, S. (2023b). “Biomass-derived carbon for supercapacitors electrodes – A review of recent advances.” *Inorg. Chem. Commun.*, 153, 110768.

Zhao, X., Liu, B., Yang, J., Hou, J., Wang, Y., and Zhu, Y. (2020). “Synthesizing LiNi0.5Co0.2Mn0.3O2 with microsized peanut-like structure for enhanced electrochemical properties of lithium ion batteries.” *J. Alloys Compd.*, 832, 154464.

Zhao, Y., and Zhang, X. (2021). “In situ activation graphitization to fabricate hierarchical porous graphitic carbon for supercapacitor.” *Sci. Rep.*, 11(1), 6825.

Zhong, C., Deng, Y., Hu, W., Qiao, J., Zhang, L., and Zhang, J. (2015). “A review of electrolyte materials and compositions for electrochemical supercapacitors.” *Chem. Soc. Rev.*, 44(21), 7484–7539.

Zhou, Y., Gao, B., Zimmerman, A. R., Fang, J., Sun, Y., and Cao, X. (2013). “Sorption of heavy metals on chitosan-modified biochars and its biological effects.” *Chem. Eng. J.*, 231, 512–518.

Zhu, F., Cao, W., Song, W., Peng, J., Yang, N., Niu, J., and Wang, F. (2022). “Biomass-derived carbon prepared through a quadruple-functional-salt approach for application in K-ion capacitors.” *Chem. Eng. J.*, 449, 137561.

PUBLICATIONS

PUBLICATIONS RELATED TO THESIS:

1. **Hegde, S. S.**, B.R. Bhat, (2024) "Impact of Electrolyte Concentration on the Electrochemical Performance of Biomass Waste-Derived High-Surface Carbon for Green Energy Storage", Fuel, 371, 131999.
2. **Hegde, S. S.**, and Bhat, B. R. (2024). "Sustainable energy storage: Mangifera indica leaf waste-derived activated carbon for long-life, high-performance supercapacitors." *RSC Adv.*, 14(12), 8028–8038.
3. **Hegde, S. S.,** and Bhat, B. R. (2024). "Biomass waste-derived porous graphitic carbon for high-performance supercapacitors." *J. Energy Storage*, 76, 109818.
4. **Hegde, S. S.,** and Bhat, B. R. (2022). "Dengue detection: Advances and challenges in diagnostic technology." *Biosens. Bioelectron. X*, 10, 100100.
5. **Hegde, S. S.,** and Bhat, B. R. (2023). "Solid Waste-Derived Carbon Materials for Electrochemical Capacitors." *Sustain. Mater. Electrochem. Capacit.*, Wiley, 19–31.
6. **Hegde, S. S.**, Naik, S., Bhat, B. R., Mishra, P., Dalimba, U., Ahmed, M. U., Santos, G. N. "A novel and ultrasensitive high-surface porous carbon-based electrochemical biosensor for early detection of dengue virus", (Biosensors and Bioelectronics:X, Under review)

PATENT RELATED TO THESIS:

7. **Hegde, S. S.,** B.R. Bhat, "PROCESS OF DERIVING POROUS GRAPHITIC CARBON FOR HIGH-PERFORMANCE SUPERCAPACITORS FROM BIOMASS WASTE" (Application Number: 202441007897, Date of Filing: 06/02/2024, Publication date: 15/03/2024)
8. **Hegde, S. S.**, B.R. Bhat, "PROCESS OF DERIVING ACTIVATED CARBON FROM DEAD MANGIFERA INDICA LEAF WASTE FOR HIGH-PERFORMANCE SUPERCAPACITORS" (Application Number: 202441030042, Date of Filing: 13/04/2024, Publication date: 07/06/2024)

9. **Hegde, S. S.,** B.R. Bhat, "PROCESS OF PREPARING COCOS NUCIFERA WASTE- DERIVED HIGH- SURFACE CARBON AND SELECTION OF ELECTROLYTE CONCENTRATION FOR GREEN ENERGY STORAGE DEVICE" (Application Number: 202441030043, Date of Filing: 13/04/2024, Publication date: 07/06/2024)
10. B.R. Bhat, **Hegde, S. S,** "THE PROCESS OF DETECTING THE DENGUE VIRUS USING AN ULTRASENSITIVE HIGH-SURFACE POROUS CARBON-BASED ELECTROCHEMICAL BIOSENSOR" (Application Number: 202441043802, Date of Filing: 06/06/2024, Publication date: 14/06/2024)

OTHER PUBLICATIONS:

11. **Hegde, S. S.**, and Bhat, B. R. "Infections, Symptoms, and Clinical Diagnostic Techniques for Dengue: A Case Study of a Neglected Tropical Disease", (Wiley-scrivener, Accepted)
12. **Hegde, S. S.**, and Bhat, B. R. "Graphene-based Electrochemical Biosensor for Environmental Monitoring", (Elsevier, Under review)
13. Adoor, P., **Hegde, S. S.,** Bhat, B. R., Yethadka, S. N., and Yeenduguli, R. (2023). "Elucidating the Role of Copper-Induced Mixed Phases on the Electrochemical Performance of Mn-Based Thin-Film Electrodes." *ACS Omega*.
14. Pramitha, A., **Hegde, S. S.,** Bhat, B. R., George, S. D., Sudhakar, Y. N., and Raviprakash, Y. (2023). "Properties of Mn_3O_4 thin film electrodes prepared using spray pyrolysis for supercapacitor application." *Mater. Chem. Phys.*, 307, 128213.
15. Mascarenhas, F. J., **Hegde, S. S.,** and Bhat, B. R. (2023). "Supercapattery." *Sustain. Mater. Electrochem. Capacit.*, Wiley, 279–290.
16. Adoor, P., **Hegde, S. S.,** Bhat, B. R., C. Yadav, S. Chakraborty, A. Ravikumar, S. George, S. D., Sudhakar, Y. N., and Raviprakash, Y. "Unveiling the Mass-loading Effect on the Electrochemical Performance of Mn_3O_4 Thin film Electrodes: A Combined Computational and Experimental Study", (Physica

Scripta, Under review)

17. Jayalakshmi, K., **Hegde, S. S.,** Bhat, B. R., Ismayil, "Exploring the microstructural properties of HPMC-based solid polymer electrolytes: A promising candidate for flexible electric double layer capacitor", (Cellulose, Under review)

AWARDS & ACHIEVEMENTS

- The article titled "Dengue detection: Advances and challenges in diagnostic technology", has been recognized by Elsevier and linked to the **United Nations Sustainable Development Goals** ("SDG 3: Ensure healthy lives and promote well-being for all at all ages"), helping to tackle some of the world's greatest challenges.
- "**Best Poster Presentation Award**" at the International Conference on Materials Chemistry for Energy and Environmental Applications 2023 (MCEEA-2023), conducted by MITS Madanapalle, during August 07-09, 2023.
- "**Visiting Researcher**" at the Faculty of Science, Universiti Brunei Darussalam, Brunei, during October 02 - 15, 2022.
- "**Visiting Scholar**" at De La Salle University in Manila, Philippines, from July 17 to 30, 2022.

CONFERENCES/SYMPOSIUMS/WORKSHOPS

- High-end Karyashala workshop on "Synthesis of electroactive hybrid composite materials and their application in supercapacitors for portable and smart electronics", conducted by NIT Rourkela, during March 04-10, 2024.
- Online Symposium "Small Bite, Big Threat: Dengue Demystified" held on 12th September 2023, organized by IIT Kharagpur, India.
- **Hegde, S. S.**, and Bhat, B. R., "Biomass-derived activated carbon as an electrode material for high-performance supercapacitor" International Conference on Materials Chemistry for Energy and Environmental Applications

2023 (MCEEA-2023), conducted by Madanapalle Institute of Technology and Science, during August 07-09, 2023.

- INUP - i2i Familiarization Workshop on Nanofabrication Technologies, held at IIT Madras, Chennai during August 21-22, 2023.
- INUP - i2i Familiarization Workshop on Nanofabrication Technologies, held at CeNSE, IISc, Bangalore during July 17-19, 2023.
- INUP - i2i, 8th User Awareness Workshop on Fabrication & Characterization Facility for Nanotechnology, held at IIT Delhi during 22 - 23 June, 2023.
- Synergistic Training program Utilizing the Scientific and Technological Infrastructure (STUTI), organized by Mangalore University Karnataka, India, during November 14-20, 2022.
- 2nd IEEE Workshop on Advances in Nanophotonic devices & Sensors organized by the Department of Electronics & Communication Engineering, NIT Karnataka, Surathkal, during October 04 - 08, 2021.
- Five-day National E Workshop on 'Advanced Materials Properties and Applications (AMPA-2021)' organized by NITK Surathkal, in association with the ESI Bangalore, during March 01 - 05, 2021.
- Five-day e-workshop titled 'Advancements in the Molecular World: Materials and Catalysis' (AMWMC-2021) conducted by NITK Surathkal, during February 15-19, 2021.
- IEEE Workshop on Advances in Nanophotonic devices & Sensors organized by the Department of Electronics & Communication Engineering, NIT Karnataka, Surathkal, during December 07 - 11, 2020.

BIO-DATA

MR. SHREEGANESH SUBRAYA HEGDE

OFFICIAL ADDRESS:

Catalysis and Materials Chemistry Laboratory

Department of Chemistry

National Institute of Technology Karnataka, Surathkal.

Mangalore – 575 025, Karnataka, India.

Email: hegdeshreeganesh@gmail.com

Phone: +91 9663541667

PERSONAL INFORMATION:

Date of Birth	**:** September 08, 1996
Gender	**:** Male
Languages	**:** English, Hindi, Kannada (Native)
Nationality	**:** Indian
Research Profile ID's	**: ORCID**: 0000-0003-2678-7481
	Google Scholar: UR3SQ8UAAAAJ
	Scopus ID: 57392690300
	Web of Science ResearcherID: AAN-2817-2021

EDUCATIONAL QUALIFICATIONS:

Doctor of Philosophy (2020-2024) in Chemistry from National Institute of Technology Karnataka, Surathkal.

Thesis: "Biomass-derived high surface porous carbon for energy and sensing applications" (Submitted: 15th April 2024)

Master of Science (2017-2019) in Chemistry from Karnatak University Dharwad.

Thesis: "Supercapacitor based on composite nanomaterials"

Bachelor of Science (2014-2017) from Karnatak University Dharwad

(Core subjects: Physics, Chemistry, Mathematics)

RESEARCH EXPERIENCE:

Visiting Researcher (Oct 2022) at Universiti Brunei Darussalam (UBD), Brunei: "Food Biosensor"

Visiting Scholar (July 2022) at De La Salle University (DLSU) Manila, Philippines: "Fabrication of Dengue Biosensor"

Junior Research Fellow (Oct 2020- Jan 2023) at National Institute of Technology Karnataka (NITK), Surathkal: "Design and Development of Non-Enzymatic Biosensors for Dengue Virus (DENV)"

Project Associate-I (Feb 2020 to Sept 2020) at Indian Institute of Science Education and Research (IISER), Pune: "High Performance Graphene-Based Supercapacitors"

Summer Research Fellow (June 2018 to July 2018) at National Institute of Technology Karnataka (NITK), Surathkal, "Supercapacitor Devices Based on Graphene Materials"

ACADEMIC SERVICE:

Journal Reviewer:

- Langmuir [American Chemical Society (ACS)]
- Recent Innovations in Chemical Engineering [Bentham Science Publishers]
- International Journal of Public Health Science (IJPHS) [Intelektual Pustaka Media Utama (IPMU)]

RESEARCH INTERESTS:

Supercapacitors, Batteries, Biosensors, Electrochemical techniques, Electrode materials, Biomass conversion, Synthesis & characterization of nanomaterials, High surface porous carbon, Graphene oxide, Reduced graphene oxide, Waste to energy applications.

RESEARCH SKILS:

Material synthesis: Biomass derived carbon materials, High surface porous carbon nanostructures, Graphene oxide, Reduced graphene oxide, Composite nanomaterials, Transition metal-based nanomaterials, Controlled atmosphere-assisted high-temperature furnace synthesis.

Material characterization techniques: X-ray diffraction (XRD), X-ray photoelectron spectroscopy (XPS), Energy Dispersive X-Ray Spectroscopy (EDX), Field Emission Scanning Electron Microscopy (FESEM), Transmission Electron Microscopy (TEM), Atomic Force Microscopy (AFM), Raman spectroscopy, Fourier-transform infrared spectroscopy (FTIR), Thermogravimetric analysis (TGA), BET surface area analysis & pore size distribution and volume analysis.

Electrochemical techniques: Cyclic voltammetry (CV), Differential pulse voltammetry (DPV), Galvanostatic charge-discharge (GCD), Electrochemical impedance spectroscopy (EIS).

Computational techniques: OriginLab (Data analysis software), ChemDraw, PANalytical X'Pert HighScore Software, ImageJ (Software for processing and analyzing scientific images) Microsoft Office Suite (Word, Excel, Access, PowerPoint), Graphic design software (Adobe Photoshop, Adobe PageMaker, CorelDRAW, Canva, PowerPoint), Mendeley (Reference Management Software), HTML (Basic web development).

RESEARCH PATENTS:

1. **Shreeganesh Subraya Hegde**, B.R. Bhat, "PROCESS OF DERIVING POROUS GRAPHITIC CARBON FOR HIGH-PERFORMANCE SUPERCAPACITORS FROM BIOMASS WASTE" (Application Number: 202441007897, Date of Filing: 06/02/2024, Publication date: 15/03/2024)
2. **Shreeganesh Subraya Hegde**, B.R. Bhat, "PROCESS OF DERIVING ACTIVATED CARBON FROM DEAD MANGIFERA INDICA LEAF WASTE FOR HIGH-PERFORMANCE SUPERCAPACITORS" (Application Number: 202441030042, Date of Filing: 13/04/2024, Publication date: 07/06/2024)
3. **Shreeganesh Subraya Hegde**, B.R. Bhat, "PROCESS OF PREPARING COCOS NUCIFERA WASTE- DERIVED HIGH- SURFACE CARBON AND SELECTION OF ELECTROLYTE CONCENTRATION FOR GREEN ENERGY STORAGE DEVICE" (Application Number: 202441030043, Date of Filing: 13/04/2024, Publication date: 07/06/2024)
4. B.R. Bhat, **Shreeganesh Subraya Hegde** "THE PROCESS OF DETECTING THE DENGUE VIRUS USING AN ULTRASENSITIVE HIGH-SURFACE

POROUS CARBON-BASED ELECTROCHEMICAL BIOSENSOR" (Application Number: 202441043802, Date of Filing: 06/06/2024, Publication date: 14/06/2024)

RESEARCH PUBLICATIONS:

1. **Shreeganesh Subraya Hegde** B.R. Bhat, "Biomass waste-derived porous graphitic carbon for high-performance supercapacitors", Journal of Energy Storage, (2024) https://doi.org/10.1016/j.est.2023.109818
2. **Shreeganesh Subraya Hegde**, B.R. Bhat, "Impact of Electrolyte Concentration on the Electrochemical Performance of Biomass Waste-Derived High-Surface Carbon for Green Energy Storage", Fuel, (2024) https://doi.org/10.1016/j.fuel.2024.131999
3. **Shreeganesh Subraya Hegde**, B.R. Bhat, "Sustainable Energy Storage: Mangifera Indica Leaf Waste-Derived Activated Carbon for Long-Life, High-Performance Supercapacitors", RSC Advances, (2024) https://doi.org/10.1039/D3RA08910J
4. P. Adoor, **Shreeganesh Subraya Hegde**, B.R. Bhat, S.N. Yethadka, R. Yeenduguli, "Elucidating the Role of Copper-Induced Mixed Phases on the Electrochemical Performance of Mn-Based Thin-Film Electrodes", ACS Omega, (2023) https://doi.org/10.1021/acsomega.3c05614
5. A. Pramitha, **Shreeganesh Subraya Hegde**, B.R. Bhat, S.D. George, Y.N. Sudhakar, Y. Raviprakash, "Properties of Mn_3O_4 thin film electrodes prepared using spray pyrolysis for supercapacitor application", Materials Chemistry and Physics, (2023) https://doi.org/10.1016/j.matchemphys.2023.128213
6. **Shreeganesh Subraya Hegde**, B.R. Bhat, "Dengue detection: Advances and challenges in diagnostic technology", Biosensors and Bioelectronics:X, (2022) https://doi.org/10.1016/j.biosx.2021.100100
7. **Shreeganesh Subraya Hegde**, Shivakumar, B.R. Bhat, P. Mishra, U. Dalimba, M.U. Ahmed, G.N. Santos, "A novel and ultrasensitive high-surface porous carbon-based electrochemical biosensor for early detection of dengue virus", (Biosensors and Bioelectronics:X, Under review)

8. A. Pramitha, **Shreeganesh Subraya Hegde**, B.R. Bhat, C. Yadav, S. Chakraborty, A. Ravikumar, S. D. George, Y. N. Sudhakar, Raviprakash Y, "Unveiling the mass-loading effect on the electrochemical performance of Mn3O4 thin film electrodes: A combined computational and experimental study", (Physica Scripta, Under review)
9. K. Jayalakshmi, **Shreeganesh Subraya Hegde,** B.R. Bhat, Ismayil, "Exploring the microstructural properties of HPMC-based solid polymer electrolytes: A promising candidate for flexible electric double layer capacitor", (Cellulose, Under review)

BOOK-CHAPTERS:

1. **Shreeganesh Subraya Hegde**, B.R. Bhat, "Solid Waste-Derived Carbon Materials for Electrochemical Capacitors", in: Sustainable Materials for Electrochemical Capacitors, Wiley, 2023: pp. 19–31. https://doi.org/10.1002/9781394167104.ch2
2. F.J. Mascarenhas, **Shreeganesh Subraya Hegde**, B.R. Bhat, "Supercapattery: An Electrochemical Energy Storage Device, in: Sustainable Materials for Electrochemical Capacitors", Wiley, 2023: pp. 279–290. https://doi.org/10.1002/9781394167104.ch11
3. **Shreeganesh Subraya Hegde**, B.R. Bhat, "Infections, Symptoms, and Clinical Diagnostic Techniques for Dengue: A Case Study of a Neglected Tropical Disease", (Wiley-scrivener, Accepted)
4. **Shreeganesh Subraya Hegde**, B.R. Bhat, "Graphene-based Electrochemical Biosensor for Environmental Monitoring", (Elsevier, Under review)

AWARDS AND ACHIEVEMENTS:

★ The article titled "Dengue detection: Advances and challenges in diagnostic technology", has been recognized by Elsevier and linked to the United Nations Sustainable Development Goals ("**SDG 3**: Ensure healthy lives and promote well-being for all at all ages"), helping to tackle some of the world's greatest challenges.

★ "**Best Poster Presentation Award**" at the International Conference on Materials Chemistry for Energy and Environmental Applications 2023 (MCEEA-2023), conducted by MITS Madanapalle, during August 07-09, 2023.

★ "**Visiting Researcher**" at the Faculty of Science, Universiti Brunei Darussalam, Brunei, during October 02 - 15, 2022.

★ "**Visiting Scholar**" at the department of Physics, De La Salle University, Manila, Philippines, during July 17 - 30, 2022.

★ "**Sahyadri Young Ecologist-2012**" award from Indian Institute of Science (IISc) Bangalore.

CONFERENCES AND WORKSHOPS:

★ High-end Karyashala workshop on "Synthesis of electroactive hybrid composite materials and their application in supercapacitors for portable and smart electronics", conducted by Dept. of Chemical engineering, NIT Rourkela, during March 04-10, 2024.

★ Symposium on “Small Bite, Big Threat: Dengue Demystified” held on 12th September 2023, organized by the Dept. of Paediatrics and Dept. of Community Medicine, Dr. B. C. Roy Multi-Speciality Medical Research Centre, IIT Kharagpur, Kharagpur, India.

★ **Hegde, S. S.**, and Bhat, B. R., “Biomass-derived activated carbon as an electrode material for high-performance supercapacitor” International Conference on “Materials Chemistry for Energy and Environmental Applications 2023” (MCEEA-2023), conducted by Dept. of Chemistry, Madanapalle Institute of Technology and Science, Andhra Pradesh, during August 07-09, 2023.

★ INUP - i2i Familiarization Workshop on Nanofabrication Technologies, held at IIT Madras, Chennai during August 21-22, 2023.

★ INUP - i2i Familiarization Workshop on Nanofabrication Technologies, held at CeNSE, IISc, Bangalore during July 17-19, 2023.

★ INUP - i2i, 8th User Awareness Workshop on Fabrication & Characterization Facility for Nanotechnology, held at IIT Delhi during 22 - 23 June, 2023.

★ DST funded “Synergistic Training program Utilizing the Scientific and Technological Infrastructure” (STUTI), organized by Mangalore University Karnataka, India, during November 14-20, 2022.

- ★ 2nd IEEE Workshop on "Advances in Nanophotonic devices & Sensors organized by the Department of Electronics & Communication Engineering", NIT Karnataka, Surathkal, during October 04 - 08, 2021.
- ★ Five-day National E Workshop on "Advanced Materials Properties and Applications (AMPA-2021)" organized by NITK Surathkal, in association with the ESI Bangalore, during March 01 - 05, 2021.
- ★ Five-day e-workshop titled "Advancements in the Molecular World: Materials and Catalysis" (AMWMC-2021) conducted by NITK Surathkal, during February 15-19, 2021.
- ★ Five-day e-workshop on Surface Characterization: Tools and Applications (SCTA-2020), conducted by NITK Surathkal, during December 14-18, 2020.
- ★ "IEEE Workshop on Advances in Nanophotonic devices & Sensors" organized by the Department of Electronics & Communication Engineering, NIT Karnataka, Surathkal, during December 07 - 11, 2020.
- ★ National conference on "Recent Advances in Chemistry" jointly organized by UGC-DSA-I and Karnatak University Chemistry Alumni Association, during March 24 - 25, 2018.
- ★ "Special lecture series (Chemical Science)-2017" organized by Karnatak University Dharwad & Karnataka Science and Technology Academy Bangalore, during October 09 - 11, 2017.

OTHER ACHIEVEMENTS:

- ★ Member of the Organizing Committee for the 3rd "International Conference on Direct Digital Manufacturing and Polymer" (ICDDMAP 2019, In collaboration with India and Portugal), during February 20 - 23, 2019.
- ★ Member of the Organizing Committee for the "Kannadadalli Vijnana mattu Tantrajnana Sammelana" conducted by Karnataka Science and Technology Academy, Dharwad Regional Science Centre & Karnatak University Dharwad.
- ★ Received **RAJYAPURASKAR** award (state level highest award for a Rover scout) from the Governor of Karnataka State and **Nipun** Rover award (District level highest award) for Rover scout achievements.

- ★ Completed two-years of volunteership under the **National Service Scheme** (NSS) and participated in the National Integration Camp 2016 held at KIIT University, Bhubaneswar, Odisha. Secured 2nd rank in the national-level nukkad competition.
- ★ Completed **National Cadet Corps** (NCC) certificate examination, and participated in many national level training camps.
- ★ Successfully cleared the **PMKVY** National Skill Qualification Framework Level-4 assessment and received certification from the National Skill Development Corporation, Government of India.